AEROSPACE RESEARCH • AERODYNAMICS • PROPULSION • STRUCTURAL DYNAMICS • ELECTRONIC SYSTEMS AND INSTRUMENTS • COMPUTER MODULES

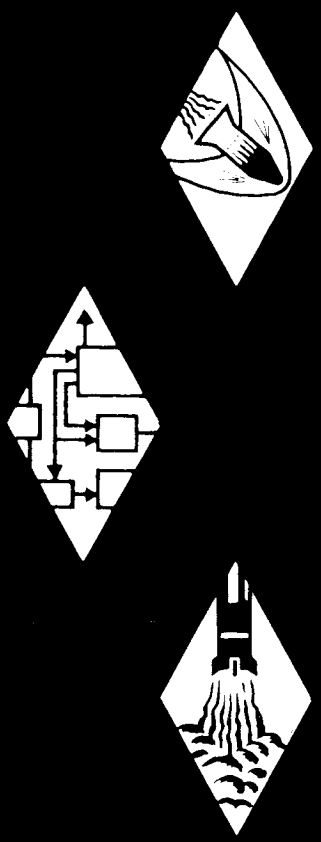

RESEARCH
ENGINEERING
PRODUCTION

Final Report

for

Development of an Electron Density Probe

(22 June 1964 - 22 March 1965)

GENERAL APPLIED SCIENCE LABORATORIES, INC.
MERRICK and STEWART AVENUES, WESTBURY, L.I., N.Y. · (516) ED 3-6960

Technical Report No. 527

Final Report

for

Development of an Electron Density Probe

(22 June 1964 - 22 March 1965)

Contract No.: NAS5-3929

Prepared by

General Applied Science Laboratories, Inc.
Merrick and Stewart Avenues
Westbury, L. I., New York

for

National Aeronautics and Space Administration
Goddard Space Flight Center
Greenbelt, Maryland

Project 8017

Total No. of Pages - viii & 135

Copy (135.

TECHNICAL REPORT NO. 527

Final Report

"Development of a Probe for the Measurement of Point Values of Electron Densities in Supersonic Flows"

(22 June 1964 - 22 March 1965)

By M. Abele
R. W. Byrne
H Medecki

Contract No : NAS5-3929

Prepared by

General Applied Science Laboratories, Inc
Merrick and Stewart Avenues
Westbury, L. I., New York

for

National Aeronautics and Space Flight Center
Goddard Space Flight Center
Greenbelt, Maryland

Approved by: _____
Antonio Ferri
President

April 9, 1965

SUMMARY

The present report describes the work completed between June 22, 1964 and March 22, 1965, on the development of electron density probes to perform measurements in flow fields similar to those estimated to exist in the local flow surrounding the Apollo spacecraft during reentry at altitudes between 350,000 and 150,000 ft.

The maximum stagnation point electron density expected during reentry of the Apollo spacecraft is 10^{16} e/cm^3 and the minimum value considered of interest is 10^8 e/cm^3.

The aerodynamic conditions taken for simulation have been computed for a typical trajectory and the point selected to perform the measurement is located aft of the heat shield where the local Mach number remains essentially constant (2.5) for a considerable portion of the trajectory.

A probe with an operating principle based on the interaction between a plasma and an electromagnetic field is considered to satisfy the main requirements of minimum size of the instrument, local supersonic flow conditions, wide range of electron densities and high spatial resolution. Three types of interaction are considered giving the basis

for three types of probes:

1. An internal cavity probe that can be used over three orders of magnitude in electron densities, the upper limit being 10^{12} e/cm^3 and can only operate in underdense plasmas.

2. An external cavity probe, also covering three orders of magnitude and operating in overdense plasmas only.

3. A low phase velocity structure which can operate in both over and underdense plasmas for a range of four orders of magnitude.

The main effort under the present development program has been the study and testing of probes of the internal cavity type. The first phase of this development program was concerned with the design of the probe to satisfy mutually interacting aerodynamic and electromagnetic requirements. The measurements of the resolution, sensitivity and range of operation were performed and the effects of a simulated plasma upon the conditions of resonance of the cavity determined.

A series of tests have been performed to determine the aerodynamic characteristics of the probe for Mach and Reynolds numbers equivalent to the ones encountered during reentry.

Finally the probes have been tested in a shock tube where the range of electron densities and Mach numbers close to the design values of the instrument were reproduced. The output from the probes was compared to the indication obtained with an independent measurement and with the values predicted for the shock tube as a function of the initial driven tube conditions and measured incident shock velocity.

This program has resulted in the development of two internal cavity type probes one operating with a 10 cm wavelength to measure electron densities in the range of 10^{8} to 10^{11} e/cm^{3} and another, a 3 cm wavelength probe to measure electron densities in the range of 10^{9}-10^{12} e/cm^{3}. Analytical studies of an external cavity probe and a low phase velocity structure probe have indicated that using these techniques the upper limit of measurable electron density levels can be extended to 10^{14} e/cm^{3}.

[illegible]

SECTION	TITLE	PAGE
1	INTRODUCTION	1
2	ELECTROMAGNETIC DEVELOPMENT PROGRAM	8
3	[illegible]	[illegible]
4	CALIBRATION OF THE PROBES	[illegible]
5	INVESTIGATION OF [illegible] TO MEASURE HIGHER ELECTRON DENSITIES	54
6	CONCLUSIONS	[illegible]
	[illegible]	
	[illegible]	[illegible]
	APPENDIX I - Principle of Operation of the Internal Cavity Probe	[illegible]
	APPENDIX II - Principle of Operation of the External Cavity Probe	II-[illegible]
	APPENDIX III - Low Phase Velocity [illegible] Probe	III-1
	APPENDIX IV - Internal Cavity Probe Operating Manual	IV-1

LIST OF FIGURES

1. Introduction. - A program to develop probes suitable for measuring electron densities of supersonic flow plasmas has been undertaken. These probes are intended to operate in a superorbital shock-tube tunnel, and are also adaptable for measurements in the ionized flow field of a spacecraft during superorbital reentry conditions. A study of different plasma diagnostic techniques has been performed to determine their possibilities and limitations for this special application. The factors considered of prime importance in the development of this type of probe are the range of electron densities to be covered, the aerodynamic conditions in which the probe is to operate, and the spatial resolution to be achieved.

The type of probe considered most adequate for performing these measurements is the one based on plasma-microwave interactions. Three possible configurations utilizing these interactions have been studied. Internal cavity, external cavity, and low phase velocity structure probes. For the lower end of the above-mentioned range two internal cavity probes have been developed. Each can cover three orders of magnitude in electron density with the range of operation depending upon the microwave frequency being used; the

ranges are 10^8 to 10^{11} e/cm^3 for a 10 cm wavelength probe and 10^9 to 10^{12} e/cm^3 for a 3 cm wavelength probe.

A region in the Apollo local flow field was chosen where the Mach number remains almost constant at a value of approximately 2.5 during reentry to establish the design operating conditions for the probe. Estimates of the electron density levels in the local flow field of the Apollo vehicle were made in order to determine the extent to which probes of a given maximum electron density measuring capability would have application. Estimates of the stagnation equilibrium electron density and the electron density existing in the local flow field where the Mach number was 2.5 were made. For the purposes of this study an Apollo reentry trajectory with an initial flight path angle of -6.4° and a reentry range of 3000 nm was selected. The stagnation equilibrium electron densities were calculated for the altitude and velocity conditions corresponding to this trajectory. The results are presented in Fig. 1, where the velocity, altitude, stagnation electron density and the electron density estimated to exist in the local flow at a Mach number of 2.5 are given as a function of time during the trajectory. The

estimates of the electron density for the local Mach number of 2.5 case were made for the 200,000 ft altitude flight condition by assuming frozen chemistry along a streamline passing from the stagnation region to a point where the local Mach number was 2.5. It was found that the local electron density was an order of magnitude lower than the corresponding stagnation point value. The local (M = 2.5) electron density curve shown in Fig. 1 was estimated by drawing a line one order of magnitude lower than the stagnation value throughout the entire trajectory. It is seen that for appreciable portions of the trajectory the electron density at the stagnation point is lower than 10^{14} e/cm^3 while at a point where the local Mach number is 2.5 the electron density is below the maximum value measurable with the 3 cm wavelength internal cavity probe (10^{12} e/cm^3). The bulk of the time spent at conditions corresponding to electron densities (at the M = 2.5 station) less than 10^{12} e/cm^3 is seen, however, to be above an altitude of 200,000 ft. In the development program presented herein, the electron densities encountered at altitudes above 200,000 ft could only be duplicated at unit Reynolds

numbers higher than those actually experienced in flight.

The diffusion of charged particles toward the wall of the duct was estimated. This effect can, under the same conditions, result in a considerable reduction of the electron density in the region of plasma-microwave interaction as compared to the free stream condition.

A simple analysis has been performed assuming a uniform flow condition and a uniform electron density distribution along the axis of the duct. Consequently only the radial diffusion was considered.

The process was considered ambipolar and the differential equation is

$$D\left(\frac{d^2 n_e}{dr^2} + \frac{1}{r}\frac{dn_e}{dr}\right) = k_d\, n_N\, n_o \left(1 - \frac{n_e^2}{n_{e_o}^2}\right)$$

where D is the ambipolar diffusion coefficient, given by the expression

$$D = \frac{4\ kT}{m_i D_i}$$

k is the Boltzman constant

T the temperature

m_i mass of the ions

D_i the ion-neutral collision frequency

k_D is the forward reaction rate

n_N n_O are the equilibrium concentration of the species N and O

n_{e_o} is the electron density at equilibrium

The only reaction considered is

$$N + O \rightleftharpoons NO^+ + e^-$$

The condition of zero electron density at the wall of the duct has been imposed.

The computation was performed for an altitude of 200,000 ft and at two points along the trajectory, one at 1 1/2 minutes and the second at 11 minutes from reentry (Fig. 1); characterized by the temperature, 5900 °K and 4880 °K respectively.

The results are plotted in Fig. 2 together with the ideal case of zero diffusion. The integration of the radial electron density referred to the ideal case gives the reduction with respect to the free stream condition. These values are:

curve (2) .12

curve (3) .07

The axial velocity has not been considered in the computation. Since it is very large and the length of the duct is only of the order of one inch the effect of the velocity is to reduce the diffusion. The numerical computation requires the solution of a partial differential equation of the parabolic type and was not performed because of restriction in time and man-power.

The problem of developing an internal cavity type electron density probe to make measurements in a partially ionized supersonic air flow can be divided into three main aspects:

(a) Electromagnetic Development Program, dealing with the electromagnetic resonant cavity; the resolution, sensitivity and range of operation of the probe.

(b) Aerodynamic Test Program, considering the basic aerodynamic conditions to be simulated, selection of the point of operation, aerodynamic design of the probe, experimental facility, instrumentation, testing and analysis of the results.

(c) Calibration of the Probe. To perform this calibration the probe is located in a plasma flow,

similar in both electron density and Mach number to the one encountered during the reentry condition and the response of the probe is correlated to the values obtained with another standard electron density measuring device.

These separate aspects of the development program are discussed in the following sections of this report. These sections are then followed by the results of an investigation of other techniques for measuring electron density levels higher than those measurable with an internal cavity probe.

The authors wish to acknowledge the contributions of Drs. V. Zakkay and R. Cresci in the design of the aerodynamic experiments; of Messrs. A. Agnone and A. Martellucci, in carrying out the aerodynamic test program, to Dr. M. Naraghi for the electron beam phase of the probe development program, and to Mr. David Attwood for his assistance in the calibration of the instruments.

2. Electromagnetic Development Program

2.1 Introduction. - The principle of operation of the internal cavity probe is based on the interaction between the electromagnetic field of a resonant cavity and an underdense plasma. The resonant frequency of an electromagnetic cavity is known to depend on the dielectric constant of the medium within. For an underdense collisionless plasma, the equivalent dielectric constant is less than one and a function of the electron density. Therefore, when a plasma is introduced into the field of the cavity the change of its resonant frequency can be related to the electron density.

It is the purpose of this probe to provide such a cavity and to allow the plasma to flow through the interaction region without an appreciable change in its properties with respect to the undisturbed flow. A schematic representation of such a probe is given in Fig. 39.

A detailed description of the principle of operation of this instrument is given in Appendix I.

2.2 Characteristics of the Probe. - The characteristics of this probe have been derived using small perturbation

considerations (Appendix I). However, such an approach cannot be used to define the upper limit of measurable electron densities because the electric field is distorted and therefore the small perturbation approximation is no longer valid. It can be accepted that the probe can, near the upper limit of electron density, start to operate in a certain higher mode resembling a coaxial structure where the center conductor is the plasma flowing through the cavity. Here effects not important in the limiting small perturbation approach play all-important roles. In this case the plasma is a lossy conductor and the conduction of current between the plasma and the walls of the channel, apart from being not well defined, introduces additional losses, increasing with ω_p. The upper limit can be taken as $\omega_p = \omega_o$ and it cannot be moved upwards by increasing the operating frequency because of viscous aerodynamic choking of the flow in the internal passage when its dimensions are reduced to correspond to the decreased wavelength. On the basis of these considerations the maximum electron density that can be measured with an internal cavity probe is 10^{12} e/cm^3 the frequency of operation being 10 kmc (3 cm wavelength).

The resolution of an internal cavity probe can be defined as an increment of electron density producing a certain resonant frequency shift; it can be taken equal to half the bandwidth $\Delta f = \frac{f_o}{2Q}$ where f_o is the resonant frequency of the cavity. The measurement technique to be used may give a better or worse resolution than the one defined in this way, but as an order of magnitude and for comparative purposes this reference is very convenient.

The minimum measurable electron density is the one that produces the minimum detectable resonant frequency shift. If this shift is taken equal to the bandwidth, both resolution and minimum electron density have the same value.

The sensitivity of the probe is the ratio between relative resonant frequency shift and relative plasma frequency when the perturbation of the field is small.

$$k = \frac{\frac{\Delta\omega}{\omega_o}}{\left(\frac{\omega_p}{\omega_o}\right)^2}$$

2.3 Design Considerations - Aerodynamic considerations lead to the selection of the cone angle. The length,

diameter and divergence angle of the duct must be adopted as a compromise among electromagnetic, aerodynamic and plasma dynamic requirements: i.e it should be short and with a large diameter and divergence angle to minimize boundary layer and diffusion effects; on the other hand, it should be long with a small diameter to avoid radiation of electromagnetic energy. Lower electron densities can be measured by increasing the diameter of the duct; i.e. by having more plasma interacting with the microwave field, provided that the Q is not affected.

The maximum electron density that can be measured with the probe corresponds to a plasma frequency equal to the operating frequency. The first 10 cm wavelength (3 kmc/sec) probe has been designed, as shown in Fig. 3 taking into account the above mentioned considerations. The resonant cavity has been distorted in order to fit within the aerodynamic configuration.

The resonant frequency of this cavity geometry is very difficult to calculate, instead it has been estimated as a transition between a cylindrical and a reentrant coaxial cavity with an additional correction for the [illegible].

The difference between the estimated and measured resonant frequency was less than 10%. In order to have a well-limited plasma a piece of teflon covers the cavity gap providing a continuous surface for the aerodynamic flow. The construction of the cavity has been made in two pieces which were soft soldered together.

2.4 Electromagnetic Calibration. - To determine the resonant frequency shift as a function of the electron density two techniques have been used. The first technique used a dielectric rod to simulate the plasma and was based on the consideration that the frequency shift resulting from the insertion of a dielectric with a dielectric constant very close to one is equivalent (apart from a sign difference) to that caused by a weakly ionized plasma. A plastic foam was found to be a satisfactory dielectric substitute for the plasma. A cylindrical cavity operating in the same mode and frequency has been built to calibrate this reference material. Samples filling completely the interaction region of the probes have been prepared. The plasma frequency simulated with this material is $\left(\frac{\omega_p}{\omega_0}\right)^2 = \left|\epsilon_r - 1\right|$, where ϵ_r is the relative dielectric constant of the material.

(The same principle has been used to calibrate the two standard electron density measuring devices described later.)

The second technique employed an electron gun to create an electron cloud equivalent in density to that found in a weakly ionized plasma. Since, in the derivation of the dielectric constant of the plasma (Appendix I) the presence of the ions and the neutrals has been neglected, one can repeat the same derivation for an electron cloud and find identical results. This is the basis of the particular technique utilized here to calibrate the internal cavity probe. If the number of electrons present in the interaction region of the cavity is the same for a body of plasma and for an electron beam passing through the plasma, then one can expect the same shift in the resonance frequency of the cavity for the two conditions. Let n_e represent the number of electrons per unit length of the beam, n_{eq} the equivalent plasma electron density, and finally, ΔL and A the length and area of the interaction region respectively, then one can write,

$$n_e \Delta L = n_{eq} A \Delta L ,$$

hence

$$n_{eq} = \frac{n_e}{A} . \qquad (1)$$

Now if e is the electronic charge, u the velocity of the electrons, and I the current carried by the beam, we have the following relation

$$n_e \, e \, u = I , \qquad (2)$$

and if V is the accelerating voltage to the gun, and m the electronic mass,

$$\frac{1}{2} m \, u^2 = e \, V . \qquad (3)$$

By combining Eqs. (2) and (3) we obtain

$$n_e = \frac{I \, V^{-\frac{1}{2}}}{e\sqrt{\frac{2e}{m}}} . \qquad (4)$$

If we substitute the quantities for the electronic mass in Kg, and the electronic charge in Coulombs in this last relation, we have

$$n_e = 1.05(10)^{19} \frac{I}{V^{\frac{1}{2}}} . \qquad (5)$$

This last relation shows the independent variables which determine the operation of the beam so far as the electron density n_e is concerned are limited to the accelerating voltage and the beam current. In Eq. (5) n_e is the number of electrons per meter of beam length, I the beam current in amperes, and V the accelerating voltage in volts.

By combining Eqs. (5) and (1), and assuming a value of A = 2.3 cm^2, which is the cross sectional area of the central duct of the first model of the 10 cm wavelength probe, we obtain

$$n_{eq} = 4.56 \times 10^{10} \frac{I}{V^{\frac{1}{2}}} \; e/cm^3 \qquad (6)$$

In order to determine the characteristic of the gun to be used, it is more convenient to use a parameter called the "perveance" of the gun, which relates the parameters I and V due to space charge effects. The perveance of the beam, or gun, is defined as

$$P = \frac{I}{V^{3/2}} \; . \qquad (7)$$

By eliminating I between the last two equations we obtain the plasma electron density simulated as a function of perveance, and accelerating voltage of the gun, i.e.

$$n_{eq} = 4.56 \times 10^{10} \text{ PV e/cm}^3 \qquad (8)$$

This last relation shows that the simulated electron density is directly proportional to the perveance of the gun. However, the perveance cannot be chosen too large, because it will result in a larger diameter of the beam and a significant number of electrons being collected on the walls of the central channel of the cavity.

The particular electron gun used here to generate an electron density of 10^8 e/cm^3, has a perveance of 1.6×10^{-6}, and a beam diameter of 3.7 mm (which is small compared to the diameter of the central channel of the cavity). The operating voltage of the gun is of the order of one KV. For short intervals, which are sufficiently long for microwave measurements, higher accelerating voltages may be used. For instance, for an accelerating voltage of about 1500 volts, the equivalent electron density can be found from relation (8) to be

$$n_{eq} = 1.1 \times 10^8 \text{ e/cm}^3$$

The gun used to generate the above test condition for the first 10 cm wavelength cavity was a Pierce type. The cathode of the gun is made of impregnated tungsten due

to its high emission properties. The gun is enclosed in a magnetically shielded housing which is connected by means of flanges to a chamber which contains the cavity as shown in Fig. 4.

An axial magnetic field was used to confine and collimate the beam to a uniform diameter. The value of this field on the axis of the beam was approximately 120 Gauss for a distance of about 7 cm. A water-cooled collector (target) was used to collect the current corresponding to the beam crossing the central channel of the cavity. The collector is insulated from the cavity as shown in Fig. 4. This insulation served to measure the current collected by the target independent of the current diffused to the walls due to runaway electrons.

The cavity used in the electron beam calibration was made of oxygen-free high conductivity copper in two parts which were brazed together. The inner dimensions of the cavity are identical to those of the first 10 cm wavelength probe shown in Fig. 3. A pick-up loop, as shown in Fig. 4 connects the cavity through a 50 ohm coaxial line to a BNC connector hermetically sealed at the collector flange.

A vacuum system consisting of a forepump, a two-inch oil diffusion pump, and a liquid nitrogen baffle was used. The pressure was measured with a cold cathode ionization gauge station provided on the line close to the chamber. The ultimate pressure obtained was 2×10^{-7} torr. The electron gun assembly, and the vacuum system are shown in Figs. 5 and 6.

Use of this technique required two sets of measurements to be made. The first involved the determination of the characteristics of the beam from which the equivalent plasma electron density could be calculated. The second set of measurements was made to determine the shift in the resonant frequency of the cavity produced by the electron beam passing through the duct of the cavity.

The schematic diagram of the set-up used to perform the above measurements is shown in Fig. 7. The current interacting with the electromagnetic field consists of two parts; one going to the collector and one diffusing toward the walls of the channel after passing through the interaction region. The second current was measured by replacing the channel of the cavity with electrodes, and found to be negligible. As a result the collector current gives an

accurate representation of the electron flux through the interaction region of the electromagnetic field of the cavity.

The current voltage characteristics of the electron gun are shown in Fig. 8. The total current and the collected current are closely related to the values obtained from the perveance (Ip) specified by the manufacturer of the electron gun. Nevertheless, the current used in obtaining n_{eq} is the measured value of the collector current which is slightly smaller than the specified values.

The maximum electron density that can be generated with the electron gun is slightly more than 10^8 e/cm^3. The fact that the current flowing in the interaction region does not affect the Q of the cavity allows the measurement of electron densities as low as 10^7 e/cm^3, one order of magnitude below the nominal resolution of the probe. The results of this experimental calibration with the electron gun are shown in Fig 9. The point values shown are the results of the electron beam calibration. The line represents the calibration performed with the dielectric rod technique described above. The resonant frequency shift is linearly related to the electron density so that the slope

is 45 degrees. The format used to locate the line was experimentally determined with a plastic foam with a dielectric constant of $\epsilon_r = 1.0336$ corresponding to an electron density of 4.37×10^9 e/cm^3 and a resonant frequency shift of 8.8 Mc. This point is not shown in Fig. 9 because it is out of scale.

The agreement of the two procedures justified the use of only the dielectric rod technique to obtain subsequent calibration charts for the final models of the probes.

2.5 Final Design of the Probes. - The first model of the 10 cm wavelength probe was designed on the basis of a first estimation of its characteristics. The Q of the cavity without plasma, Q_o, was lower than expected by a factor of three and a perturbation analysis can be performed to determine the effect of this reduction of Q upon the range of electron densities covered with this instrument.

If a uniform plasma is assumed the resonant frequency shift is

$$\frac{\Delta \omega}{\omega_o} \sim \frac{1}{2} \frac{n_e}{n_c} \frac{\int_{V_p} E^2 dV}{\int_V E^2 dV} \cdot \frac{1}{1 - \frac{\nu^2}{\omega_o^2}} \qquad (1)$$

where E is the electric field intensity in the cavity without plasma; V_p is the plasma volume and V the cavity volume.

Equation (1) can be written

$$\frac{\Delta\omega}{\omega_o} \sim k \frac{n_e}{n_c} \qquad \text{where} \qquad k = \frac{1}{2} \frac{1}{1+\frac{\nu^2}{\omega_o^2}} \int_{V_p} E^2 dV \Big/ \int_V E^2 dV \qquad (2)$$

is defined as the sensitivity of the instrument.

The change of the Q of the cavity is

$$\Delta\left(\frac{1}{Q}\right) = \frac{1}{Q} - \frac{1}{Q_c} \sim \frac{n_e}{n_c} \frac{\nu}{\omega_o} \frac{1}{1-\frac{\nu^2}{\omega_o^2}} \int_{V_p} E^2 dV \Big/ \int_V E^2 dV \qquad (3)$$

The value of Q_o is determined by the losses in the walls of the cavity, in the dielectric window and the radiation losses at the opening of the duct.

The minimum electron density which can be detected, $n_{e_{min}}$, correspond to an ideal situation where $\frac{\nu}{\omega_o} \ll 1$ and is given by $\frac{n_{e_{min}}}{n_c} \sim \frac{1}{k_o} \frac{(\Delta\omega)_{min}}{\omega_o} \sim \frac{1}{2k_oQ_o}$ where k_o is the sensitivity corresponding to $\nu = 0$. Thus in order to minimize the value of $n_{e_{min}}$ it is necessary to have the product k_oQ_o as large as possible. According to Eq (2) the value of k_o can be increased by enlarging the diameter of the duct. This may reduce the Q A compromise solution should be taken to get the desired minimum measurable electron density.

Two possible modes of operation of the electromagnetic cavity have been considered for the probes, transmission and reaction.

In the former, the input and output of the cavity are independent, connected only by a resonant condition in the cavity, while out of resonance there is no output.

In the latter there is only one magnetic coupling loop, with the cavity acting as a terminating impedance of the line. A change of this impedance is indicative of a resonant condition and it appears as a shift of the standing wave pattern. This reaction mode was used with the first 10 cm wavelength probe because the obtainable Q is higher than with the transmission mode. However, the measured Q was lower than expected and additional losses were anticipated with the introduction of the plasma. For these reasons the transmission mode was adopted for the final models of the probes.

In order to provide a margin of safety against detachment of the external shock from the leading edge at the zero and nonzero angle of attack, as well as to allow the probe to operate at a Mach number as low as two, the half angle of the cone was reduced from 25 to 20 degrees.

A second probe operating with a 10 cm wavelength was designed and built incorporating the experience gained from the first model. It is shown in Fig. 10. The duct diameter was increased from .5 to .7 inches.

A third probe, operating with a 3 cm wavelength (10 kmc), has also been built as shown in Fig. 11. The same consideration made before for the cone angle and divergence of the channel apply here. The range of operation of this probe is 10^9 to 10^{12} e/cm^3. The resonant frequency shift obtained using the dielectric rod technique is shown as a function of electron density for the three probes in Fig. 12. The material used to produce the perturbation of the electromagnetic field has a relative dielectric constant $\epsilon_r = 1.0336$ corresponding to a value of $n_e/n_c = .0336$. The three experimentally determined calibration points are given. The minimum detectable frequency shift has been taken equal to $\Delta f = f_o/2Q_o$, and the maximum measurable electron density corresponds to a microwave frequency equal to the plasma frequency.

The principal characteristics of the three probes are listed in the following table:

Name of Probe	Minimum Detectable Electron Density (e/cm^3)	Critical Electron Density (e/cm^3)	Resonant Frequency (mc/sec)	Quality Factor (Q)	Sensitivity $k = \frac{\frac{\Delta f}{f_o}}{\frac{n_e}{n_c}}$
10 cm Probe (1st Model)	4.1×10^{6}	1.3×10^{11}	3200	3400	.042
10 cm Probe (2nd Model)	7×10^{7}	5.4×10^{12}	2080	3200	.118
3 cm Probe	8.5×10^{8}	9.0×10^{11}	8684	2000	270

3. Aerodynamic Development Program

3.1 Introduction. - In order to obtain accurate electron density measurements the internal cavity probe design requires that a streamtube of supersonic flow be introduced undisturbed, into a small diameter duct with a length of about five (5) entrance diameters. The boundary layer thickness at the duct exit may under some conditions, be comparable to the duct radius. The fluid in the duct could under these conditions, decelerate supersonically and may even choke causing a normal shock to stand in front of the probe entrance.

The presence of the shock will influence the static temperature and pressure of the flow within the duct. This in turn will influence the electron density measurement. In order to obtain a flow of fluid through the tube at the free stream temperature and pressure, it is necessary to compensate for the "effective" reduction in streamtube area due to frictional effects. This is accomplished by increasing the tube diameter in the downstream direction.

In view of the lack of an adequate theory to describe the flow field in the entrance region of a tube, and in the absence of experimental data at the low Reynolds numbers of interest, an experimental aerodynamics program was found necessary in order to determine if the duct entrance streamtube is captured and if the flow field within the duct is free of significant disturbances.

In order to establish a set of design flow conditions which would be representative of those which might be encountered in the local flow field about the Apollo vehicle, use was made of the pressure distribution data contained in NASA TM-X-705. The data presented therein for the nose shape with an edge radius of 5 percent D (D is the overall body

diameter) were used. These data indicated that the flow external to the boundary layer reached a Mach number of 2.5 in a region between S/D ≅ 0 and S/D = 0.125 [S is the distance measured from the juncture of the nose section with the afterbody (see TM-X-705)], for angles of attack of 0 to 25°, in both the leeward and windward flow regions in the pitch plane. Since no data were presented for S/D values between -0.06 and +0.11, it is difficult to define precisely where the local Mach number reaches a value of 2.5.

Since the local flow Mach numbers in this vicinity will remain essentially constant throughout the hypersonic flight regime, this region just outside the boundary layer (and also just ahead of the indicated separated flow region over the afterbody), appeared to be a suitable location for the probe. Accordingly, the design Mach number of the probe was selected as 2.5. This value of the Mach number essentially fixed the maximum value of the cone angle of the external surface of the probe, Fig. 3. The value of the cone half angle selected initially was 25°. This value was used in the design of the early models of the 10 cm wavelength probe. Later in the program and for the final probe

designs, the value of the cone half angle was reduced to a value of 20° (corresponding to a critical Mach number equal to two) to provide for operation of the probe at angles of attack with respect to the local flow direction ahead of the probe.

3 2 Estimated Flight Local Flow Conditions. - The conditions required to be simulated then are those encountered in the local flow field surrounding the Apollo vehicle aft of the heat shield where the local Mach number is 2.5 over the altitude range extending from 350,000 ft to 150,000 ft. These flight conditions lead to the following estimated local conditions:

Altitude kft	Reynolds Number/ft	Mean Free Path (mm)	Length of Slip Flow Region (mm)
350	2.3	445	4200
300	38.8	26.0	245
250	543	1.88	17.5
200	4,269	0.24	2.23
150	14,050	0.07	0 68

The length of slip flow is based on criteria given in Ref. 1.

These local flow conditions were determined by considering the flow to be in thermochemical equilibrium at the stagnation region followed by an equilibrium isentropic expansion to a point in the local flow field where the local Mach number is 2.5. In the absence of specific trajectory information, the following flight conditions were assumed for the purpose of making these calculations:

h, kft	V, fps
350	37,150
300	37,100
250	36,800
200	29,700
150	9,950

These conditions were later found to correspond closely with the initial trajectory conditions (in the altitude range between 350 kft to 200 kft), later supplied to us for a 3000 nm reentry range trajectory with an initial flight path angle of -6.4°, and with the 150 kft conditions during final descent on the same trajectory.

The blowdown wind tunnel test facilities available at GASL can simulate the conditions existing in the local

flow field for the 150,000 ft case. It was not found possible to simulate the local flow conditions above this altitude because of the limited vacuum levels available in a vacuum sphere and because of the low local Mach numbers involved. The particular conditions of very low Reynolds numbers and low supersonic Mach numbers required for the simulation of higher altitude cases represent unusual test conditions for which it is difficult to find facilities with the necessary characteristics. The only facility found which might be adequate is the low density tunnel at the University of California, Berkeley. However, it is seen from examination of the above table, that above 200,000 ft continuum considerations no longer apply because of the length of the ambient mean free path and the small probe dimensions (5 mm internal probe diameter). It is therefore not believed necessary to carry out aerodynamic tests of the probe for conditions corresponding to 250,000 ft and above. The flow conditions corresponding to the altitudes in the vicinity of 200,000 ft, however, represent a flow range where tests are desirable but cannot be achieved with the existing GASL blowdown test facilities.

Calculations were made which indicated that when a normal shock is caused to stand at the entrance of the internal passage of the probe, the electron densities indicated by the probe can be in error by about two orders of magnitude. Such discrepancies could therefore be used as an indication of faulty aerodynamic performance (choked passage) during the shock tube calibration tests.

The calculated performance of our high driver pressure shock tube facility indicated that it would be possible to achieve the proper Reynolds number and Mach number conditions corresponding to the 200,000 ft altitude case in this facility. The estimated electron density level available in the shock tube would not, however, correspond to the level anticipated in the local flow field in the flight situation. However, it was thought that using the above considerations, one could determine whether or not a normal shock is caused to stand ahead of the probe due to internal viscous choking by comparing the indicated electron density level with the level calculated to be generated by the shock tube facility. Accordingly several snock tube tests were made in an attempt to achieve the proper test

conditions. Difficulties associated with the improper response of triggering circuits due to the low pressures involved prevented the collection of meaningful data. Time and funds did not allow the development of new instrumentation for operation at the low pressure levels required. Consequently no experimental proof could be furnished for the performance of the probes at altitudes above 150,000 ft.

The remainder of this section, then is devoted to a description of the tests conducted in the GASL blowdown wind tunnel facilities and the results obtained.

3.3 Aerodynamic Tests

3.3.1 Previous Investigations - The problem of flow through a tube has been investigated at higher Reynolds numbers, both theoretically and experimentally, by other authors. Shapiro (Ref. 2) presents the solution for flow in a constant area duct with friction. Toong and Kay (Ref. 3) investigated the viscous flow problem associated with the entrance region of a tube. For given free stream conditions, Shapiro presents a working formula which predicts the maximum tube length required to choke the flow (i.e. to decelerate the flow to sonic conditions), with the

skin friction as an input to the problem. Toong and Kay present a method for evaluating the local friction coefficient, which can then be used as an input to Shapiro's formula for determining the maximum tube length. Although the flow conditions of the present investigation are outside of the range of applicability of the theory of Toong and Kay, the method was applied to the present problem to obtain a rough estimate of the behavior which might be expected. The method predicts that choking would occur at approximately nine-tenths of the duct length.

Recently Collins (Ref. 4) experimentally investigated the problem of diffuser performance at low density in supersonic flow. The flow conditions were similar to the present investigation and his primary purpose was to determine if the bow shock would be swallowed under the ambient low Reynolds number conditions. Although the internal geometry of a diffuser is different from the probe internal geometry, the general conclusions reached by Collins may be extended to the present case. That is, the bow shock can be swallowed, in spite of the diffuser's initial contraction and the rapid boundary layer growth.

The unit Reynolds number of the GASL tests were slightly smaller than those of Collins and the probe internal duct dimensions were considerably smaller.

3.3 2 Experimental Apparatus

3.3.2.1 Facility. - The tests were conducted in the GASL Pebble Bed Heater facility. This facility (Fig. 13) consists of a pebble bed heater and a Mach 6 conical nozzle which is connected to a forty (40) foot diameter vacuum sphere. A Mach 2.5 contoured nozzle is mounted in the test section of the Mach 6 nozzle and provides the test conditions for the electron density probe.

The mode of operation of the facility is to expand the heated air (T_o = 1400° R) at the plenum chamber pressure ($15 < P_{p.c.} < 22$ psia) by means of the Mach 6 nozzle to a low static pressure (P ~ 50 μ). Then, it is shocked down to a low stagnation pressure (P_T ~ 1 to 1.4 psia) at the entrance of the Mach 2.5 nozzle while keeping the flow supersonic around and at the exhaust of the nozzle, (Fig. 14). In this way, a Mach 2.5 flow could be obtained in the contoured nozzle with low stagnation pressure and hence, low Reynolds numbers. This technique has been used

successfully by other experiments (see Ref. 5) and allows low density tests to be performed in relatively high pressure facilities.

3.3.2.2 Model. - The electron density probe geometry used in the aerodynamic tests and pressure tap locations are shown in Fig. 15. The duct entrance diameter was 0.2 inches and the length was five entrance diameters. The internal diameter in later designs was increased as a result of preliminary developments. The results obtained for this smaller internal diameter are conservative when the larger diameter internal duct is considered. The duct was expanded with a half angle of 2°30', to compensate for boundary layer growth. The expansion was determined from calculations of the boundary layer displacement thickness, which would be obtained over a flat plate of a length equal to the duct length and subjected to conditions similar to those experienced by the probe. This criterion was used in the design on the basis of the findings of Ref. 3.

The leading edge of the probe was made sharp ($R \approx .0005$ in.). The 25° semi-vertex angle of the external cone was chosen in accordance with the previous

discussions. As mentioned there, the final probe designs incorporated a 20° semi-vertex angle for the external cone shape. However, the results presented herein for the 25° semi-vertex angle apply equally well to the 20° semi-vertex angle geometry since the lip shock apparently remained attached throughout the tests and the internal passages were the same in all cases. The duct was machined to a polished surface. Three static pressure taps were located at various axial locations. These ports were placed at different azimuthal planes so as to avoid their mutual interference due to the restricted space available. The pitot tube was located at the exit plane.

3.3.2.3 Instrumentation - Total pressures were measured by means of Statham pressure transducers, which were calibrated prior to the test program and zeroed at the beginning of each test. The transducer output was continuously recorded on a Visicorder Oscillograph recorder. The flow total temperatures were sensed by means of chromel-alumel thermocouples and their outputs were also recorded on the oscillograph recorder.

The static pressures were measured by means of Hastings-Raydist heated thermopile vacuum gauges. Because of the logarithmic output of the gauges, they were carefully calibrated periodically during the test program. A typical calibration curve is shown in Fig. 16.

3.3.3 Discussion of Experimental Results. - To insure that the Mach 2.5 nozzle had started and that a plane normal shock existed at the entrance of the nozzle, a pitot pressure survey was made in the test section of the nozzle. The results are shown in Fig. 17. The Mach number was determined both from the measured pitot pressure in the test section (P_{T_2}) and the measured total pressure (P_{T_1}) at the entrance of the Mach 2.5 nozzle, and from the pitot pressure (P_{T_2}) and the nozzle wall static pressure (P_∞). The two methods agreed to within 7%. It can be seen that a uniform core of approximately two (2) inches exists in the test section. For comparison, the probe inlet diameter is also shown in the figure.

Steady flow was found to exist for approximately six seconds, during which time the data was obtained. At later times, the Mach 6 flow separated from the nozzle

walls and the tunnel unstarted. The minimum Reynolds number which was obtained before separation occurred was approximately 40,000 per ft. This unit Reynolds number is higher than that required for complete simulation of the 150,000 ft case. However, the unit Reynolds number is believed close enough so that the results obtained are indicative of the aerodynamic behavior of the final probe designs at local flow conditions encountered at an altitude of 150,000 ft (Ref. 6).

The static pressure distribution along the probe internal duct for various free-stream Reynolds numbers, nondimensionalized with respect to the static pressure on the wall of the nozzle, is shown in Fig. 18. These data were obtained without the presence of the pitot tube at the exit of the duct. It is seen that the pressures are within 30% of the free-stream value. With the probe at zero angle of attack, the pitot tube was located at the center of and normal to the exit plane of the duct. The pitot pressure measured at this point is shown plotted in Fig. 19. Also shown is the static pressure along the duct when the pitot tube is in place. The disturbing influence

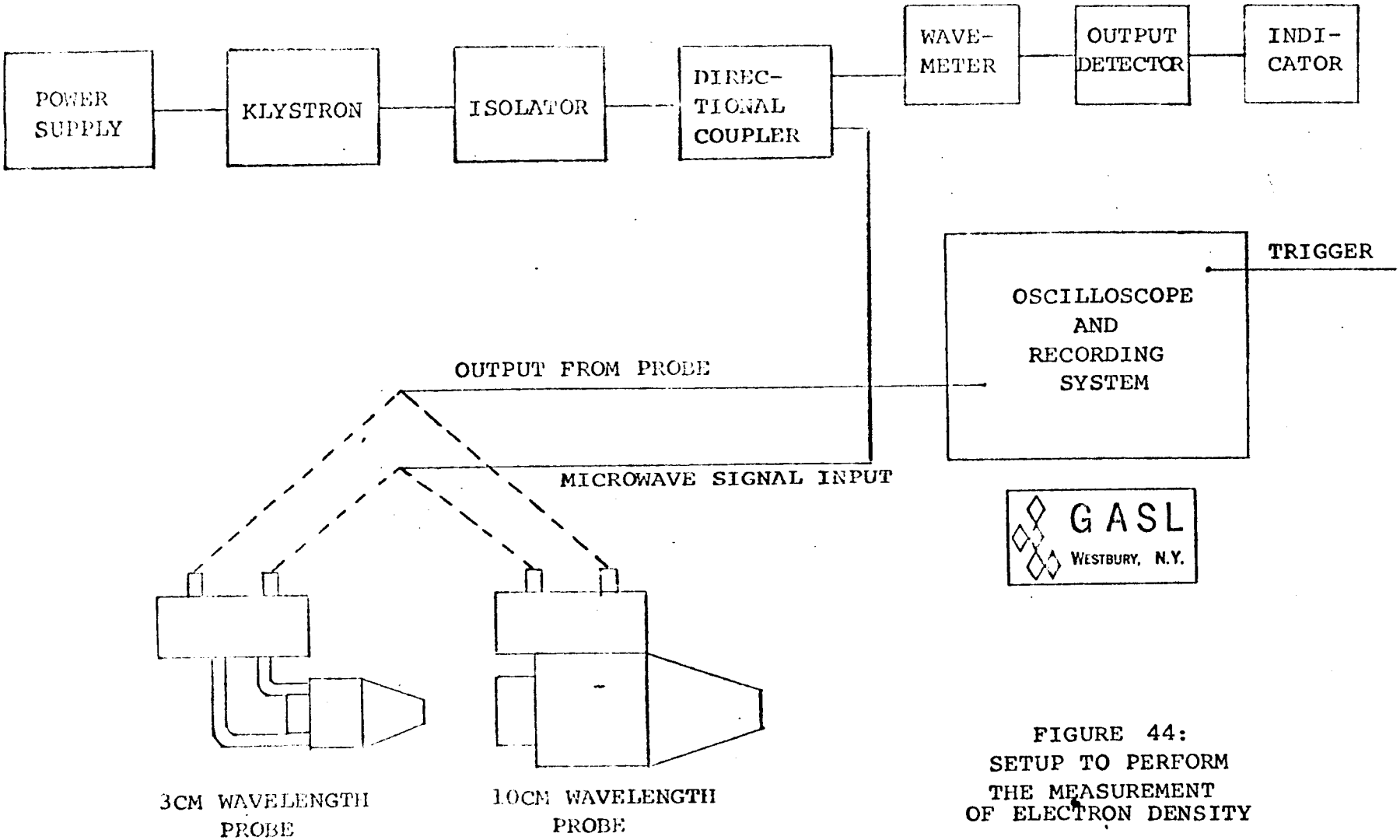

FIGURE 44:
SETUP TO PERFORM
THE MEASUREMENT
OF ELECTRON DENSITY

of the pitot tube on the wall static pressure is readily evident when compared to those of the probe-free duct..

The static pressure in the duct with the probe at a 5° angle of attack is shown in Fig. 20. The probe was at a negative angle of attack ($\alpha = -5°$), and the pressure taps are on the expansion side of the duct. The static pressure is seen to drop initially and then increase to the free-stream value. The initial drop is due to the expansion from the upper edge of the lip of the duct, and the subsequent rise is due to the impingement of the attenuated shock (emanating from the lower lip).

3.3.4 Conclusions of the Aerodynamic Tests. - The static pressure measurements in the duct indicate that:

1) The flow in the duct was supersonic without the presence of normal shock, either at the lip or in the duct. The existence of a normal shock would cause the average static pressure to be several times higher than the free stream static pressure.

2) The flow in the duct is accelerating, which implies that the passage is slightly over-expanded for the Reynolds numbers of the test.

3) The static pressure in the probe remains nominally at the free-stream value with the probe at a 5° angle of attack.

4. Calibration of the Probes

4.1 Introduction. - The probe considered here is a self-calibrating device in that the resonant frequency shift it experiences corresponds to the electron density existing within the interaction region. This, however, may differ from that found in the free stream due to the disturbances caused by the probe. To determine this difference in the properties of the plasma, simultaneous measurements of electron density are made in a shock tube with the probe and with a standard, nondisturbing technique consisting of a 1 cm wavelength interferometer and a 30 cm wavelength resonant cavity located just upstream of the testing area.

The probe is mounted inside the shock tube in a chamber designed so as to pick up the plasma without affecting its properties.

4.2 Shock Tube Facility. - The GASL low pressure shock tube was used to carry out the calibration of the probe. Its operational capabilities, important to the probe calibration, are presented in Fig. 21. Details of the shock tube design can be found in Ref. 7. The driven section is 50' long and has a 3" internal diameter. The driver and diaphragm section of the conventional shock tube configuration are replaced by a pressure chamber with a volume equivalent to a conventional driver section and a quick-acting mechanical valve. The velocity of the shock wave is measured with heat transfer gauges located along the tube; the output from these detectors can be connected to an oscilloscope or, for higher accuracy, to a counter. It operates with hot hydrogen (500°K) with driver pressures of the order of 400 psi.

4.3 Technique to Perform the Measurement. - The technique used to detect the plasma microwave interaction in

the probe is based on the fact that the resonant frequency of the cavity increases with the plasma electron density, as shown in the calibration chart of Fig. 12. The microwave setup is such that there is output from the detector only when the resonant condition is achieved. Plasmas with electron densities either below or above that corresponding to resonance allow no output. The procedure used is as follows. The microwave generator is present at a certain frequency $f_o + \Delta f$. f_o being the resonant frequency when no plasma is present. According to the calibration chart, this Δf should correspond to a certain electron density n_e, and only this particular electron density will give an output in the detector.

It should be noted that the plasma obtained in the shock tube depends on two parameters, initial driven pressure and incident shock wave velocity, as shown in Fig. 21. The plasma column so produced moves down the shock tube with a certain electron density profile along the axis of the tube, or as a function of time for a detector such as the probe. Except for a small region near the wall, the electron density can be taken as a constant across the cross section of the shock tube.

The electron density profile along the time axis starts from zero before the shock front, increases to a maximum, and then decays. For a small Δf the resonant condition is found once in the buildup of the plasma profile and once in the decay. If the value of Δf corresponds to an electron density not obtained during the test no resonance is achieved.

The repeatibility of the low pressure shock tube number three is good enough to obtain the same plasma conditions for successive shots while changing the frequency of the microwave generator. The information so obtained in a series of runs makes it possible to follow the electron density profile for the conditions maintained.

This technique is illustrated in Fig. 22. On the left side is a hypothetical electron density profile, where the electron density is shown as a function of the distance d behind the shock front, or as a function of time, t, for a stationary object. The vertical scale represents either electron density or the equivalent resonant frequency obtained from the calibration chart. On the right side of the figure is the output of the microwave detector, as seen on the oscilloscopes as a function of time. The distance

between the two peaks corresponds to the time elapsing between the two resonant conditions for the given value of microwave frequency. By increasing the frequency the two peaks indicating resonance move closer together until for the maximum electron density they coalesce into one. With an additional frequency increase the output of the detector goes rapidly to zero because no resonance is achieved.

4.4 Independent Measurements - Interferometer and 30 cm Resonant Cavity. - The final check of the probe was performed by simultaneously measuring the electron density in the undisturbed flow with an independent system and with the probe as explained above. The scheme adopted to independently measure the electron density is also based on plasma-microwave interactions. The range from 10^{8} to 10^{10} e/cm^{3} was planned to be covered with a resonant cylindrical cavity located coaxially with the shock tube It operates in the TM-010 mode with a 30 cm wavelength. The plasma flows through the center of the cavity interacting with the electric field. The range from 10^{10} to 10^{11} e/cm^{3} was checked independently with an interferometer operating with a 1 cm wavelength.

In the former device (30 cm wavelength cavity) the refractive index of the plasma is taken as $\varkappa = 1 - \delta$, where δ is a complex quantity such that

$$|\delta| \ll 1$$

The angular resonant frequency of the cavity will change from ω_o (corresponding to $\delta = 0$) to

$$\omega = \omega_o + \Delta\omega$$

In general one will have $\frac{\Delta\omega}{\omega_o} \ll 1$. The relative increment of resonant frequency can be calculated (Appendix I) and shown to be

$$\frac{\Delta\omega}{\omega_o} = 3.71 \left(\frac{r_1}{r_2}\right)^2 \left[J_o^2 \left(2.4 \frac{r_1}{r_2}\right) + J_1^2 \left(2.4 \frac{r_1}{r_2}\right)\right] \delta$$

where r_2 is the radius of the cavity and r_1 is the radius of the plasma within the cavity. This gives the change of resonant frequency due to the plasma, assuming the plasma represents a small perturbation of the empty cylindrical cavity. In order to detect a change of the resonant frequency of the cavity the imaginary part of $\frac{\Delta\omega}{\omega_o}$, responsible for the reduction of the Q, should be smaller than the real

part which corresponds to the actual frequency shift Otherwise the effect of the plasma would be primarily a broadening of the resonance curve of the cavity. This condition can be taken as

$$\nu \ll \omega_o$$

where ν is the electron collision frequency. Since the condition $|\delta| \ll 1$ requires that $\omega_p \ll \omega_o$ the upper limit of operation of the cavity must be taken as $\omega_p = \omega_o$ which for the 30 cm calibrating cavity corresponds to an electron density of 10^{10} e/cm^3.

The second technique used to measure electron densities from 10^{10} to 10^{-} e/cm^3, was an interferometer operating with a 1 cm wavelength. Basically an electromagnetic plane wave is sent across the plasma and the changes in amplitude and phase of the transmitted signal are measured and related to the electron density and collision frequency. Let us consider a plane electromagnetic wave propagating across a plasma slab of thickness x_o. Due to the small transversal dimensions of the electromagnetic beam one can assume a uniform plasma distribution perpendicular to the microwave beam axes. The plasma frequency

is considered lower than the microwave frequency.

In this case the plasma introduces a phase shift

$$\Delta \Phi = \frac{\pi}{\lambda n_o} \frac{1}{1+\frac{\nu^2}{\omega^2}} \int_o^{x_o} n \, dx$$

where λ is the wavelength in a vacuum and n_o is given by

$$n_o = \frac{\epsilon_o m_e \omega^2}{e^2}$$

where ω is the angular frequency, ϵ_o the permittivity of a vacuum, and where e and m are the electron charge and mass respectively. At the same time the amplitude of the electromagnetic wave is attenuated by a factor of $e^{-\gamma}$ where

$$\gamma = \frac{\pi}{\lambda n_o} \frac{\frac{\nu}{\omega}}{1+\frac{\nu^2}{\omega^2}} \int_o^{x_o} n \, dx$$

A direct measurement of $\Delta \Phi$ and γ provides the values of ν and the integrated value of n along the path of the microwave beam.

Since one does not expect variations of electron density over the cross section of the plasma column, except

for a small region near the walls of the tube, the interferometer technique should provide accurate information. The limitation of such a device for this particular investigation is that for small electron densities (less than 10^{10} e/cm^3) the phase shift due to the plasma is too small to be detected hence the requirement of another technique capable of operating at a lower frequency. The circuit of the one centimeter wavelength microwave interferometer is shown in Fig. 23 and construction details in Fig. 24.

The signal generated in a klystron is fed through a flexible waveguide to avoid the effect of mechanical vibrations, and through an attenuator in order to eliminate reflected signals. A cavity wave meter is inserted at this point whenever the frequency of operation of the klystron has to be checked. A directional coupler sends a reference signal to the two detectors. The main signal goes through a calibrated variable attenuator and a calibrated variable phase shifter to the transmitting horn antenna located against the pyrex tubing confining the plasma to be measured. A receiving antenna collects the signal that goes across the interaction region and delivers it to the two

detectors whose outputs are the combination of reference and transmitted signal. The horns are matched to the glass window and the effect of the plasma, being underdense, is a change in amplitude and phase of the transmitted signal, the reflections being negligible.

The detectors are located in the two arms of a magic tee. As a result, their outputs are 90° out of phase. When no plasma is present the calibrated variable attenuator is set so as to make the transmitted signal equal in amplitude to the reference signal. With the response of the detectors made equal, the phase shifter is adjusted so as to have zero output in the difference circuit. The summing circuit adds both outputs. This circuit is particularly convenient for measuring small phase shifts, the response being close to linear for the phase shift obtained from the differential circuit. The attenuation of the signal is obtained from the summing circuit. The measurement is performed by recording the sum and difference of the detector outputs in an oscilloscope. The values obtained during the tests are then reproduced on the oscilloscope by adjusting the phase shifter and attenuator. In this way the effect

of the plasma upon the transmitted signal can be determined and from this the properties of the plasma may be found. In general, the absorption was found to be very small for the conditions of operation of the shock tube, thus simplifying the measurement

The resonant cavity and the horn antennas of the interferometer are mounted in the shock tube inside a high pressure chamber designed to support the equipment as shown in Figs 24, 25 and 26. The plasma container in the region of interaction of the cavity and interferometer is a section of pyrex tubing made with the same internal diameter as the shock tube so as to avoid perturbation of the flow. Both the interferometer and the 30 cm wavelength cavity have been calibrated with a known perturbation produced by using a plastic foam and following the same technique already described for the probes The resulting calibration charts are shown in Figs. 27 and 28. However the plasma generated in the shock tube had a collision frequency of the same order of magnitude as the frequency of operation of the 30 cm wavelength cavity. This resulted in a low output and a tendency to indicate lower electron

densities than actually existed.

Rather than compute the resonant frequency shift for a lossy plasma and use the cavity at an off-design condition, it was decided to calibrate the 10 cm wavelength probe in the range of 10^8 to 10^{10} e/cm^3 with the shock tube calibration chart which is known to be accurate within a factor of two for this range.

4.5 Experimental Setup. - The experimental setup is shown in Fig. 29. It provides for the measurement and recording of the following quantities:

a) Shock wave velocity

b) Electron density as determined with standard measuring devices

c) Probe output

d) Shock wave pressure profile

The probe is mounted in a chamber immediately after the interferometer and pressure pickup. The shock wave velocity is obtained by measuring the time interval between two pulses generated by the shock wave when it travels a known distance. These pulses are obtained from heat transfer gauges flush-mounted in the inner wall of the shock tube.

The level of these pulses is raised to 40 volts and shaped so as to have constant output for a wide range of operating conditions

The first trigger starts a counter and the second one stops it. Two dual beam oscilloscopes were used; the sweeps started with the second trigger and the traces used record the sum and difference of the signals from the interferometer detectors, the response of the 30 cm wavelength resonant cavity and the response of the probe. This technique is repeated several times in the shock tube for identical flow conditions until the electron density has been determined by varying the operating frequencies of the probe and the 30 cm wavelength cavity as described previously. The shock wave pressure profile is recorded to check the repeatibility of the aerodynamic conditions. The test results are shown in Figs 33 and 34 for the 10 and 3 cm wavelength probes, respectively.

Two typical sets of pictures are presented in Figs. 30 and 31 one for the 10 cm wavelength probe and the other for the 3 cm wavelength probe.

In each case the three pictures have been selected in the neighborhood of the preset frequency corresponding to the peak electron density. In the set of pictures corresponding to the 10 cm wavelength probe a pressure trace used to measure the shock velocity is shown, while the 3 cm wavelength probe pictures show the trace of the interferometer.

The total set of pictures is as follows:

10 cm Wavelength Probe

Picture	Δ f (Mcs)
1	6 (shown)
2	8 (not shown)
3	9 (shown)
4	10 (shown)
5	14 (not shown)
6	22 (not shown)

3 cm Wavelength Probe

Picture	Δ f (Mcs)
1	35 (shown)
2	64 (shown)
3	97 (shown)
4	138 (not shown)

A typical trace of the 1 cm interferometer is shown

in Fig. 32 along with the corresponding 3 cm probe output for a specified preset frequency

According to the adopted definition of resolution there is an indetermination associated with each measurement of frequency due to the finite Q of the cavity. The corresponding frequency bandwidth for the particular measurement is expressed as a spreading of electron densities as shown in Figs. 33 and 34.

To determine the resolution of the probes for the conditions under which they have been calibrated the operating Q was measured using the traces obtained during the calibration and considering the amplitude of the resonance peaks. Figs.35 and 36 show the general trend of the Q decay and the corresponding change in bandwidth as a function of the electron density for the particular conditions under which these tests have been performed.

These values of Q are lower than the ones computed by using in Eq. (3) the values of ν given by the properties of the flow. In other words the apparent value of ν is larger than the value predicted by the performance chart of the shock tube, indicating that additional mechanisms of energy losses are present. In particular the plasma sheath, the thin region close to the walls of the duct where the elementary plasma model is not valid may introduce the detected absorption of energy.

5. Investigation of Techniques to Measure Higher Electron Densities. - As explained before, the upper limit of operation of the internal cavity probe cannot be extended above 10^{12} e/cm^3 because of the viscous aerodynamic choking of the flow in the channel when its dimensions are reduced to correspond to the decreased wavelength. Therefore two other possible principles of operation have been studied in order to determine the possibility of measuring higher electron densities with probe devices. These are discussed in the following paragraphs.

5.1 External Cavity Probe. - The principle of operation of this instrument is based on the penetration characteristics of an electromagnetic wave in an overdense plasma. A partially open resonant cavity is surrounded by an overdense plasma; the resonant frequency of this structure is a function of the penetration of the field inside the plasma which in turn is related to the electron density. Consequently, a correlation between resonant frequency and electron density can be established. A description of the principle of operation is given in Appendix II. It is shown there that this principle can be used to cover three

orders of magnitude in electron density. A practical upper limit at wnich the penetration depth becomes comparable to the thickness of the region where the plasma properties are affected by boundary effects is 10^{14} e/cm^3. The minimum measurable electron density corresponds to the critical plasma frequency, where the cavity begins to radiate energy, consequently reducing the Q and the resolution of the probe. A range of 10^{11} to 10^{14} e/cm^3 seems to be appropriate for this instrument.

5.2 Low Phase Velocity Structure. - In this proposed technique an evanescent wave is generated with a structure equivalent to a dielectric. In this condition there is no radiation of energy when no plasma is present. The penetration depth of this evanescent wave is, like in the external cavity probe, a function of the plasma electron density in the interaction region. Here too a correlation between resonance frequency and electron density can be established. The principle of operation of this technique is given in Appendix III.

The fact that there is no radiation when a plasma is not present allows measurements in underdense as well as overdense plasmas. Studies described in Appendix III

indicate that four orders of magnitude in electron density can be covered, going from one order of magnitude below the critical electron density to the region where the limitations similar to those of the external cavity probe are encountered. With these limitations the range of measurable electron densities is estimated to be from 10^{10} to 10^{14} e/cm^3.

These two techniques appear to be particularly convenient for measuring a broad range of several orders of magnitude in electron densities at plasma frequencies equal to or larger than the operating microwave frequency of the instrument. It is worthwhile noting that using the above-mentioned techniques electron densities in the range up to 10^{14} e/cm^3 can be measured using S and X band frequencies. Conventional interferometric techniques when applied to measurements in this range would require the use of millimeter wavelengths. The high sensitivity obtained with these techniques is due to the large values of Q which can be achieved with the two resonant structures.

6. Conclusions

6.1 With a given operating frequency the internal cavity probe can be used to measure electron densities over a range of three orders of magnitude. Aerodynamic considerations limit the upper range of measurable electron densities by this technique to 10^{13} e/cm^3.

6.2 Aerodynamic conditions were simulated for an altitude of 150,000 ft during the reentry of the Apollo spacecraft, and a model of the 3 cm wavelength probe was determined to fulfill the basic aerodynamic requirements of sampling the flow without significantly changing its properties. The angles of attack tested were 0 and 5°.

6.3 The electromagnetic calibration was performed to determine the resolution, sensitivity and range of electron density of two models of a 10 cm wavelength and one model of a 3 cm wavelength probe. Two methods have been used to measure the characteristics mentioned above and the results have been found to agree.

6.4 The measurement of electron densities in a shock tube with the 3 cm wavelength probe was compared to the one obtained with a one centimeter interferometer. They have

been found to agree within a factor of two in electron densities.

6.5 The 10 cm wavelength probe was checked against the value of electron densities predicted for the shock tube as a function of incident Mach number and initial driven pressure. The results have been found to agree. The 30 cm wavelength resonant cavity could not be used because the plasma generated in the shock tube has a too-high collision frequency for the frequency of operation of this particular cavity.

6.6 This program has resulted in the development of two operational internal cavity electron density probes. One of these probes operates with a 10 cm wavelength and measures electron densities in the range of 10^8 to 10^{11} e/cm^3. The other operates with a 3 cm wavelength and measures electron densities in the range of 10^9 to 10^{12} e/cm^3.

6.7 Theoretical investigations have indicated that by using other techniques, such as the external cavity and the low phase velocity structure, it should be possible to extend the upper limit of measurable electron densities to 10^{14} e/cm^3.

REFERENCES

1. Nagamatsu, H T., Weil, J. A., and Sheer, R E. Jr , Leading Edge Bluntness and Slip Flow Effects in High Temperature Hypervelocity Flow Over a Flat Plate, AGARD Specialists' Meeting, Rhode-Saint-Genese, Belgium, April 3-6, 1962.

2. Shapiro, A. H., The Dynamics and Thermodynamics of Compressible Fluid Flow (Vol. I, Chapter 6) Ronald Press Company, New York 1953

3 Toong Tau-Yi and Kaye, J., Theoretical Solutions for a Steady Laminar Flow of a Compressible Fluid in the Entrance Region of a Tube, Massachusetts Institute of Technology TR No 7359-11, March 1916.

4. Collins, A. M., Low Density Supersonic Diffuser Performance, TR No. He-150-164, Univ. of California, Berkeley, California, January 15, 1959.

5 Ferri, A. and Zakkay, V., Measurements of Stagnation Point Heat Transfer at Low Reynolds Numbers, J. Aero. Space Sci., Vol. 29. No 7, p. 847 July 1962.

6. Arens, M. and Speigler, E., Shock-Induced Boundary Layer Separation in Over-expanded Conical Exhaust Nozzles, Amer. Inst. Aero and Astro Vol. 1. No 3, p. 578, March 1963.

7. Abele, M., Medecki H., and Tomboulian R., Electromagnetic Studies in Shock-Produced Plasmas CASL TR-338, April 1964.

8. Abele, M., Byrne, R. W., and West, J , Preliminary Design of an Electron Probe GASL TR-188. October 1960

9. Abele, M., Theory of Propagation of an Electromagnetic Field in a Dielectric Circular Waveguide, Nuovo Cem. N 9, 1948

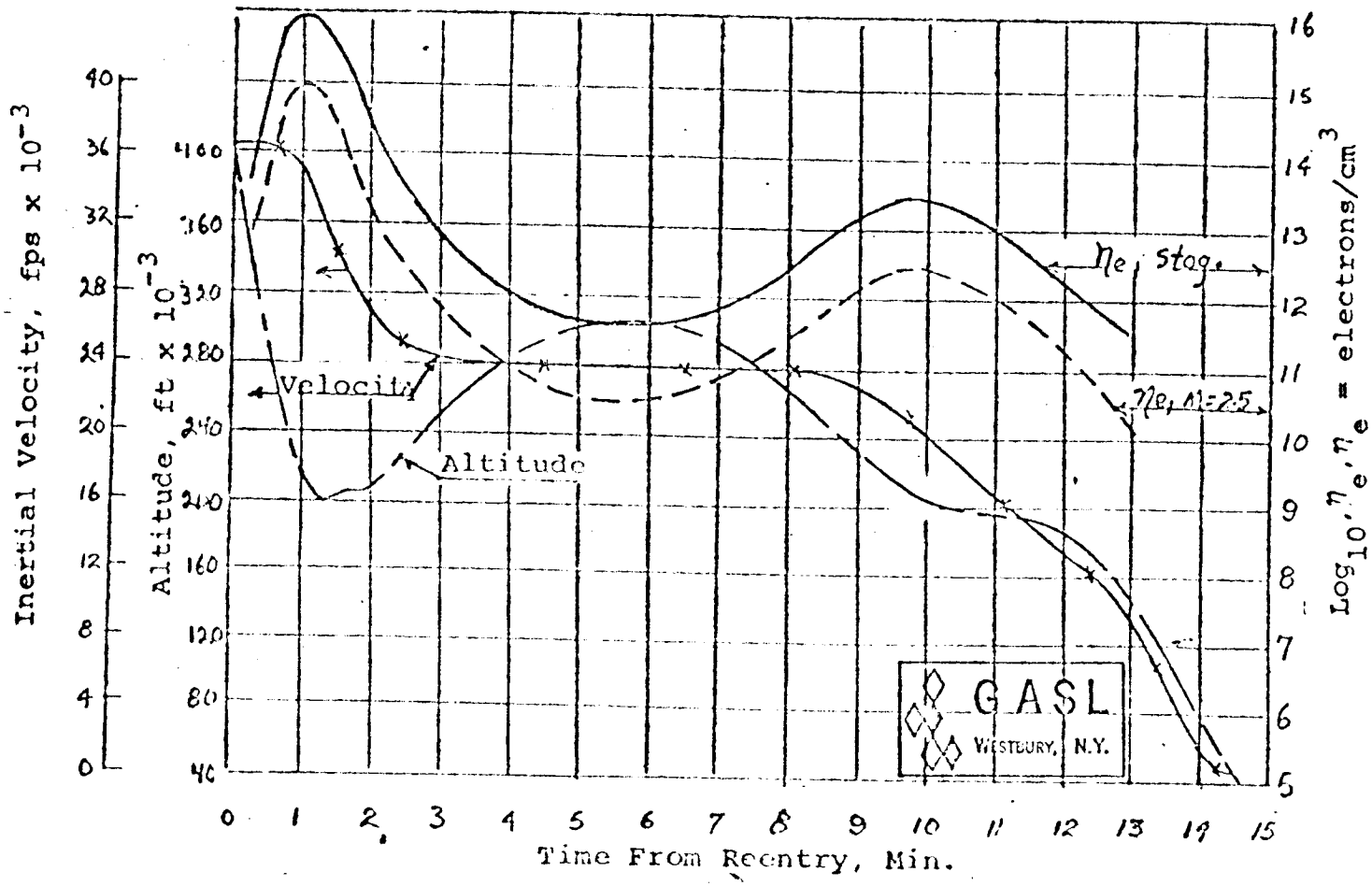

TRAJECTORY DURING REENTRY

FIGURE 1 : ESTIMATED ELECTRON DENSITIES, INITIAL FLIGHT - PATH ANGLE = 6.4°, REENTRY RANGE 3000 n.m.

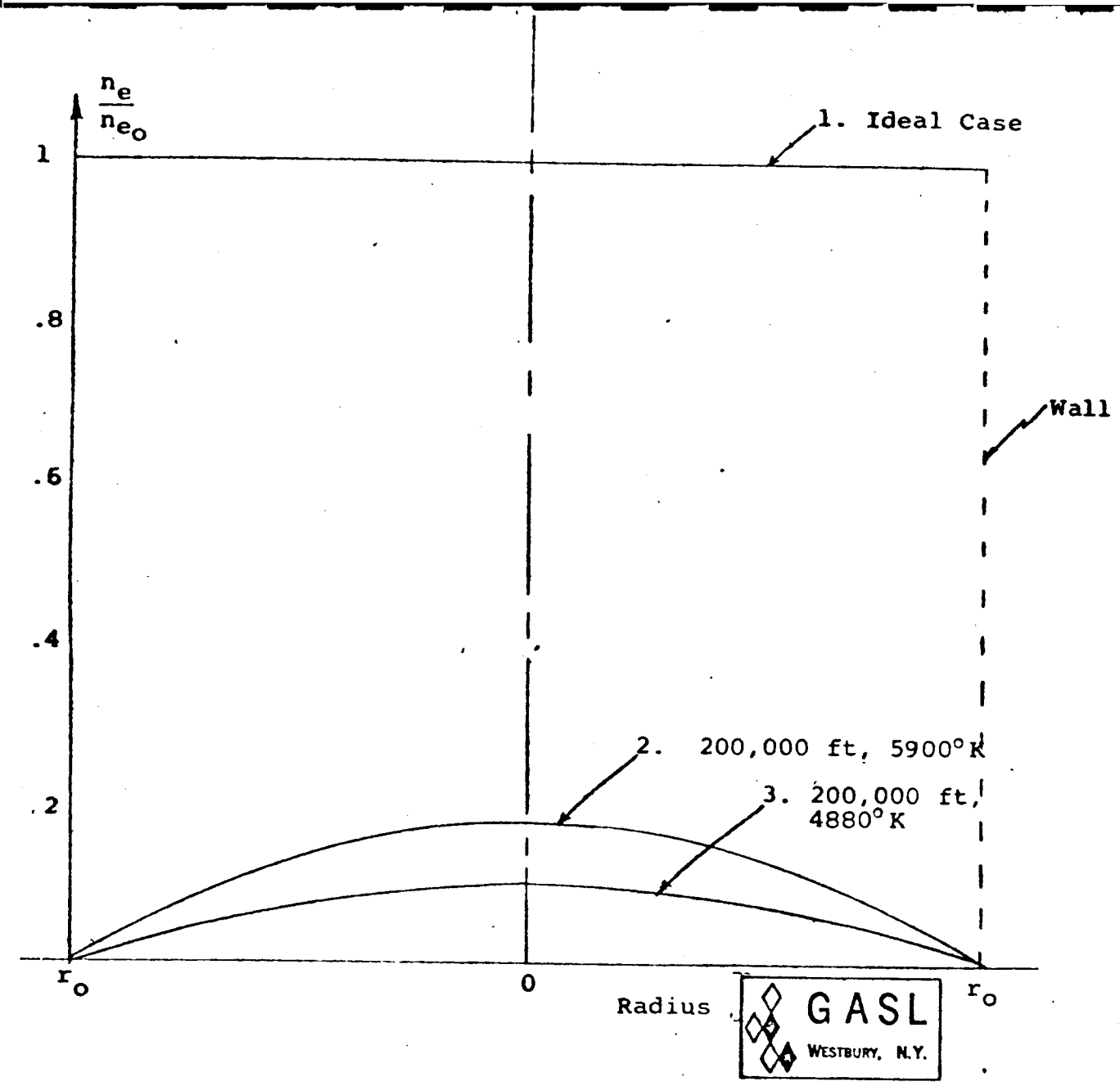

Fig. 2. Effects of Diffusion on Transversal Electron Density Distribution

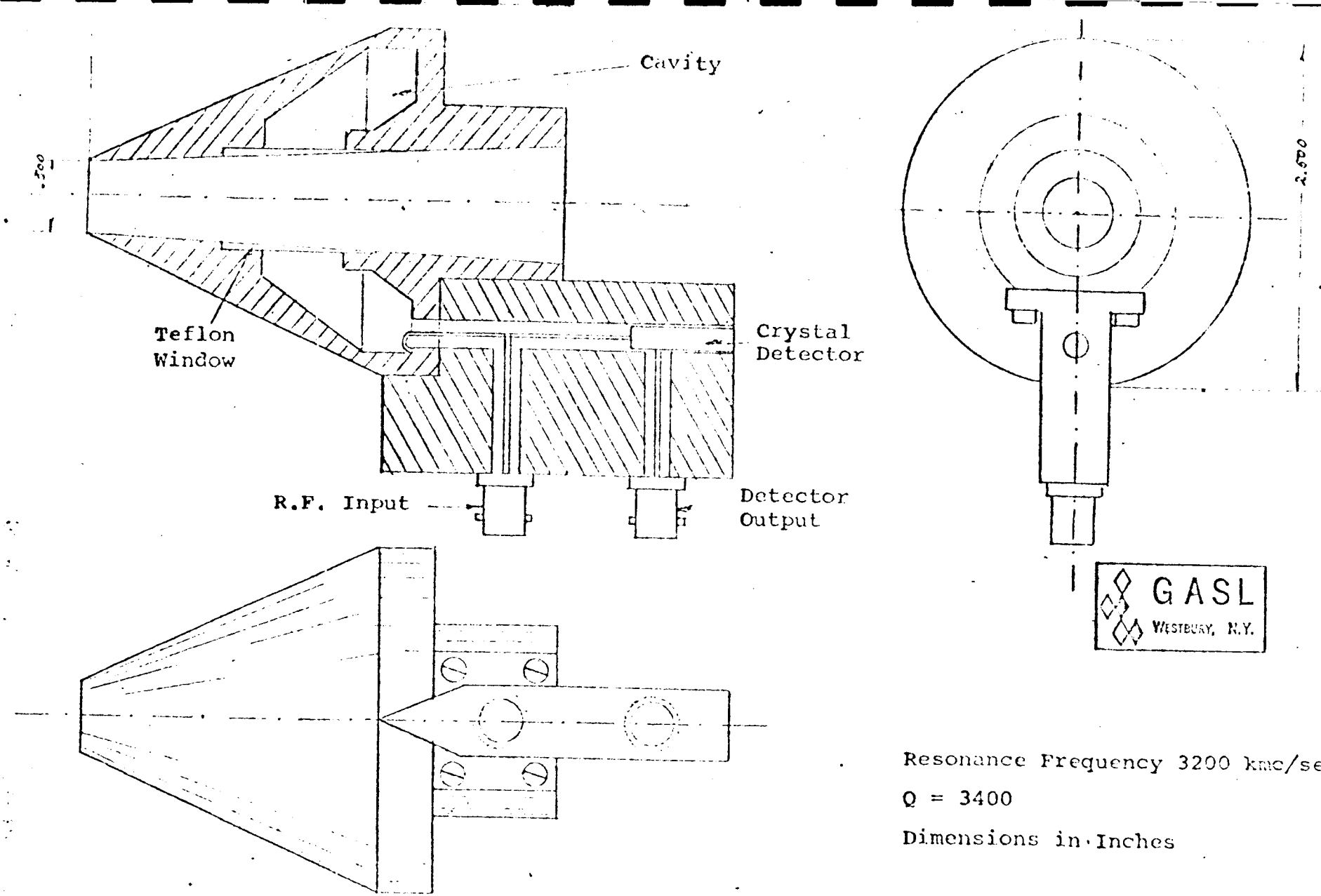

Fig. 3: 10 cm Wavelength Electron Density Probe (First Model)
TR No. 527 - NASA Contract NAS5-3929

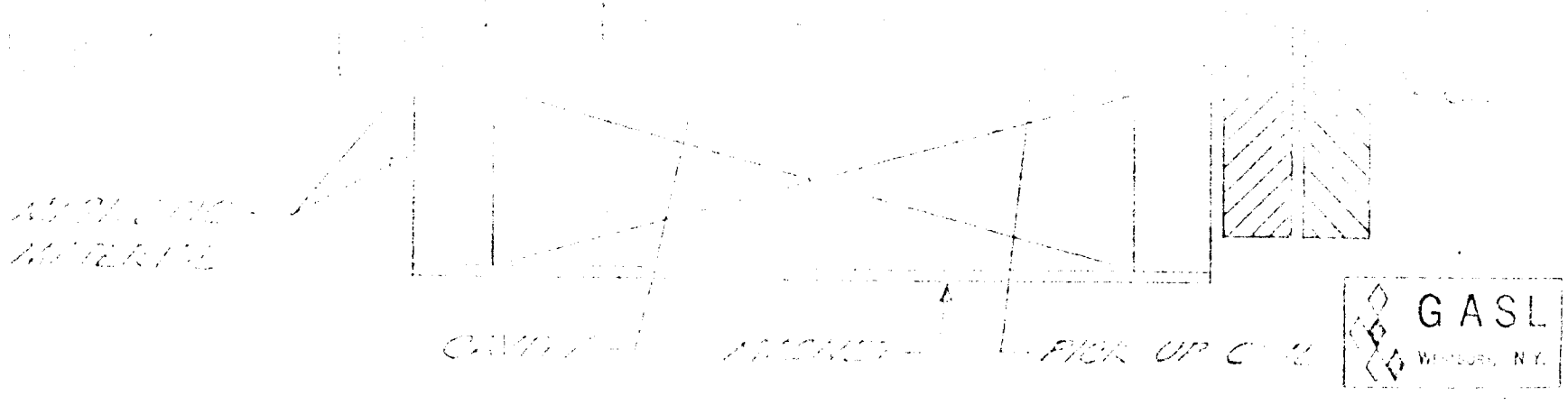
GASL

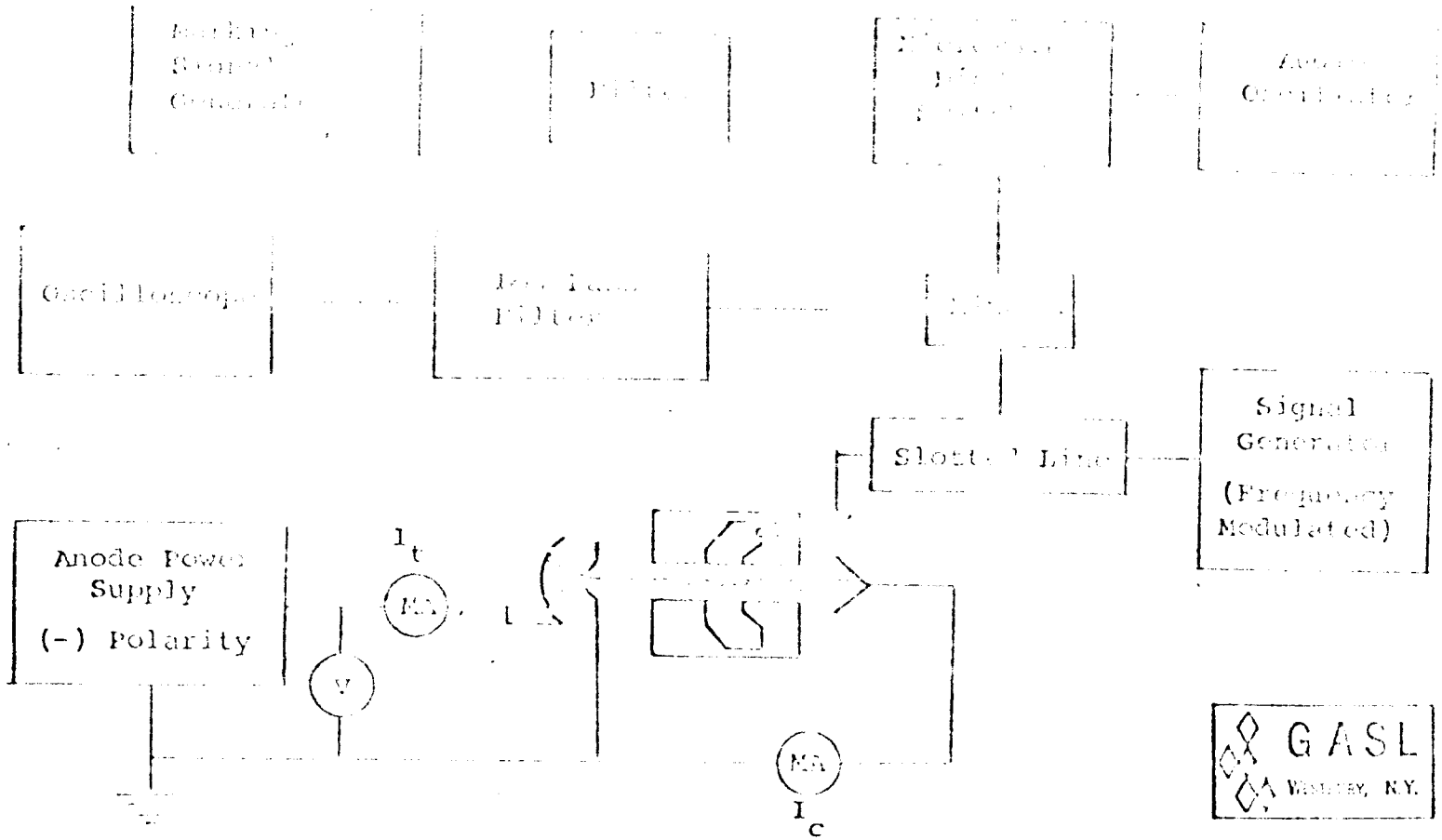

FIGURE 7 : BLOCK DIAGRAM OF MEASURING EQUIPMENT FOR ELECTRONIC CALIBRATION

TR No. 527 - NASA Contract NAS5-3929

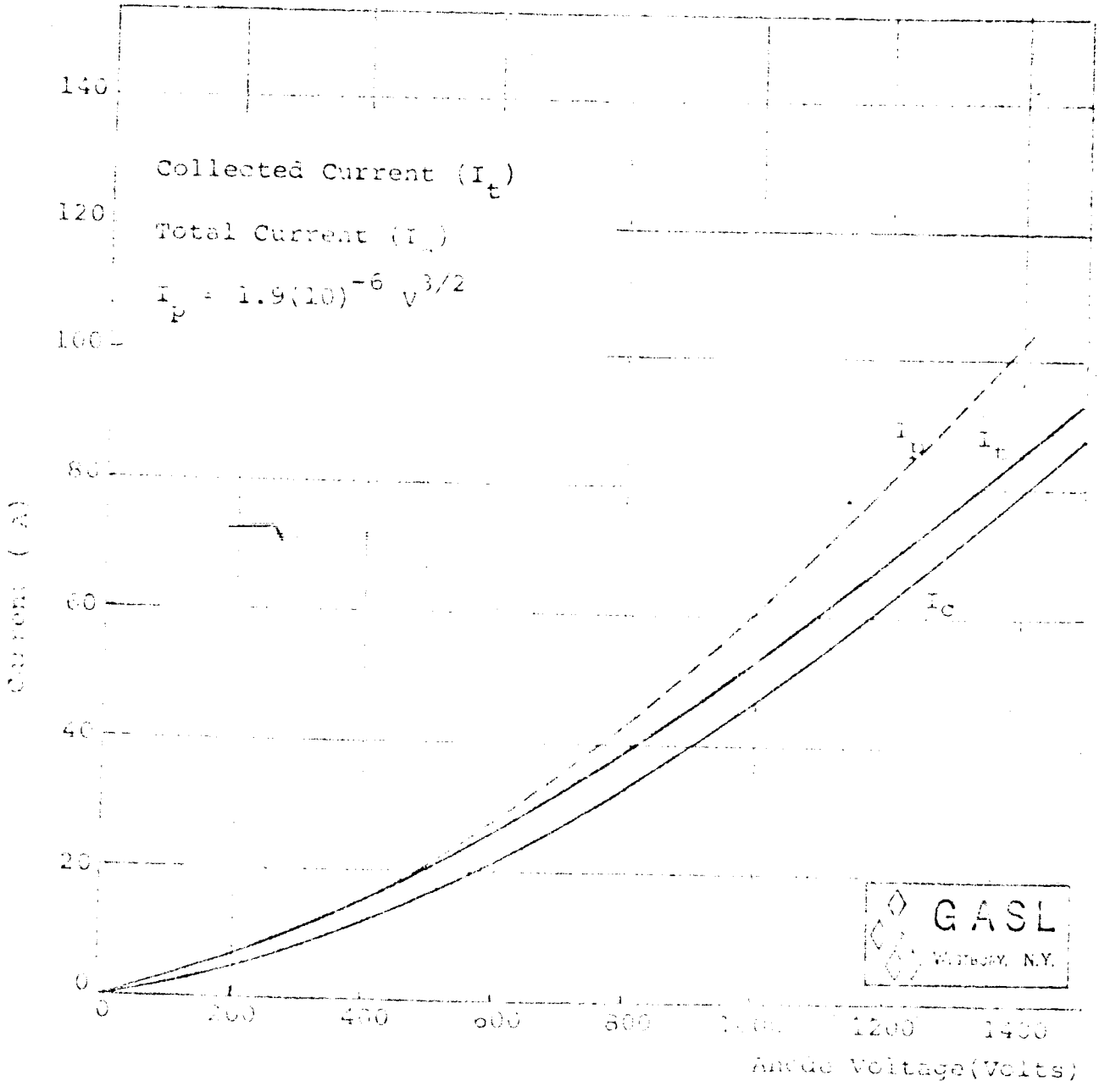

FIGURE 8: CURRENT-VOLTAGE CHARACTERISTICS OF THE ELECTRON GUN

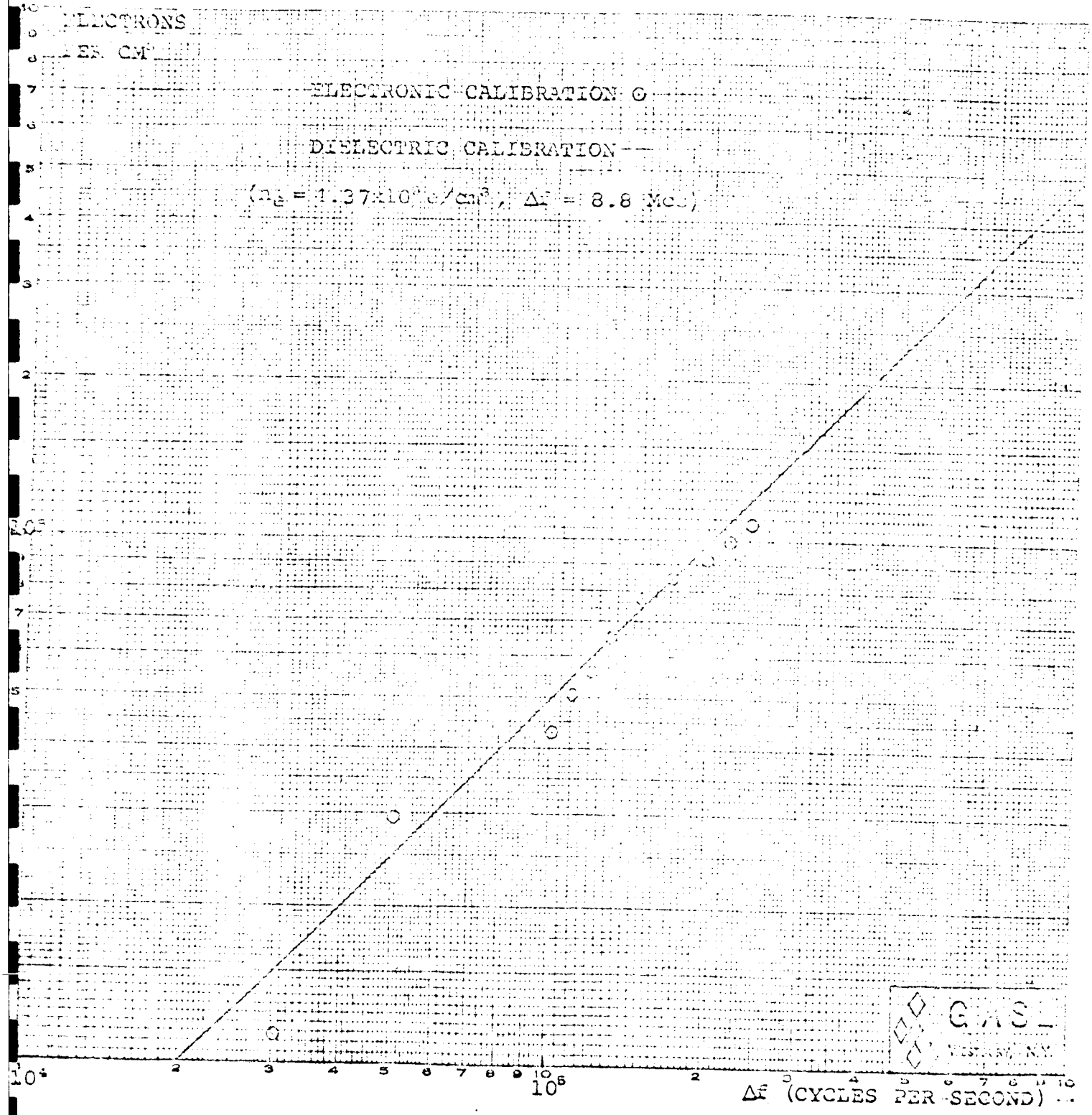

COMPARISON OF DIELECTRIC CALIBRATION WITH ELECTRONIC CALIBRATION

FIG. 9

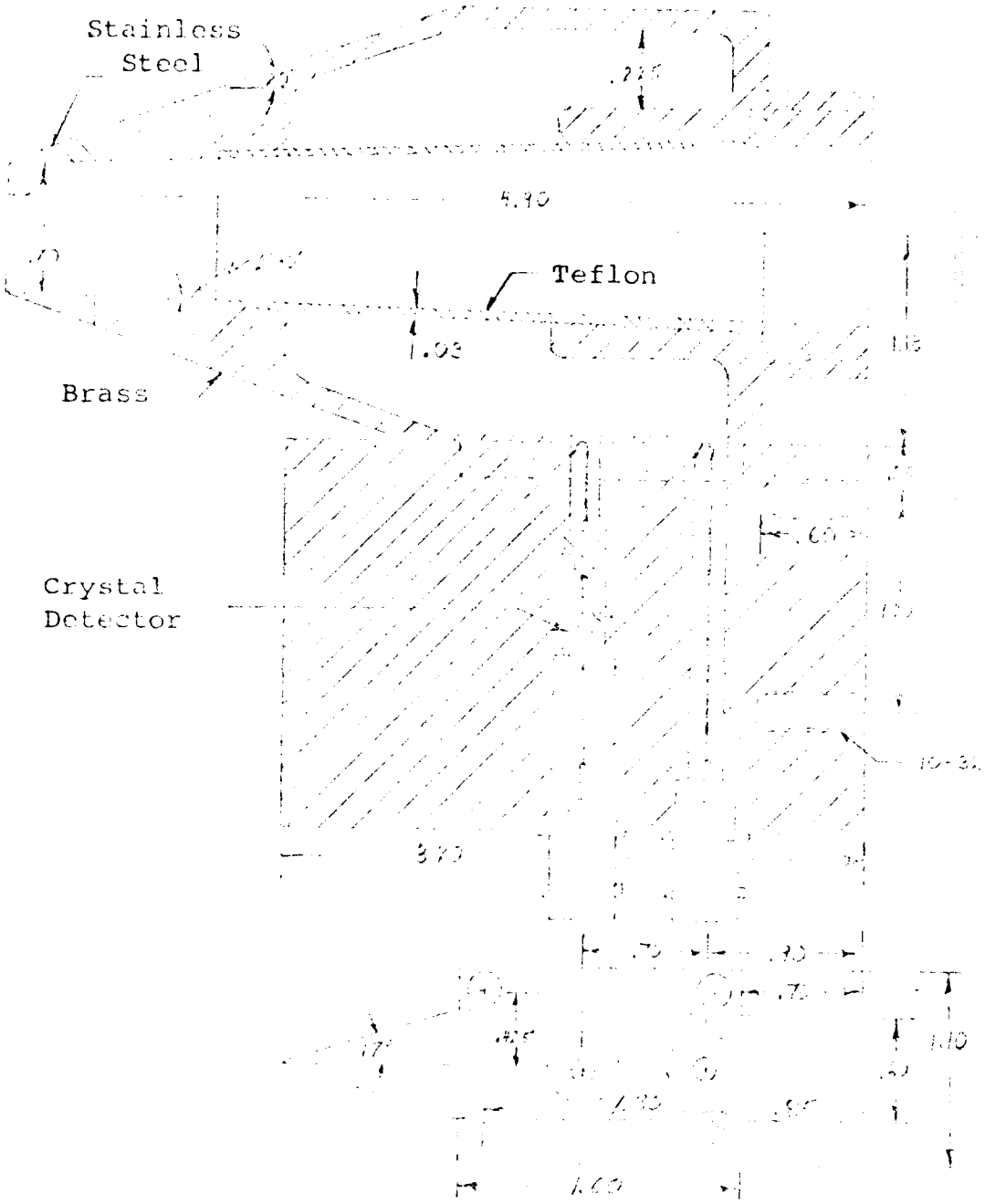

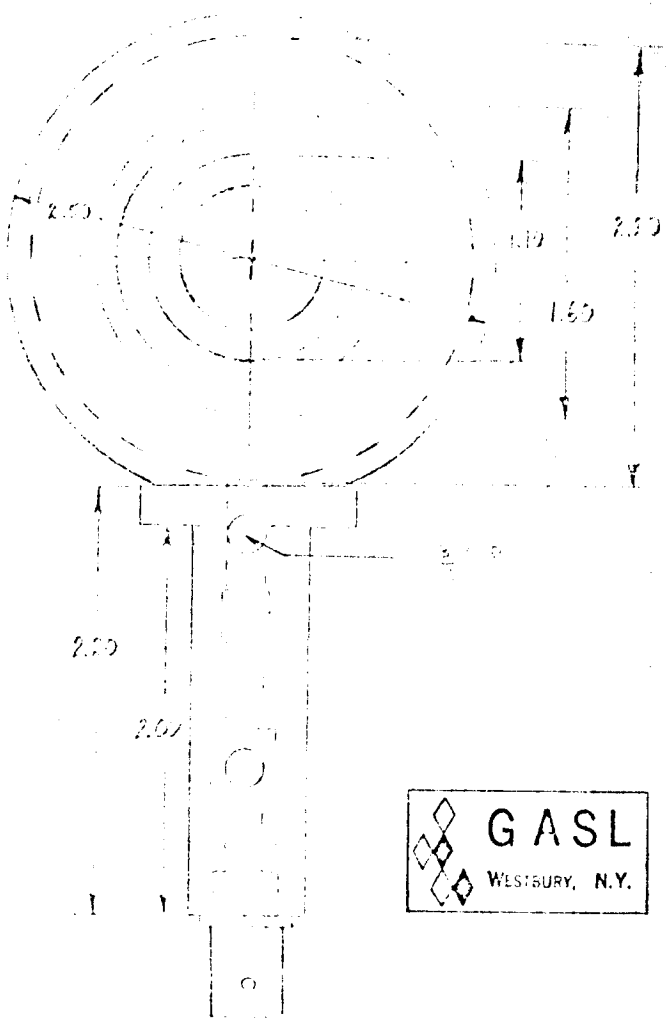

Fig. 10. 10 cm Wavelength Probe and Mounting (Second Model)

f_o = 2.08 KMc; Q = 3200

Dimensions in Inches

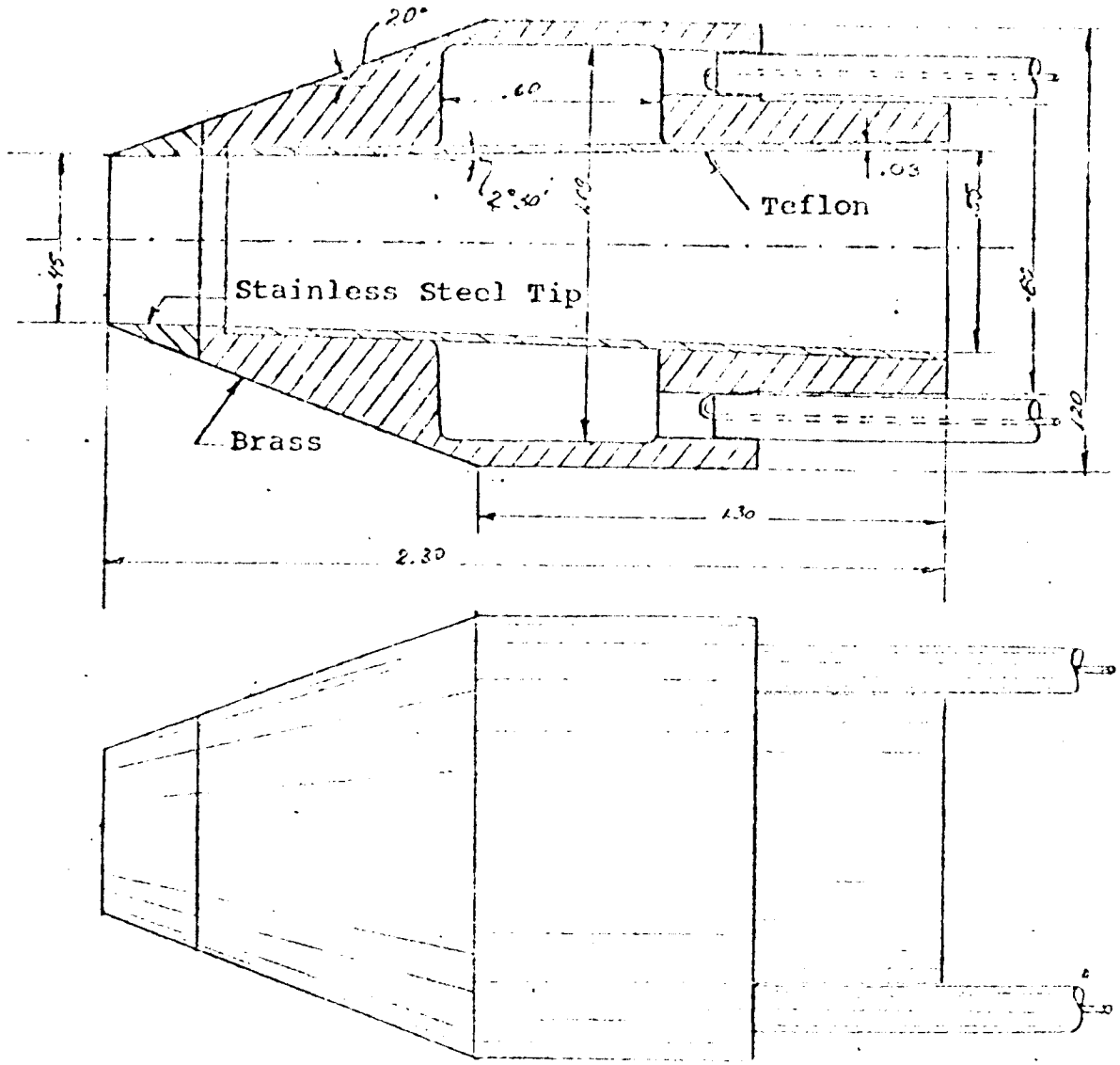

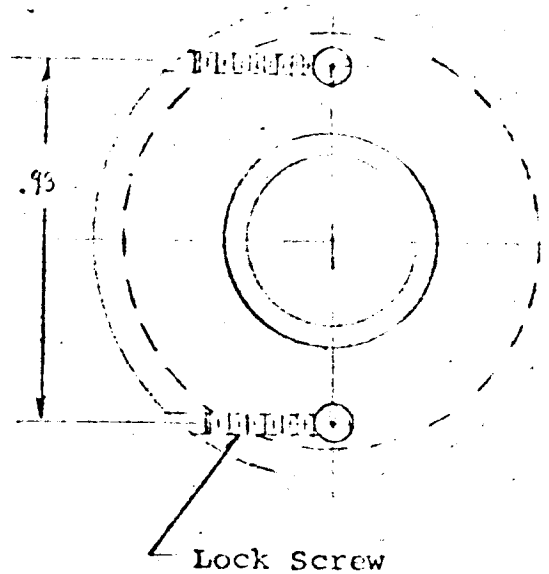

GASL
WESTBURY, N.Y.

Figure 11:

3 cm Wavelength Probe

Frequency of Resonance 8.68 KM

Q = 2000

Dimensions in Inches

TR No. 527 - NASA Contract NAS5-39

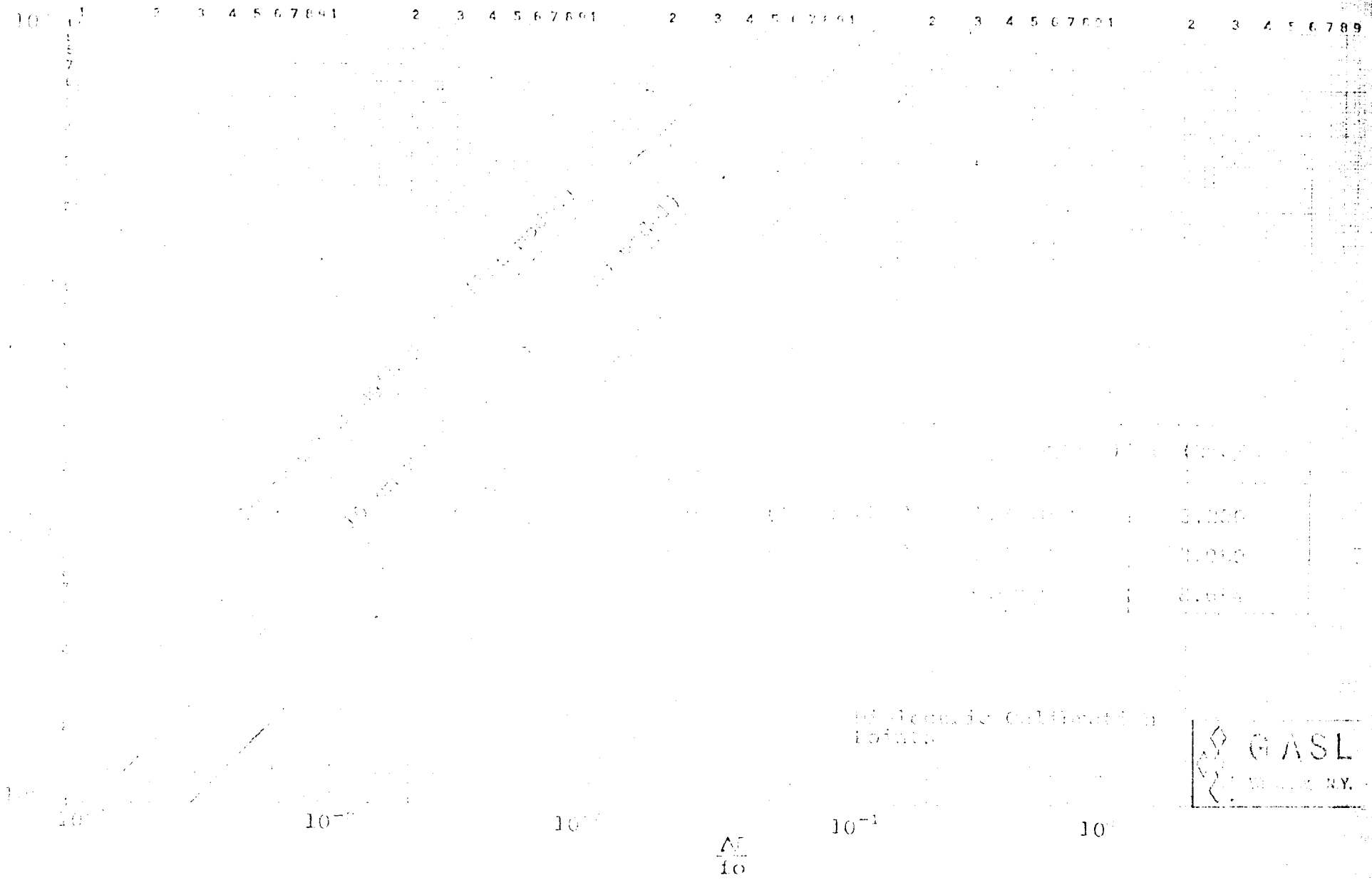

Fig. 12: Elect[illegible] Calibration Chart
TR No. 527 - 2 Attachment E(15-3929)

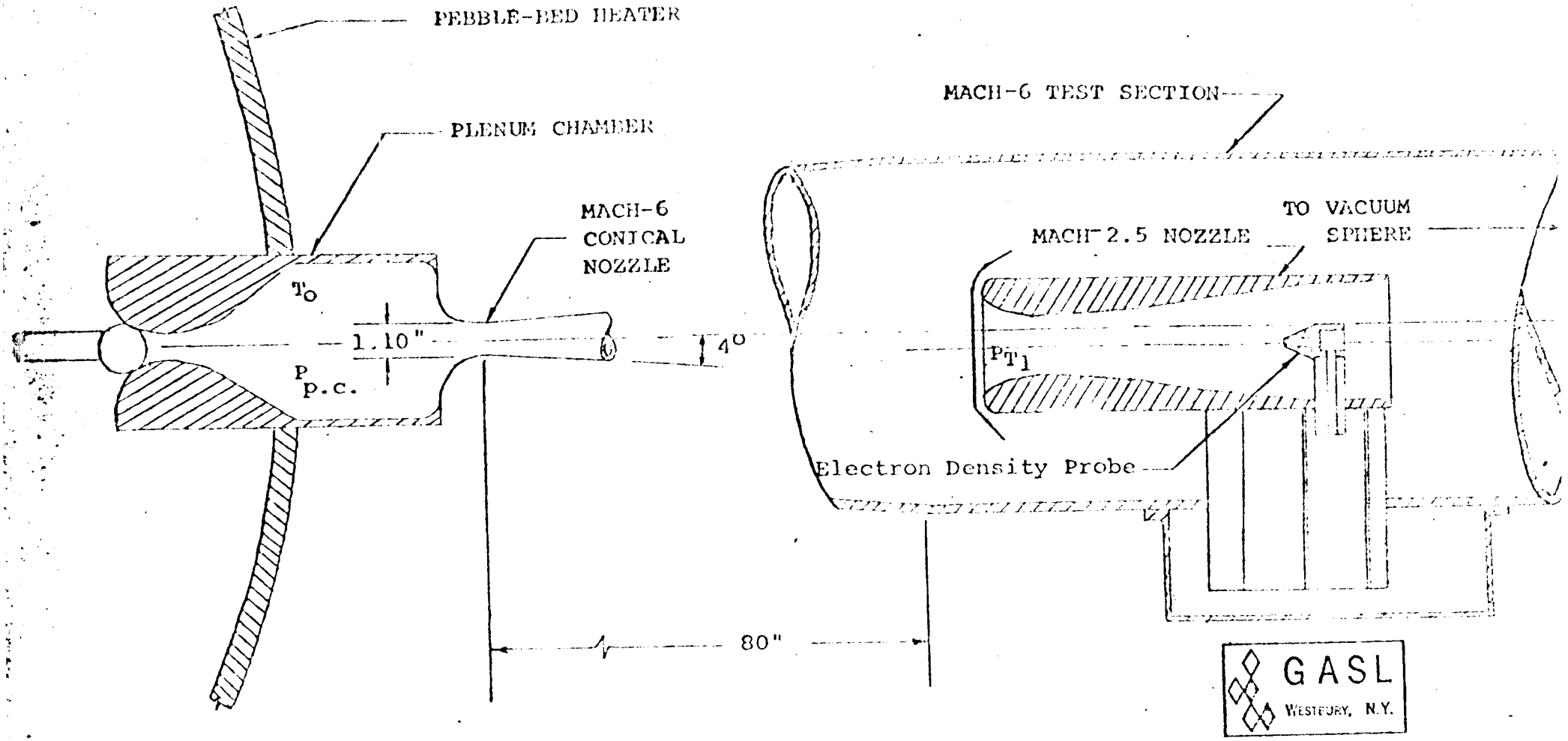

FIGURE 13: AERODYNAMIC TEST FACILITY - SCHEMATIC
TR No. 527 - NASA Contract NAS5-3929

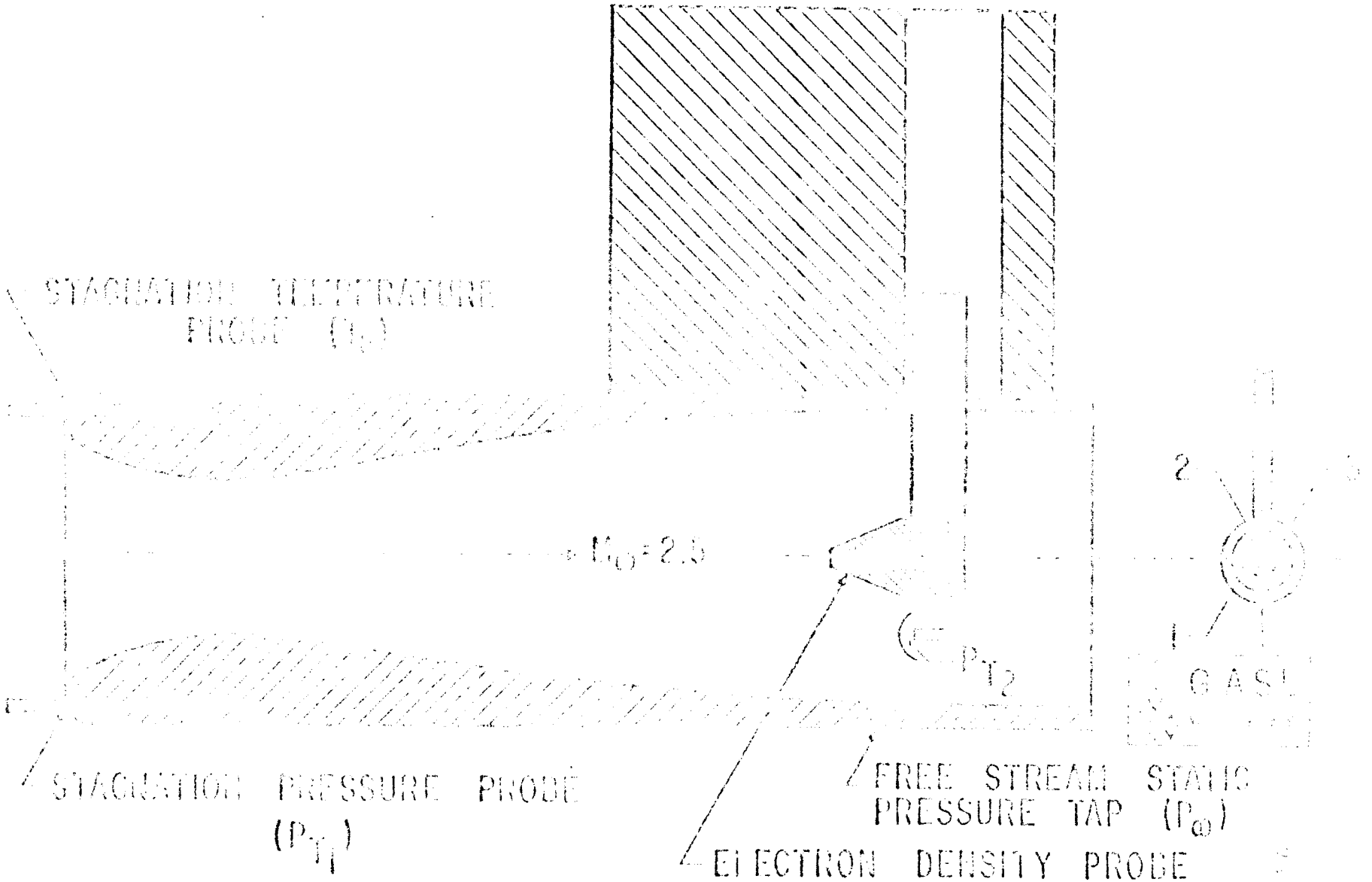

FIG. 1: ELECTRON DENSITY PROBE INSTALLATION IN MACH 2.5 NOZZLE

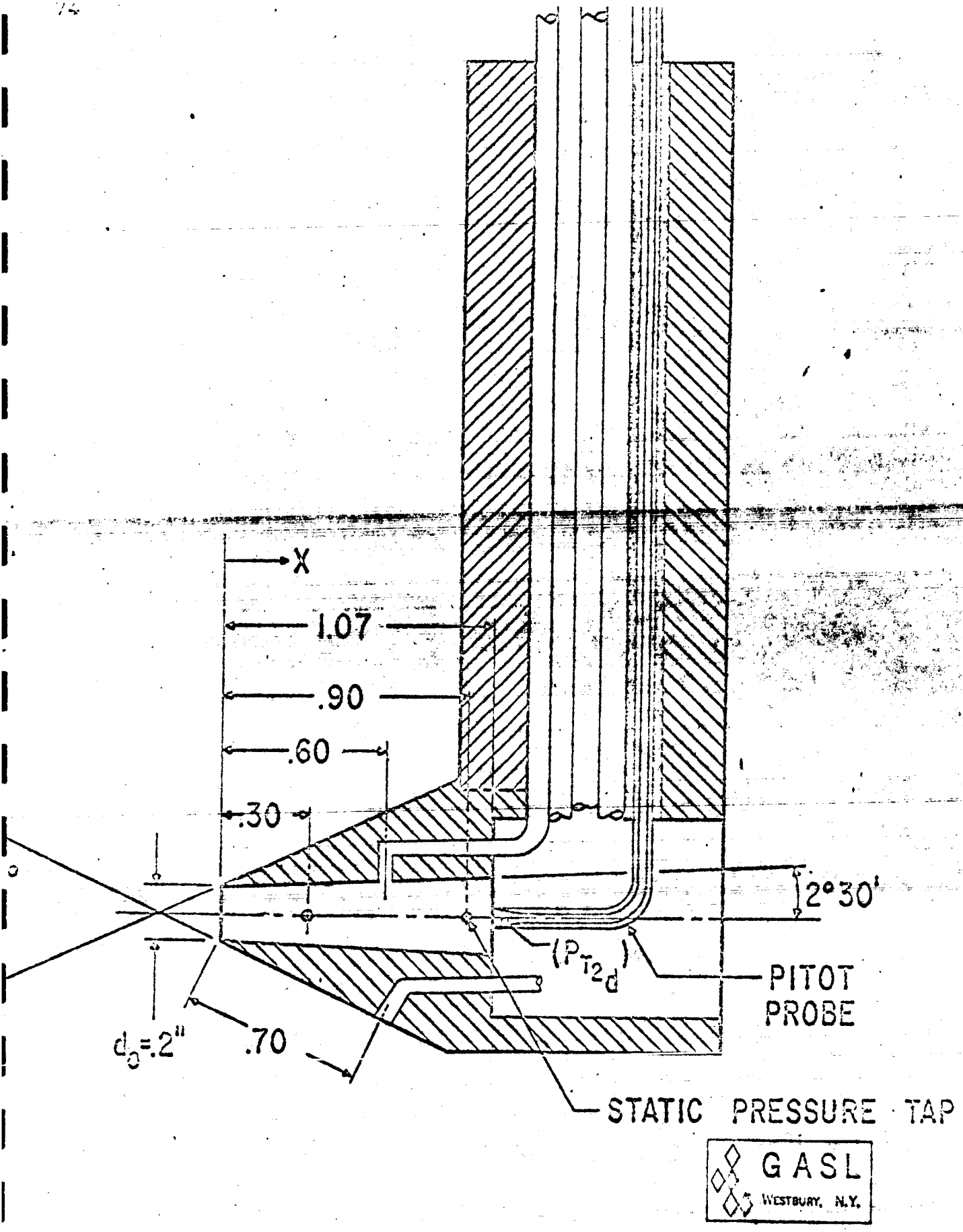

FIGURE 15: AERODYNAMIC MODEL OF THE ELECTRON DENSITY PROBE

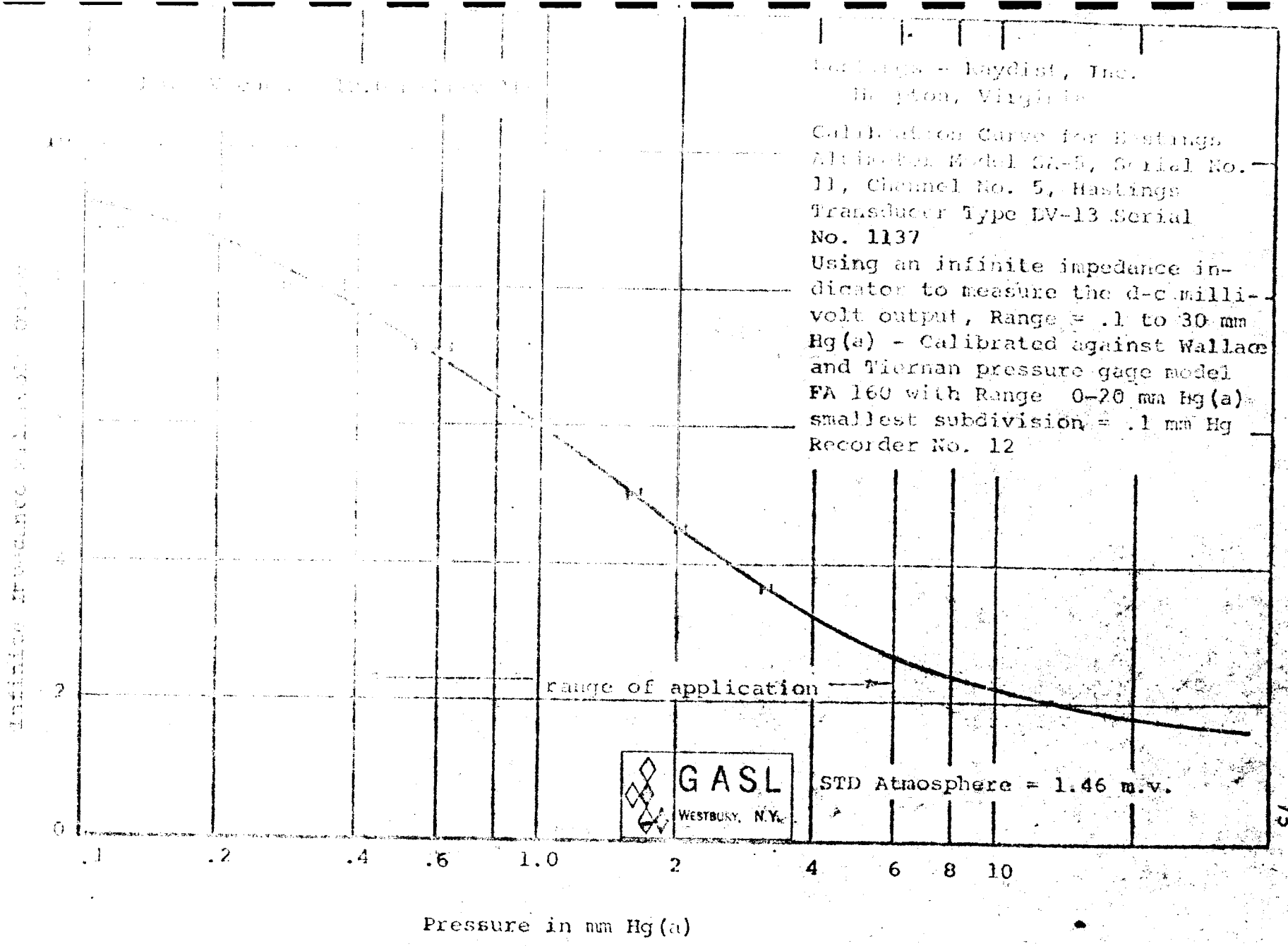

Figure 16 : Typical Calibration Curve of a Hastings-Raydist Heated Thermopile Vacuum gauge

Tr No. 527 - NASA Contract NAS5-3929

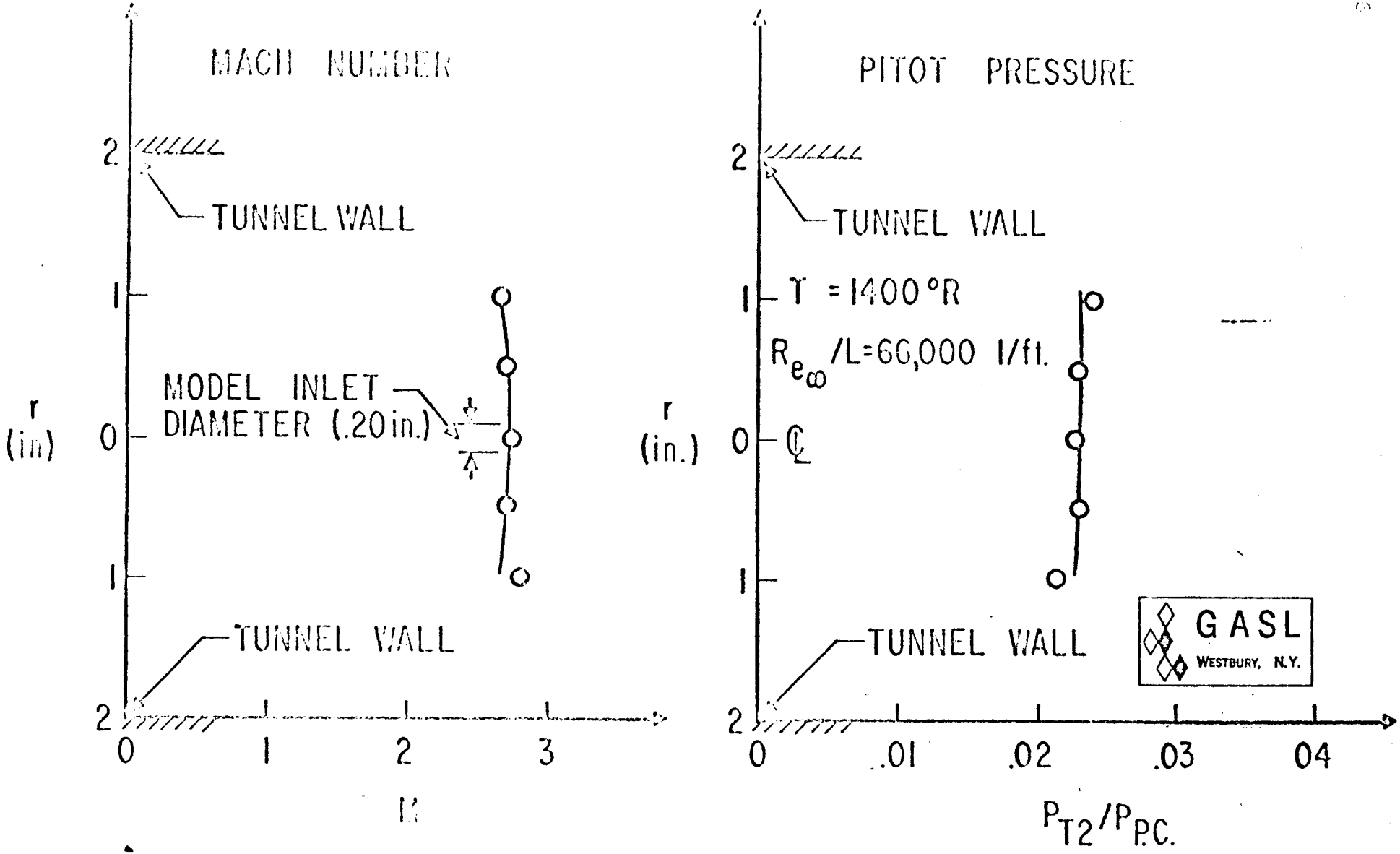

FIG. 17: MACH 2.5 NOZZLE CALIBRATION

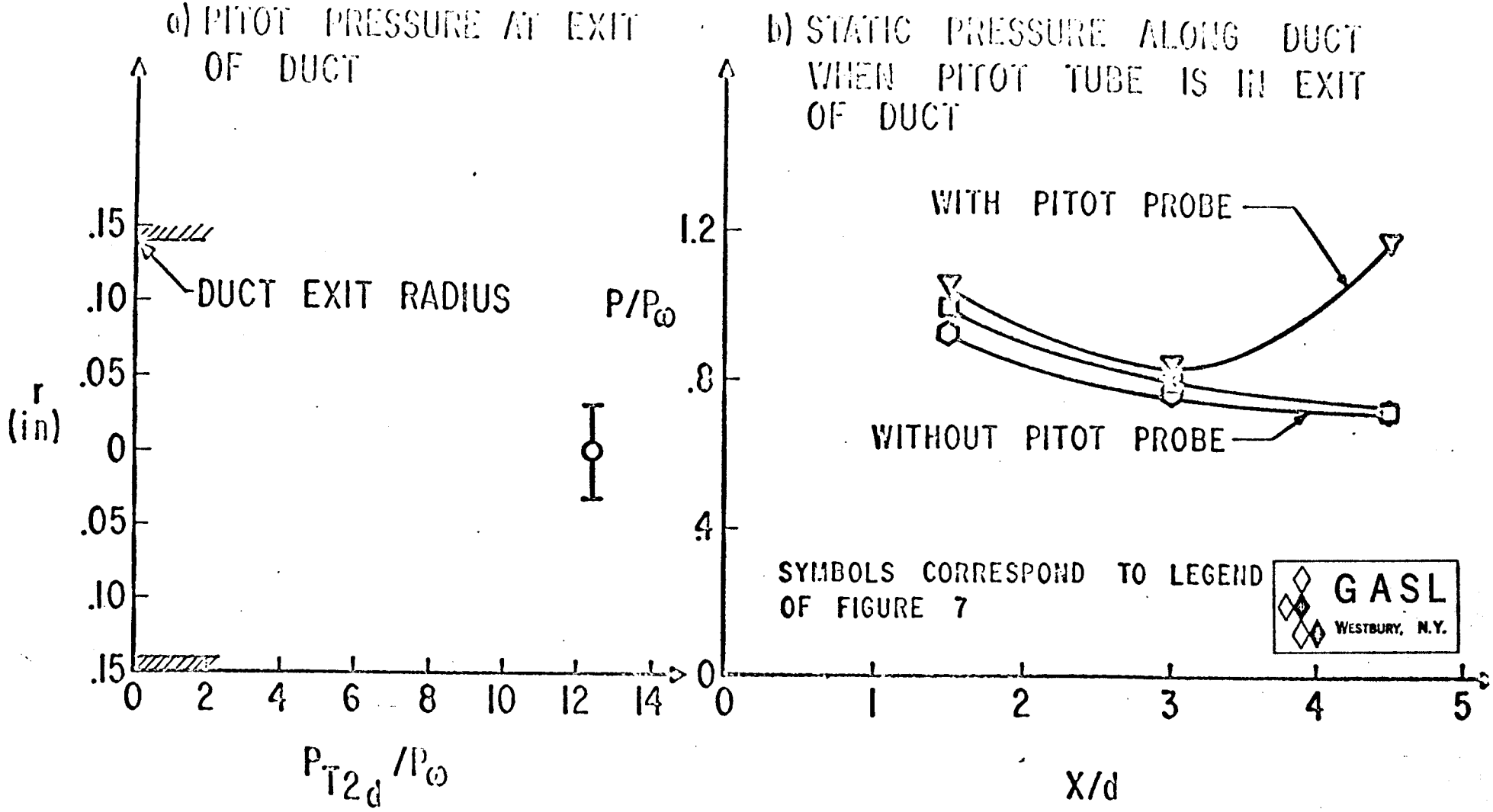

FIG. 19: PITOT PRESSURE AT EXIT OF DUCT

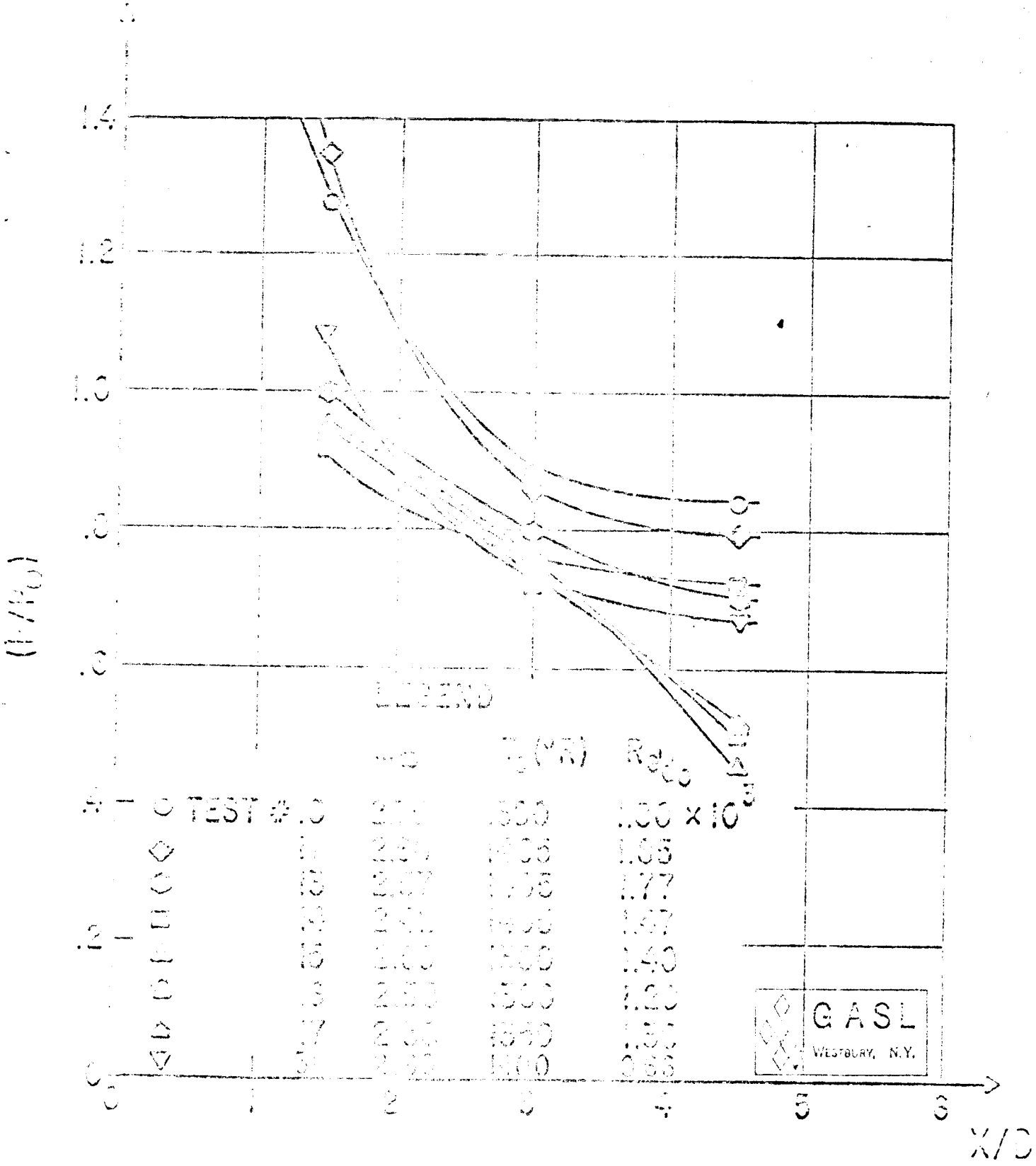

FIG. 5

ELECTRON DENSITY PROBE BUOY STATIC PRESSURE

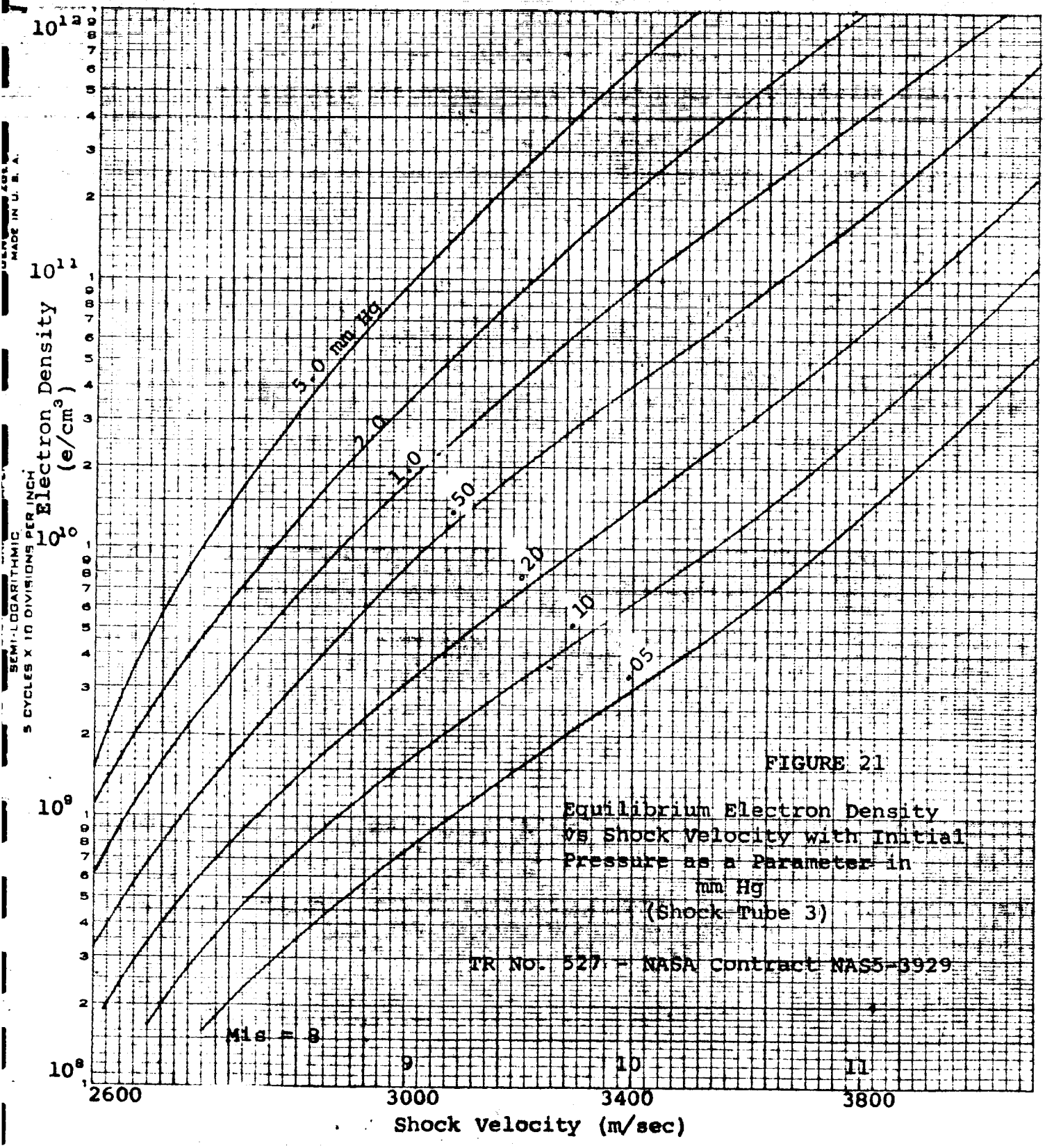

FIGURE 21

Equilibrium Electron Density vs Shock Velocity with Initial Pressure as a Parameter in mm Hg (Shock Tube 3)

TR No. 527 - NASA Contract NAS5-3929

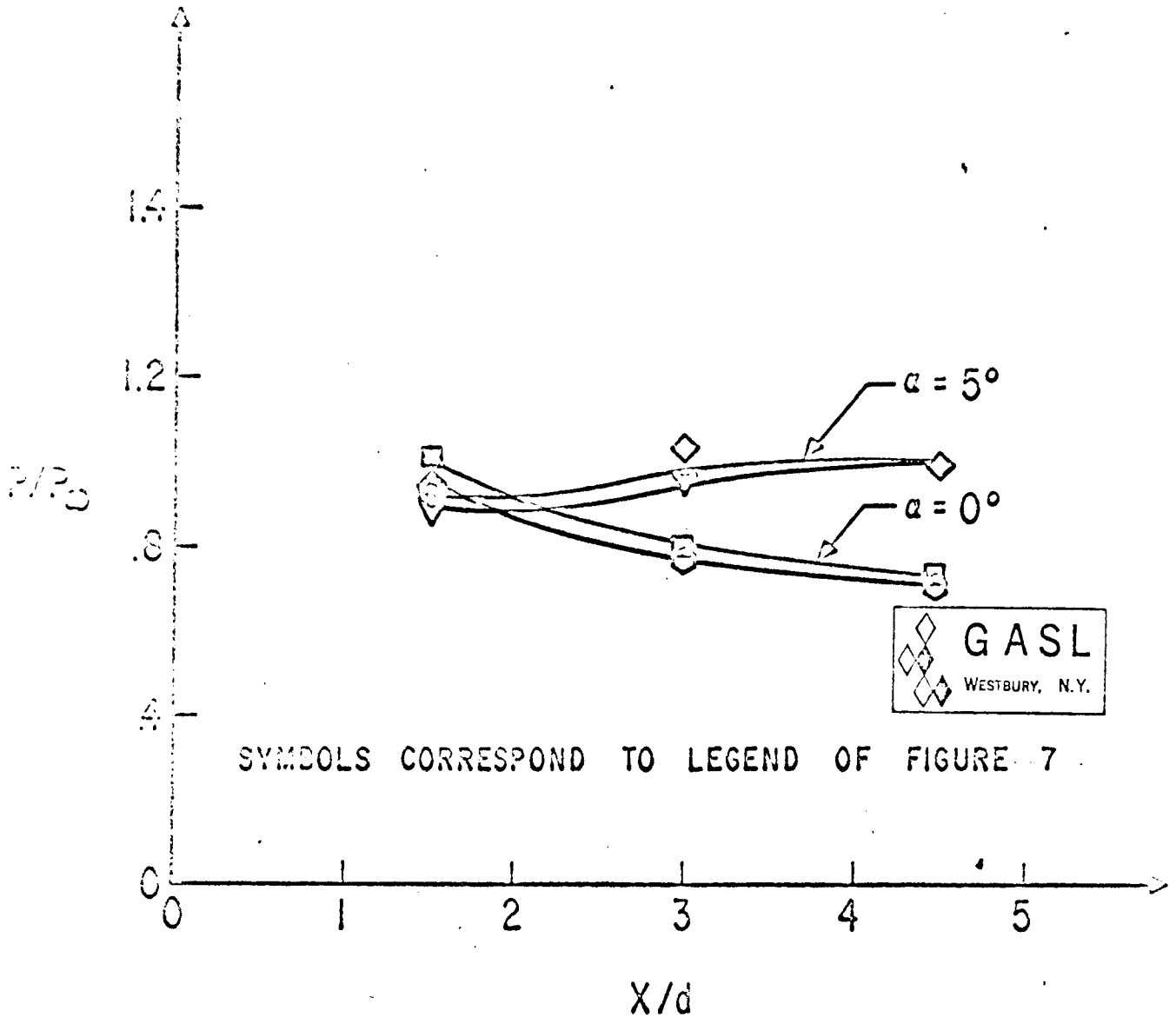

FIG. 20: STATIC PRESSURE DISTRIBUTION IN DUCT (PROBE AT ANGLE OF ATTACK)

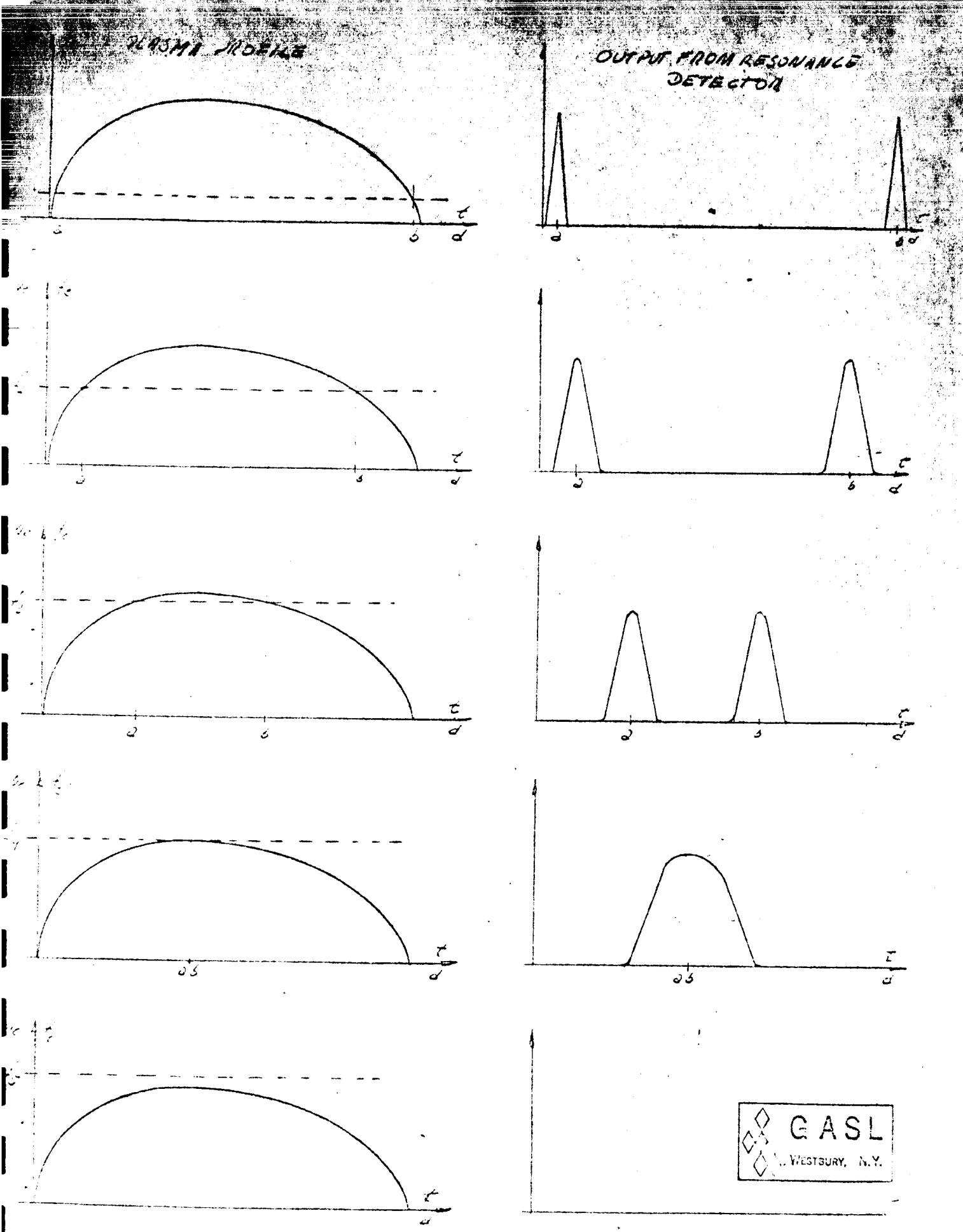

Fig. 22. Technique to Determine the Electron Density Profile

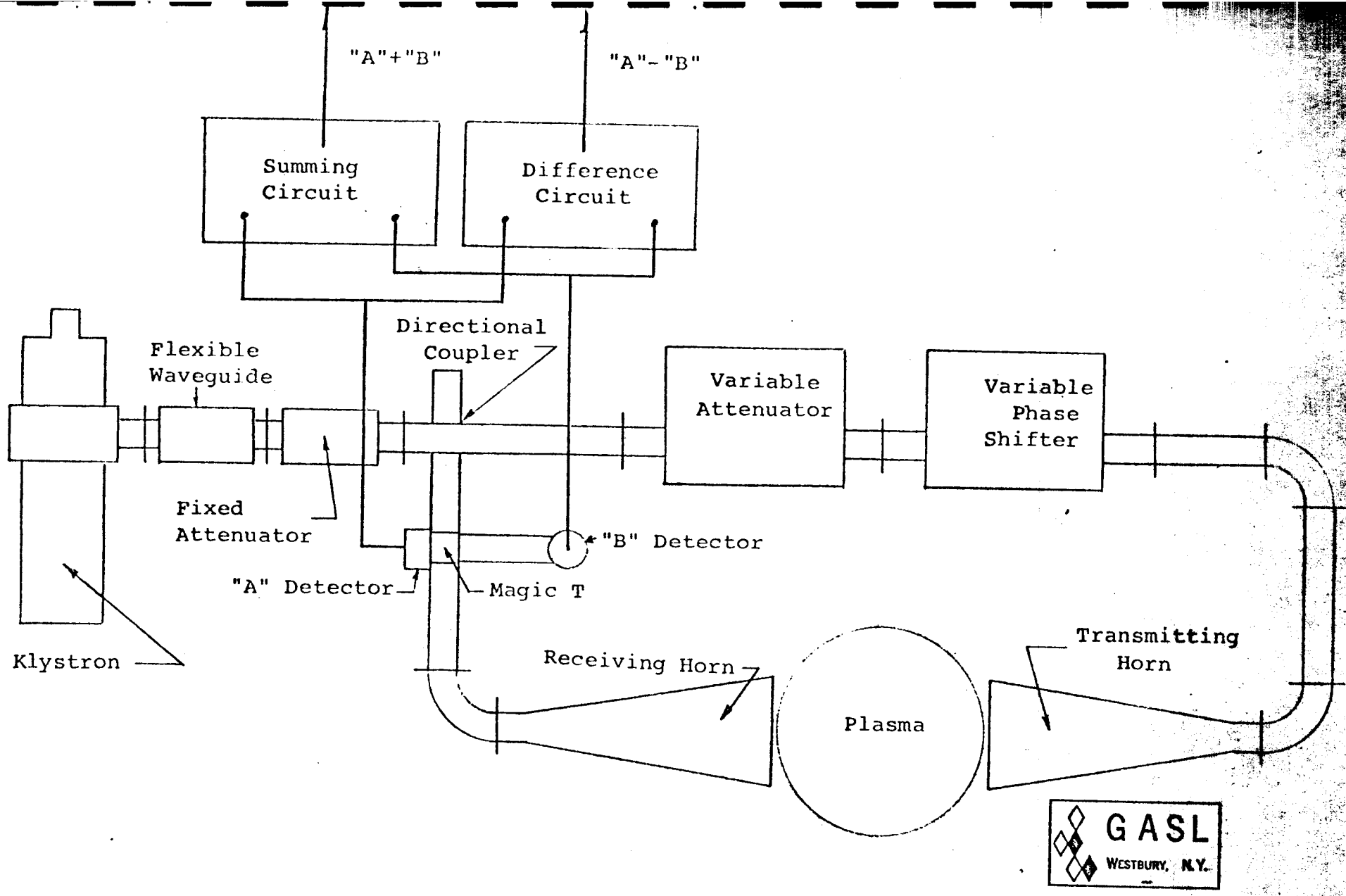

FIGURE 23 : ONE CENTIMETER WAVELENGTH INTERFEROMETER CIRCUIT
TR No. 527 - NASA Contract NAS5-3929

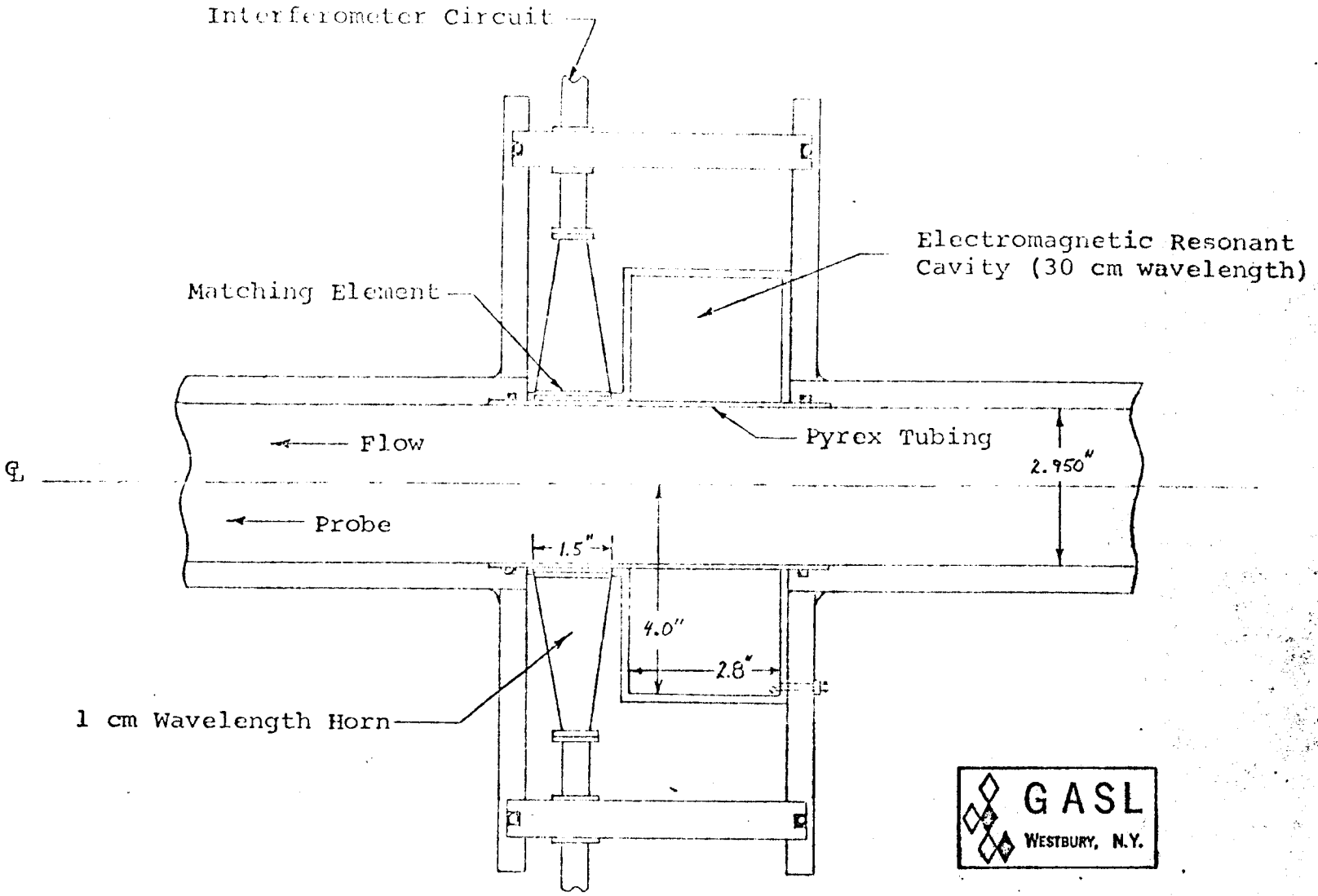

Fig. 24 : Standard Measuring Device Assembly
TR No. 527 - NASA Contract NAS5-3929

FIGURE 26: INTERFEROMETER AND CAVITY TEST SECTION

TR No. 527 - NASA Contract NAS5-3929

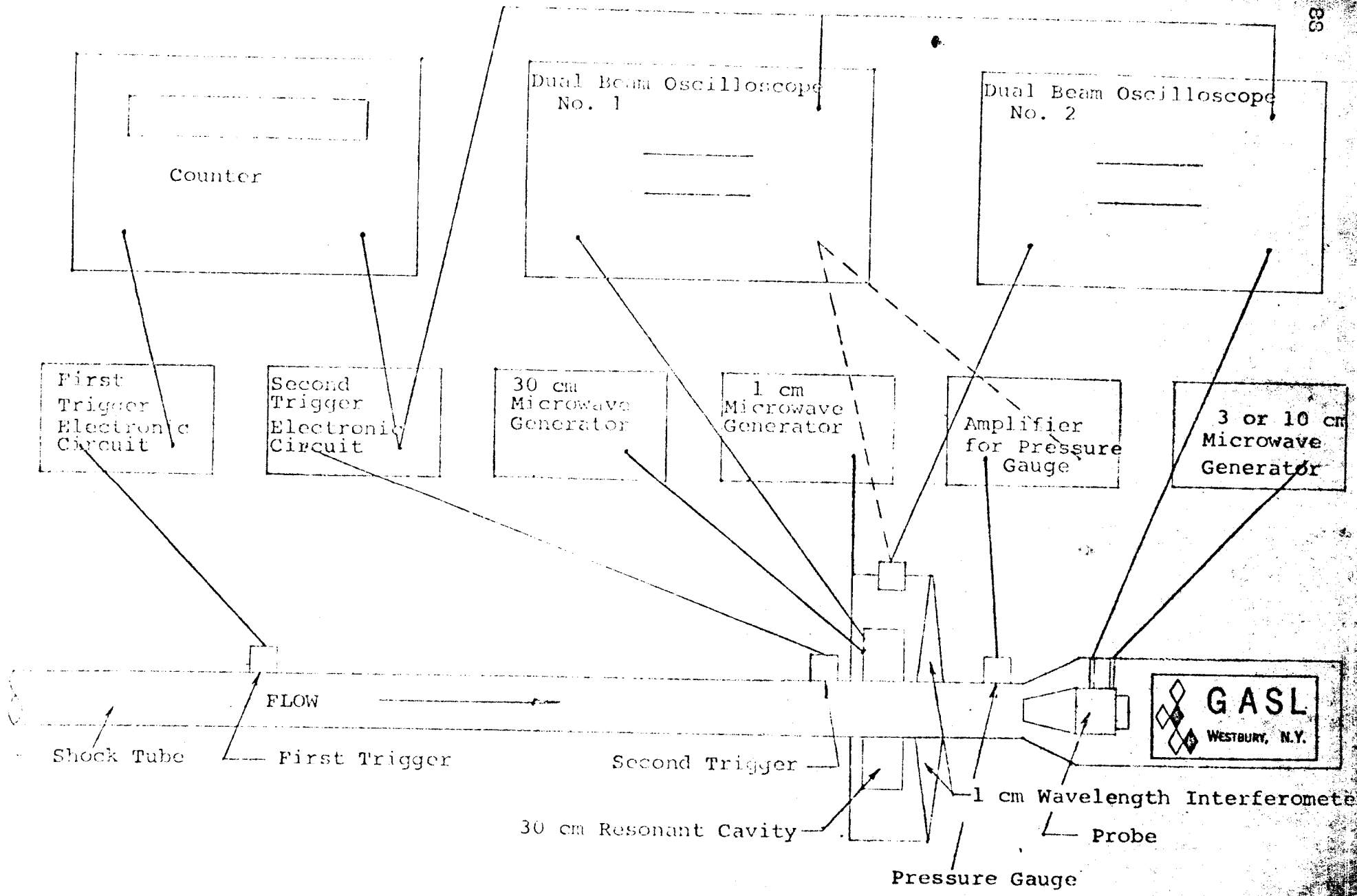

FIGURE 2: SHOCK TUBE INSTRUMENTATION DIAGRAM
AR No. 527 - NASA Contract NAS5-3929

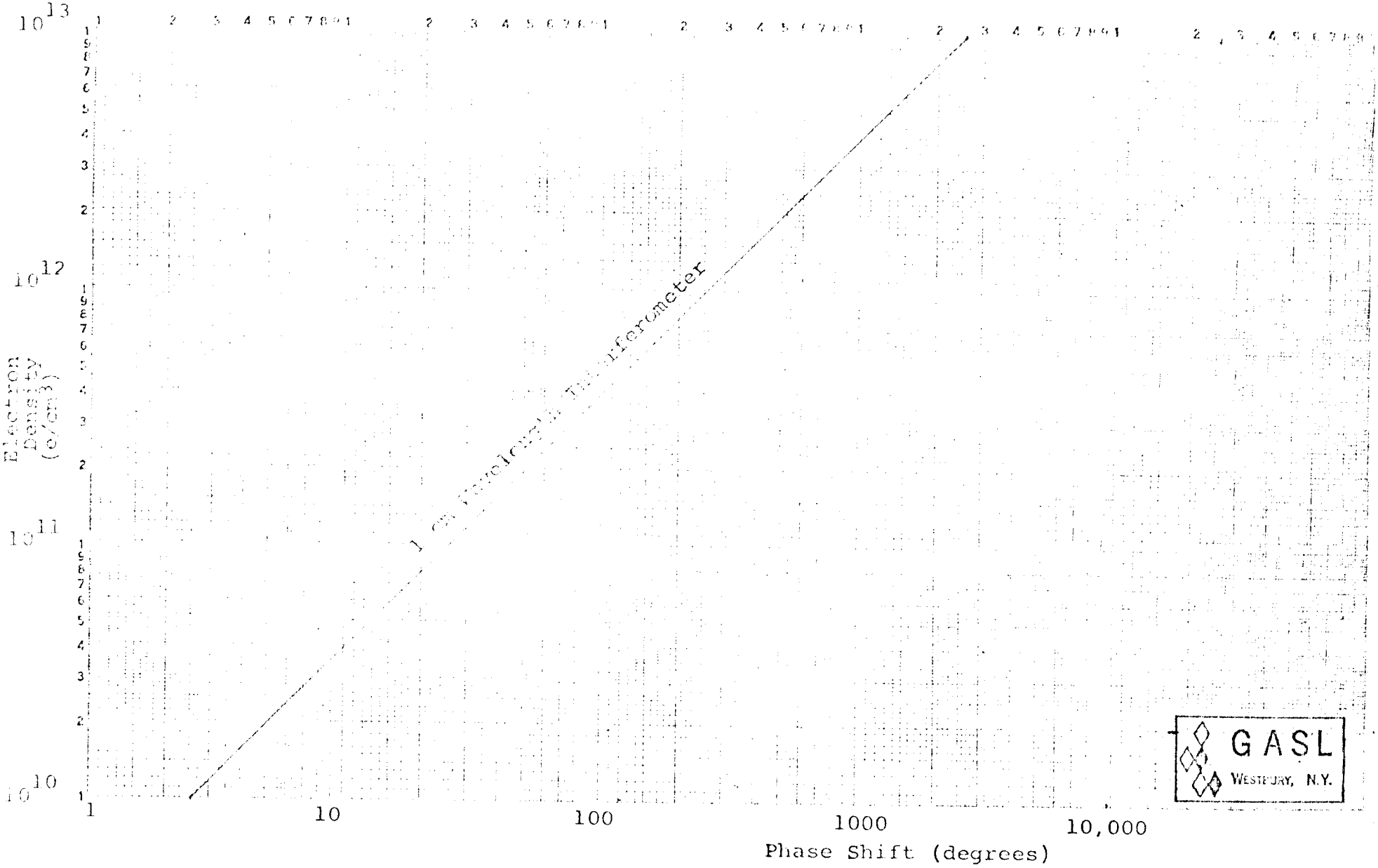

FIGURE 27 : INTERFEROMETER CALIBRATION CURVE
TR No. 527 - NASA Contract NAS5-3929

a) Δ f = 35 Mcs

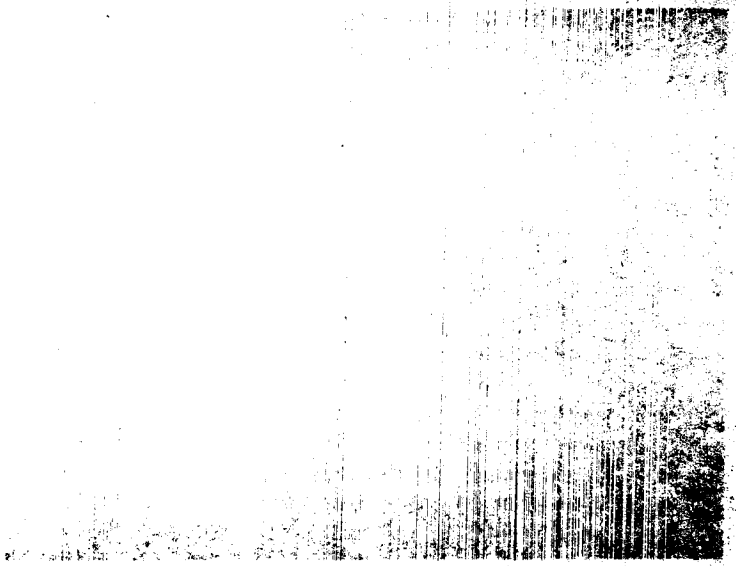

c) Δ f = 97 Mcs

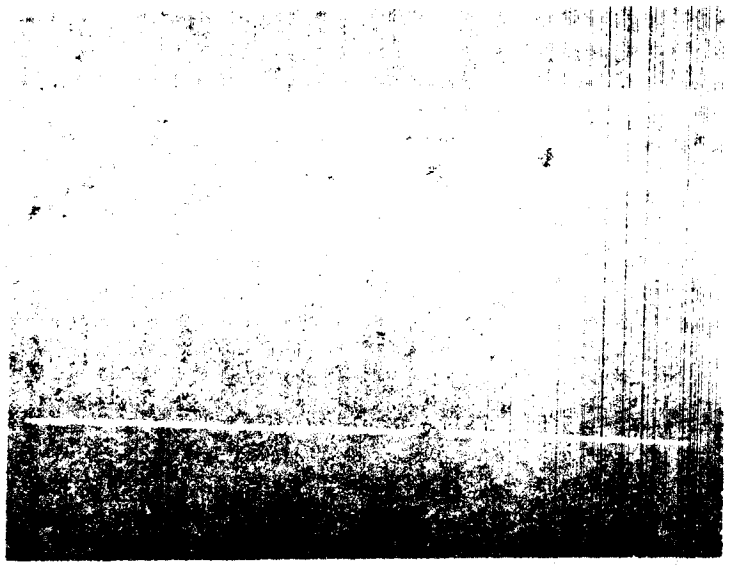

b) Δ f = 64 Mcs
$n_e = 2.5 \times 10^{10}$ e/cm^3

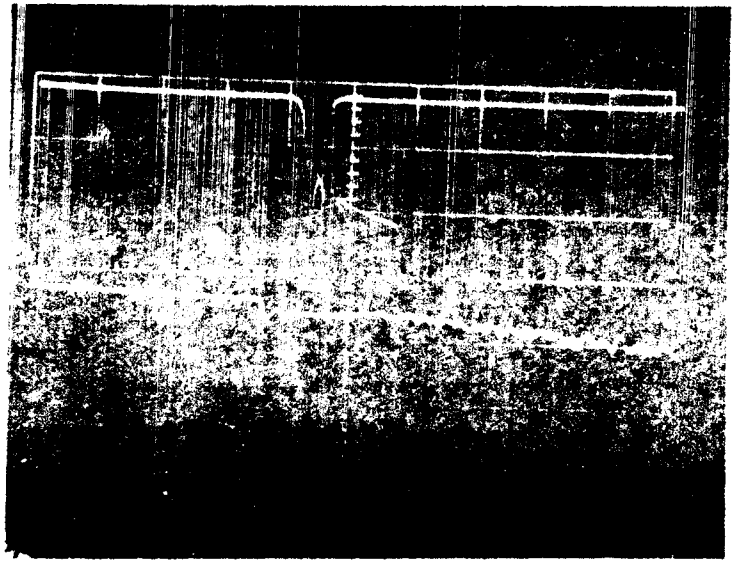

a) $\Delta f = 6$ Mcs

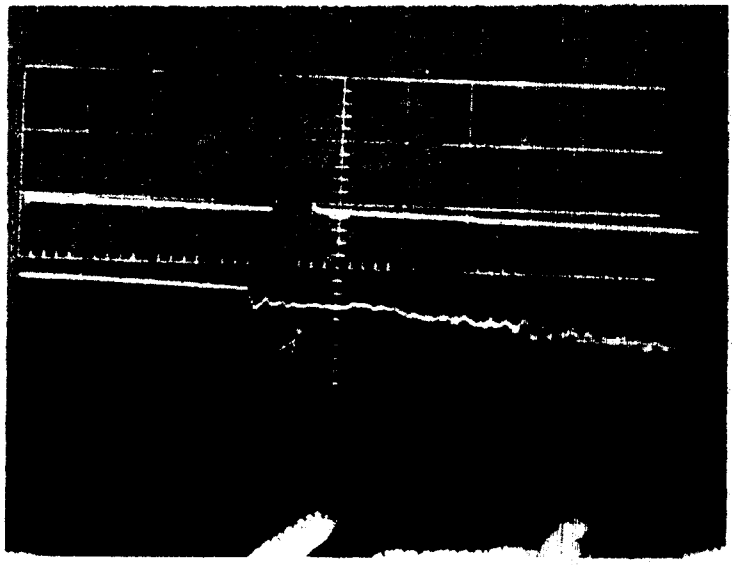

b) $\Delta f = 9$ Mcs
$n_e = 2.0 \times 10^9$ e/cm^3

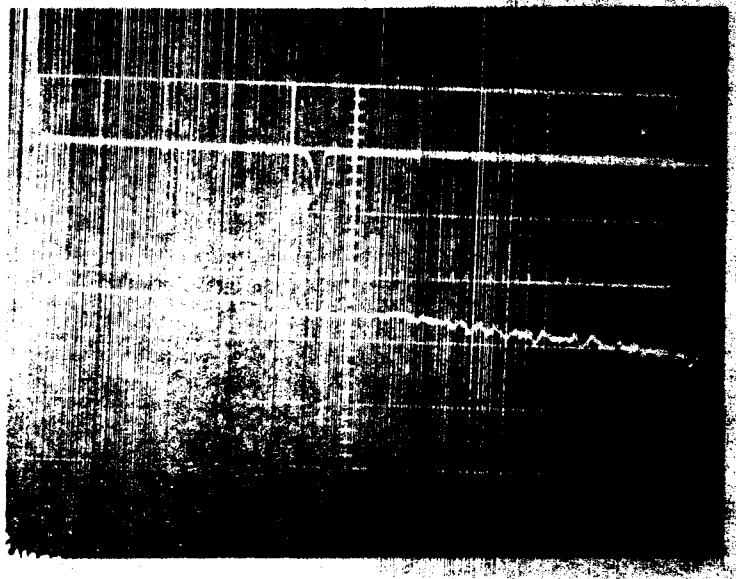

c) $\Delta f = 10$ Mcs

FIG. 30. Example of the Experimental Determination of Electron Density. Upper Trace: output of the 10^{-} cm wavelength probe. Lower Trace: pressure transducer output used to measure velocity.

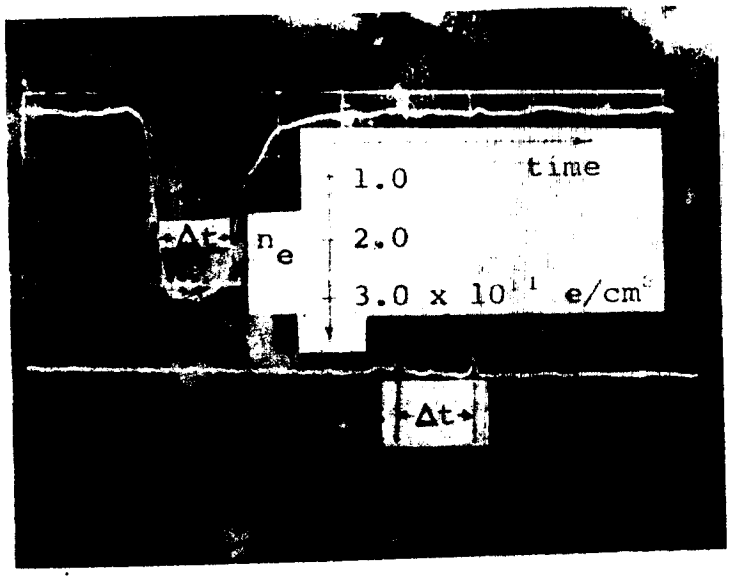

GASL
WESTBURY, N.Y.

Upper Trace: Interferometer trace indicating electron density profile along time axis with respect to the probe. Arrows indicate points where n_e corresponded to the preset cavity frequency for resonant condition.

Lower Trace: Output of the 3 cm wavelength probe indicating resonant peaks due to $\Delta f = 500$ Mcs setting. This setting corresponds to $n_e = 2.0 \times 10^{11}$ e/cm^3 which is indicated by the arrows in the interferometer trace.

FIG. 32. Typical Interferometer Trace

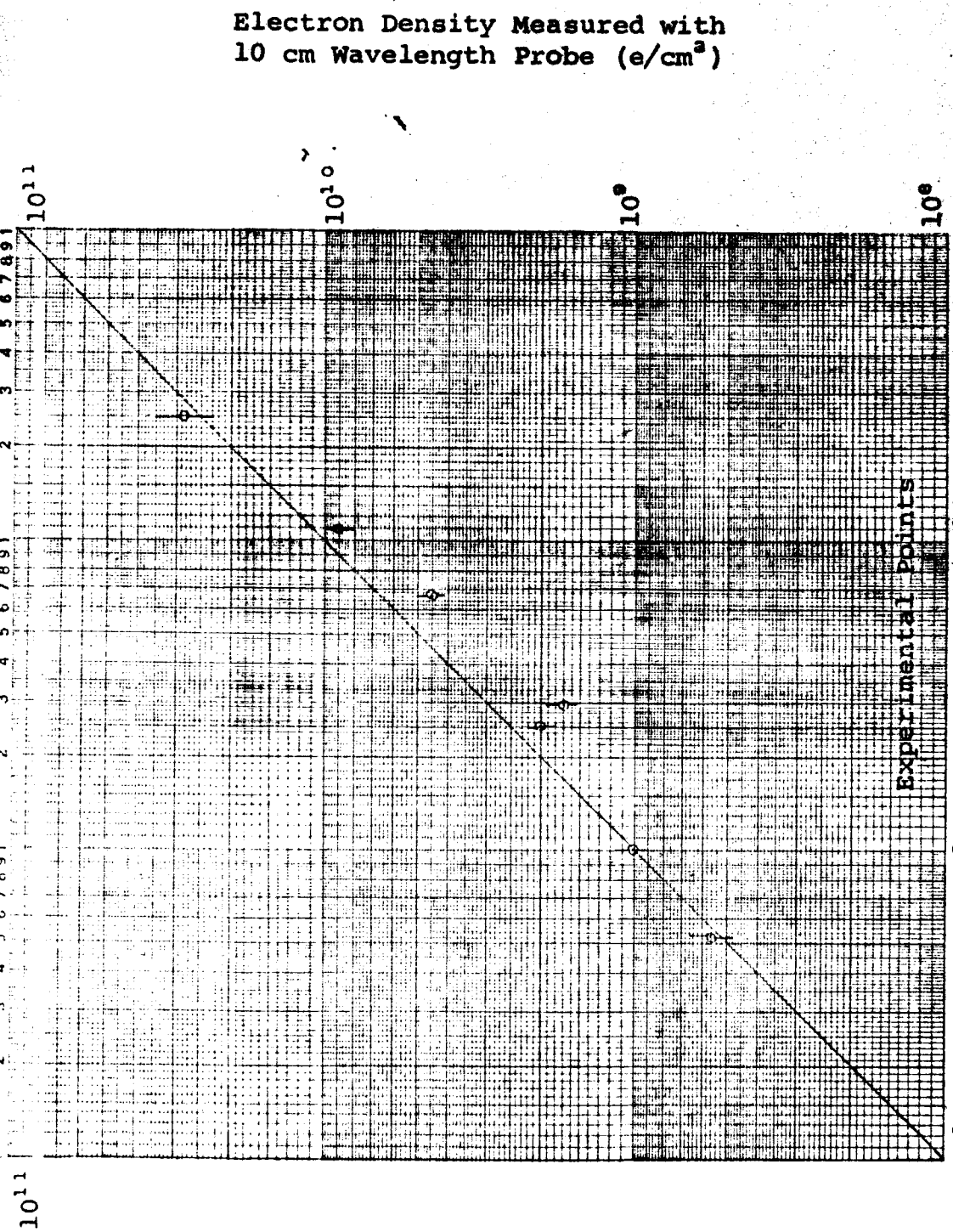

Figure 33: CORRELATION OF ELECTRON DENSITY INDICATIONS FOR THE 10 CM WAVELENGTH PROBE

TR No. 527 - NASA Contract NAS5-3929

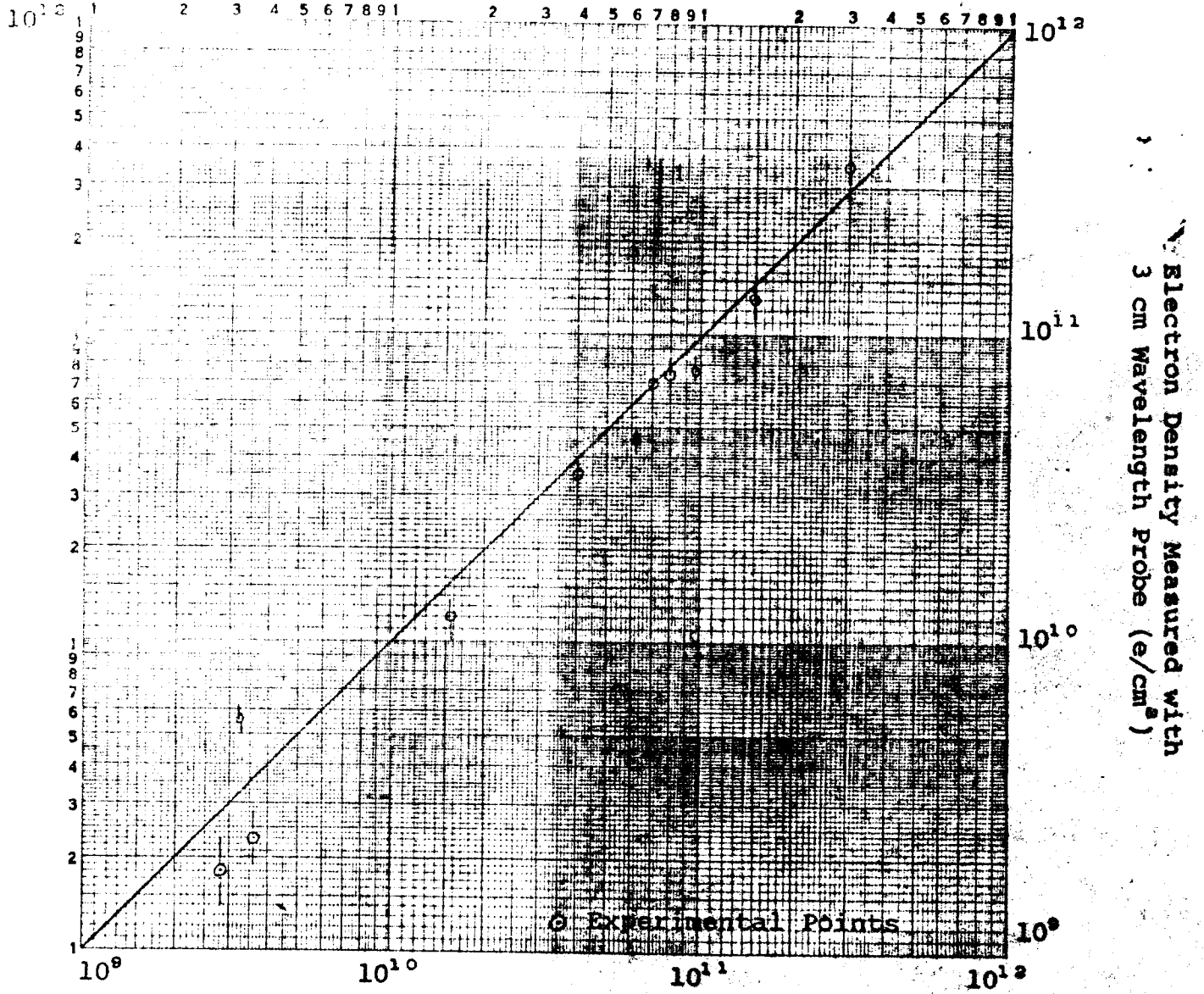

Figure 34: CORRELATION OF ELECTRON DENSITY INDICATIONS FOR THE 3 CM WAVELENGTH PROBE

TR No. 527 - NASA Contract NAS5-3929

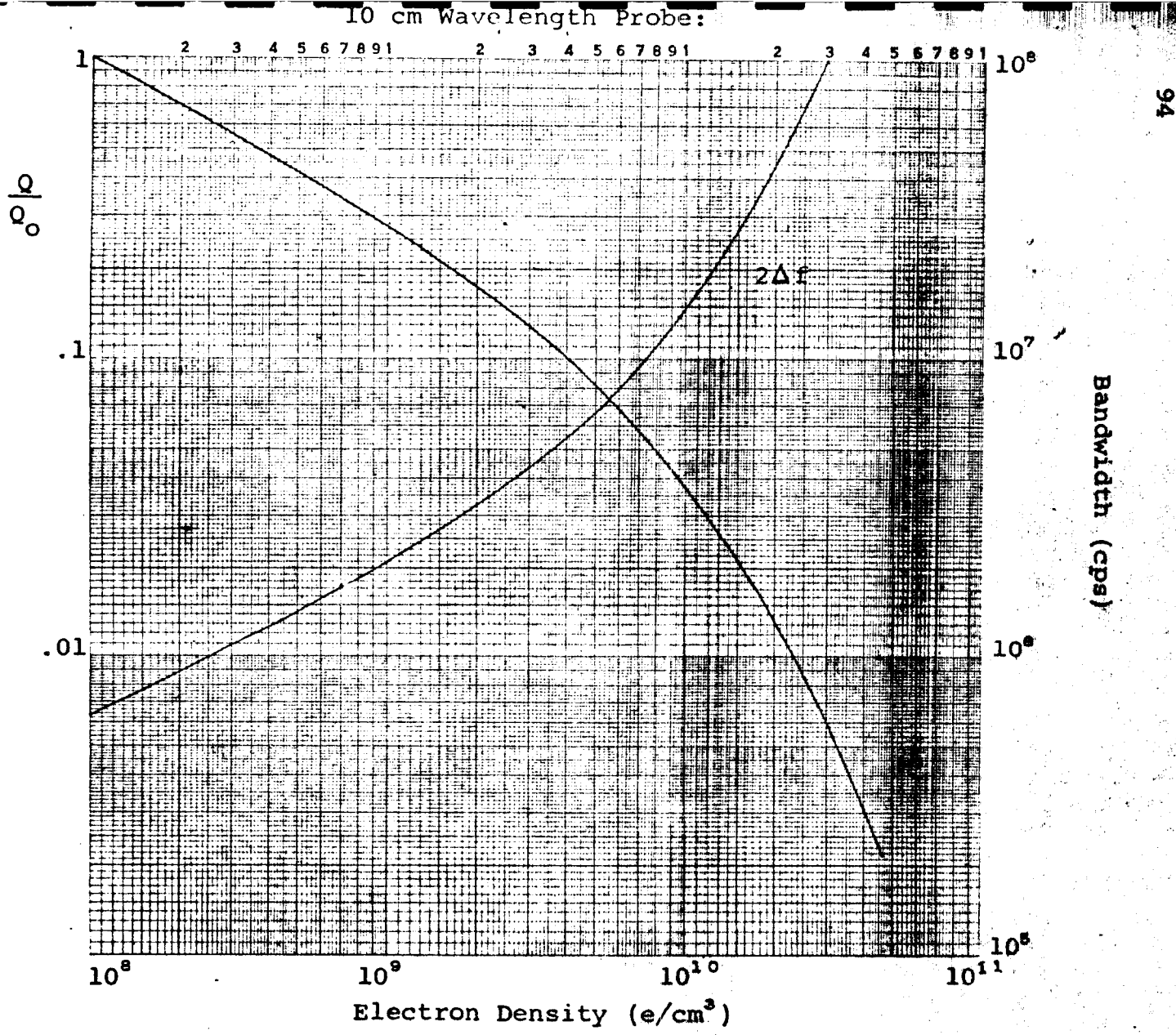

Figure 35: OBSERVED DECAY OF THE QUALITY FACTOR (10 cm Probe)

TR No. 527 - NASA Contract NAS5-3929

3 cm Wavelength Probe:

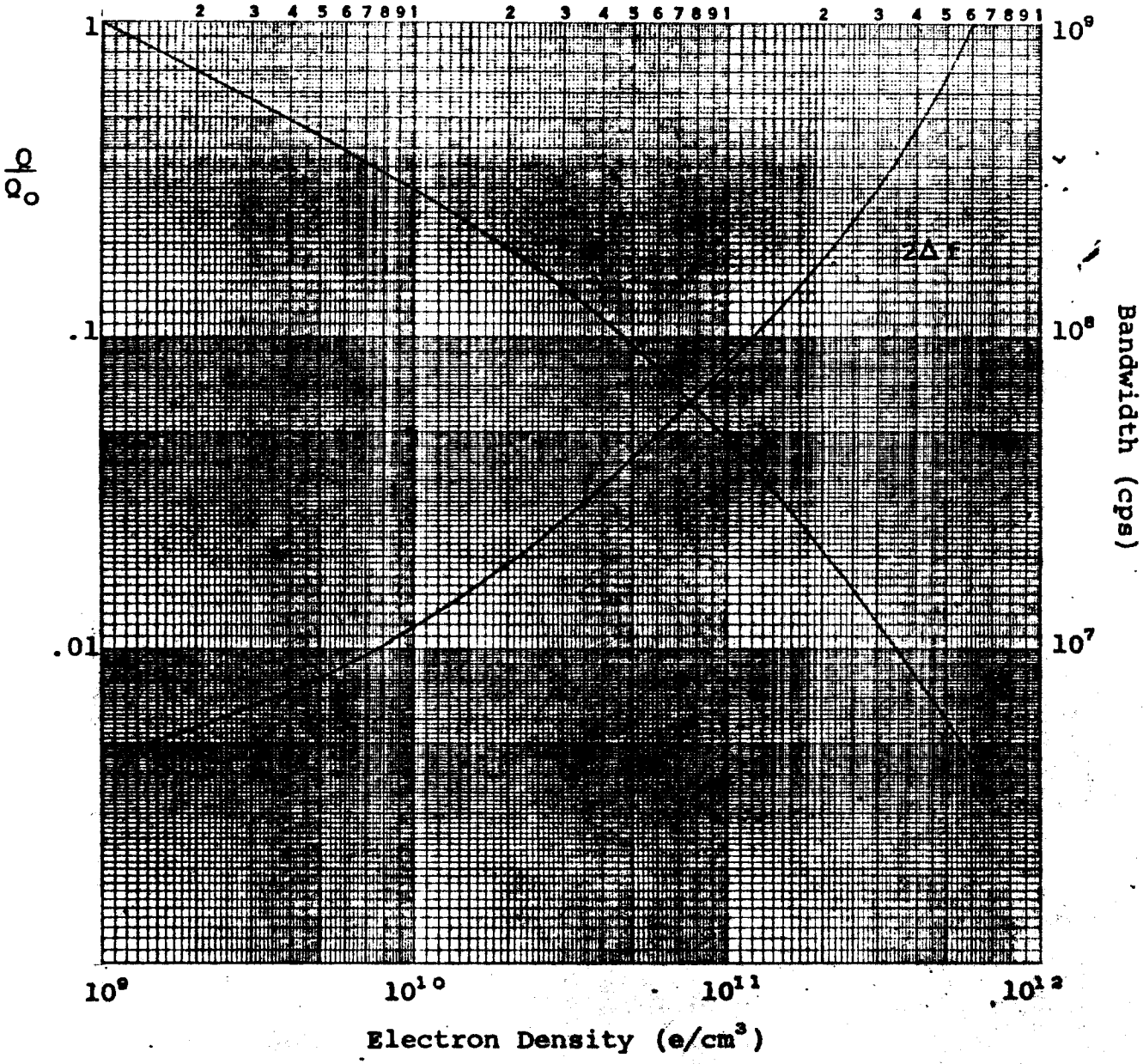

Figure 36: OBSERVED DECAY OF THE QUALITY FACTOR (3 cm Probe)

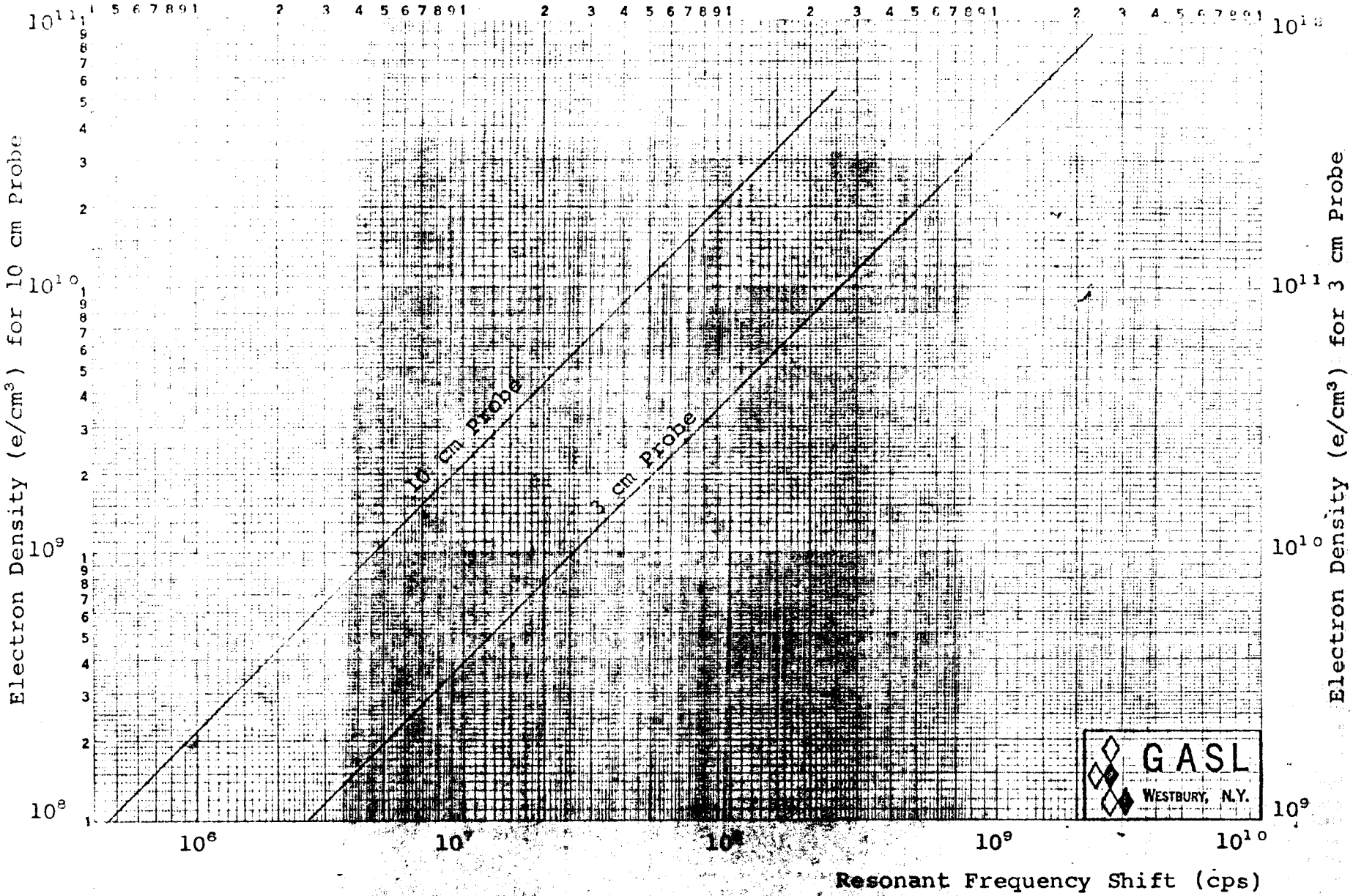

Figure 37: ELECTROMAGNETIC CALIBRATION CHART

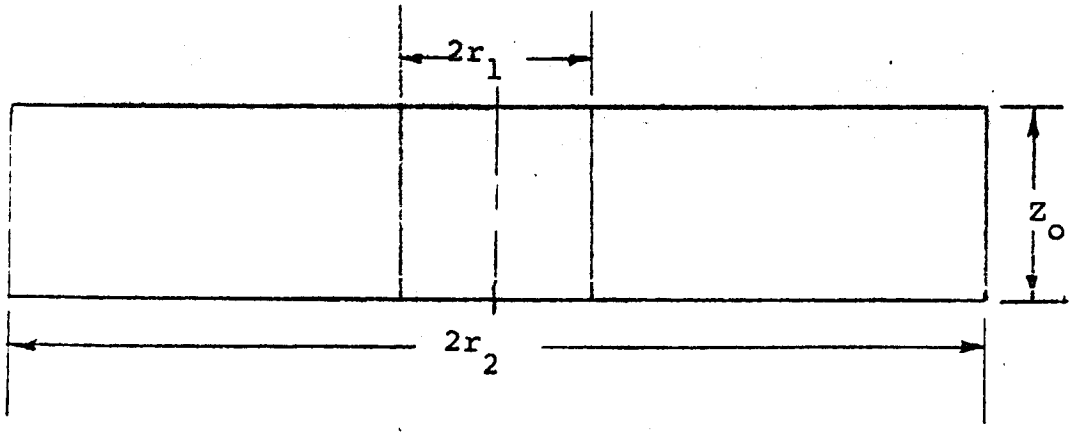

FIGURE 38 : CYLINDRICAL CAVITY

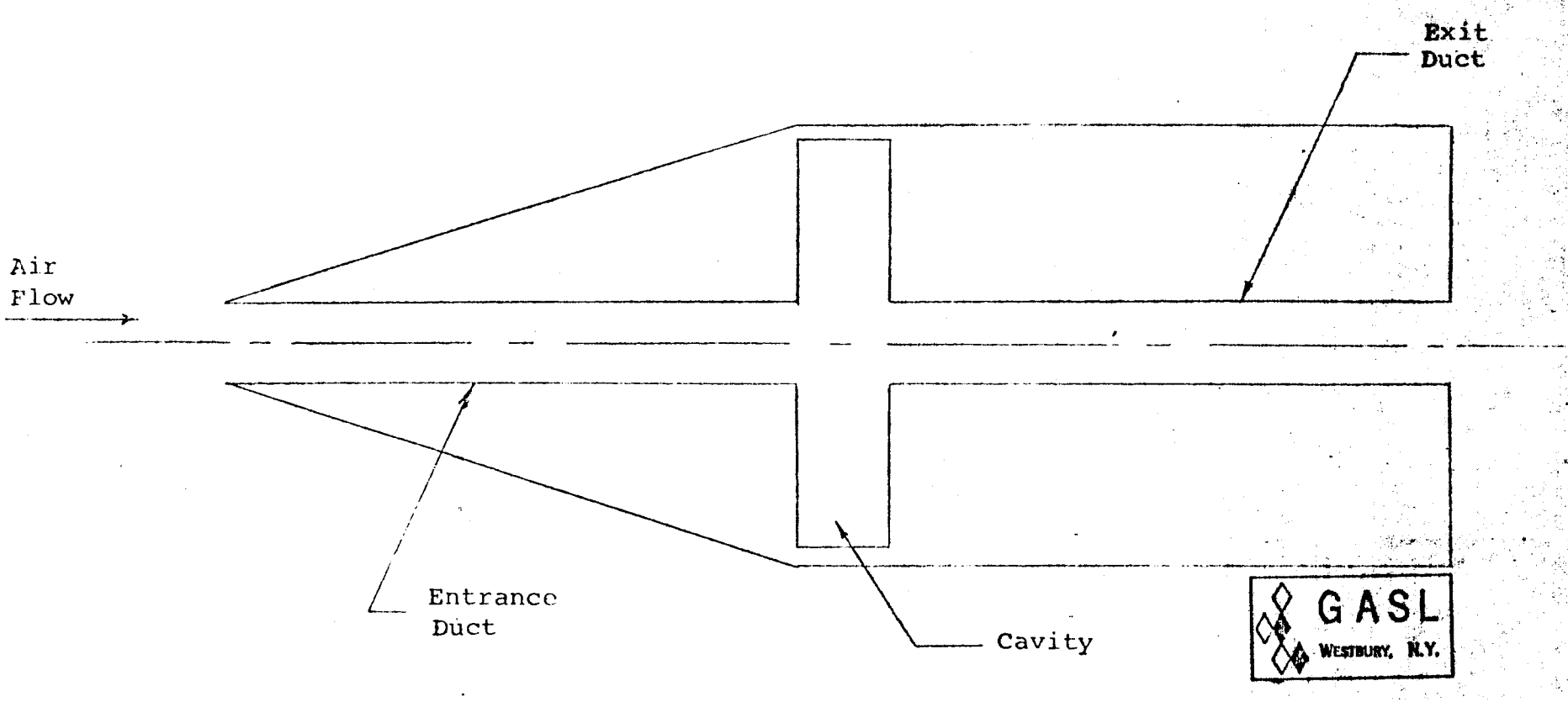

FIGURE 39: GENERALIZED PROBE GEOMETRY

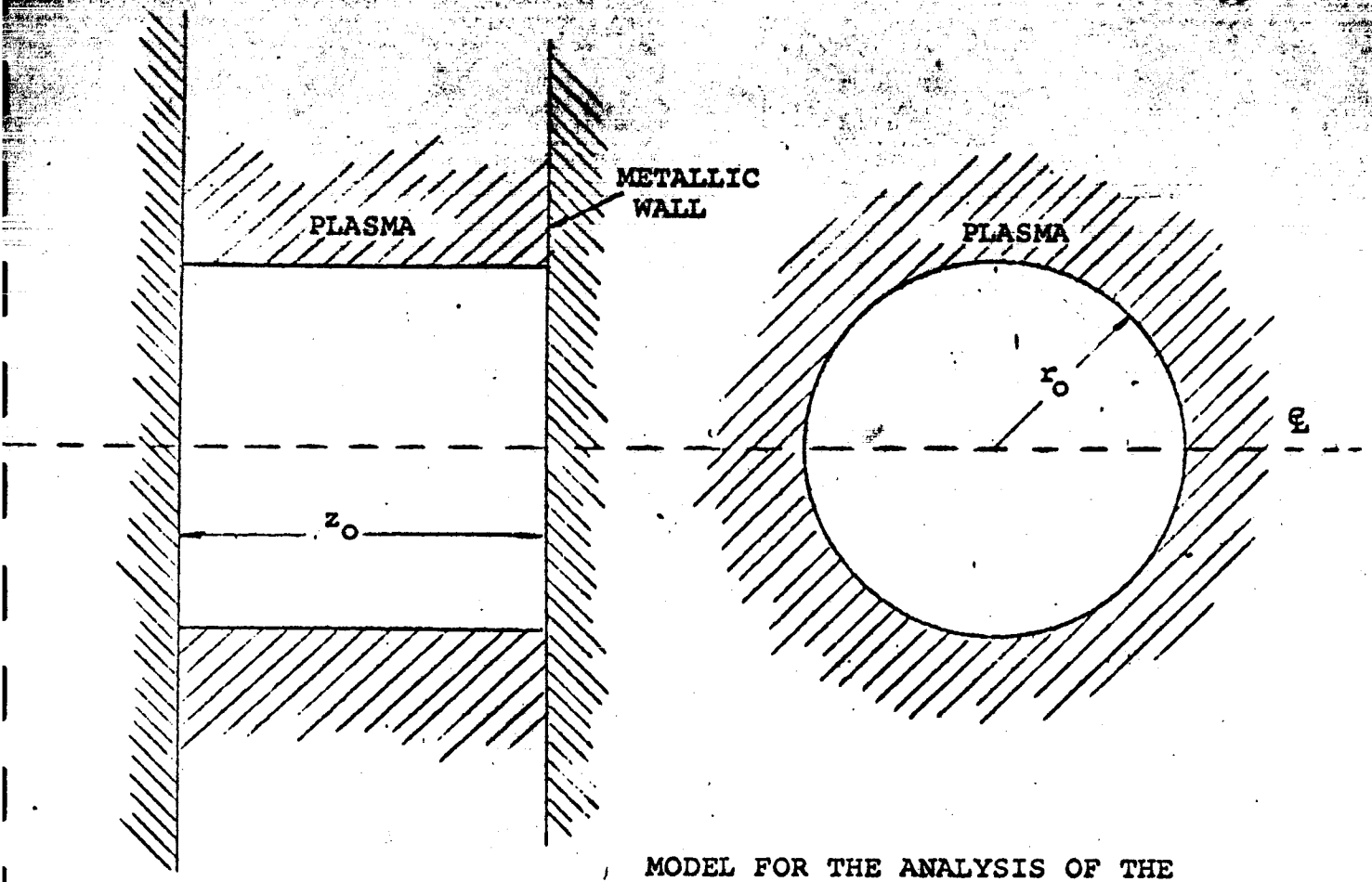

FIGURE 40: MODEL FOR THE ANALYSIS OF THE EXTERNAL CAVITY PROBE

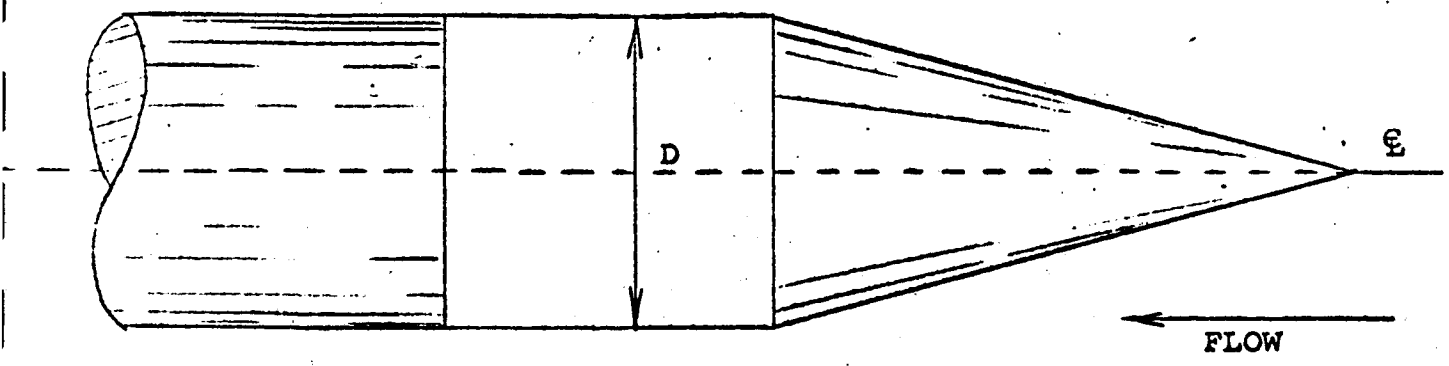

FIG. 41: POSSIBLE CONFIGURATION OF THE EXTERNAL CAVITY PROBE FOR SUPERSONIC FLOW

APPENDIX I

PRINCIPLE OF OPERATION OF THE INTERNAL CAVITY PROBE

This appendix presents an analysis of the operation of an internal cavity probe which essentially follows that given in Ref. 8. The resonant frequency of a cavity depends upon its geometrical shape and the properties of the medium contained inside the cavity. If the cavity is partially filled with a plasma, for small values of both the plasma frequency and the collision frequency compared to the resonant frequency of the cavity the plasma behaves primarily like a dielectric medium, whose index of refraction depends upon the electron concentration. Consequently, the resonant frequency ω of the cavity will depend upon the electron density n_e. The analysis of the resonant condition is performed assuming a cylindrical cavity whose central duct contains a uniform plasma.

A. Oscillation of the Cylindrical Cavity

Let us consider a cylindrical cavity of radius r_2 and height z_o, and let us choose a system of cylindrical coordinates r, θ, z, coaxial with the cavity. The region of the cavity:

$$0 < r < r_1 \quad (r_1 << r_2) \tag{I-1}$$

is assumed to contain a plasma defined by a plasma frequency, ω_p, and an electron collision frequency, ν. The geometry of the cavity is shown in Fig. 38.

We will analyze now the mode of oscillation of the cavity corresponding to a distribution of electromagnetic field with the electric field given by the component E_z and the magnetic field given by the component H_θ. Furthermore, in the region (I-1) in a first-order approximation, the distribution of electric current, due to the electron oscillations, is oriented in the z-direction. Thus the electric current density is given by the component j_z.

If E_z, H_θ, j_z depend upon time t in the form:

$$E_z = E\, e^{i\omega t},\ H_\theta = H\, e^{i\omega t},\ j_z = I\, e^{i\omega t} \tag{I-2}$$

the governing equations in region (I-1) become:

$$\frac{dE}{dr} = i\omega \mu_o H \tag{I-3}$$

$$\frac{1}{r}\frac{d}{dr}(rH) = i\omega \epsilon_o E + I \tag{I-4}$$

$$(\nu + i\omega)\, I = \epsilon_o \omega_p^2 E \tag{I-5}$$

where ϵ_o, μ_o are the electric and magnetic permeabilities of a vacuum, respectively. From the system of Eqs. (I-3), (I-4), and (I-5), we obtain:

$$\frac{1}{r}\frac{d}{dr}\left(r\frac{dE}{dr}\right) + \frac{\omega^2}{c^2}\varkappa^2 E = 0 \qquad \text{(I-6)}$$

where c is the velocity of light in a vacuum:

$$c = (\epsilon_o \mu_o)^{-\frac{1}{2}} \qquad \text{(I-7)}$$

and $\varkappa$ is the refractive index of the plasma:

$$\varkappa = \left(1 - \frac{\omega_p^2}{\omega^2}\frac{1}{1 - i\frac{\nu}{\omega}}\right)^{\frac{1}{2}} \qquad \text{(I-8)}$$

The solution of Eq. (I-6) is:

$$E = E_1 J_o\left(\frac{\omega}{c}\varkappa r\right) + E_2 Y_o\left(\frac{\omega}{c}\varkappa r\right) \qquad \text{(I-9)}$$

where J_o, Y_o are Bessel functions of order zero and of the first and second kind, respectively. E_1, E_2 are arbitrary constants. By virtue of (I-9) and (I-3), we obtain:

$$H = i\sqrt{\frac{\epsilon_o}{\mu_o}}\,\varkappa\left[E_1 J_1\left(\frac{\omega}{c}\varkappa r\right) + E_2 Y_1\left(\frac{\omega}{c}\varkappa r\right)\right] \qquad \text{(I-10)}$$

In the region of the cavity:

$$r_1 < r < r_2 \tag{I-11}$$

we have $\varkappa = 1$ and E, H are given by:

$$E = E_3 \, J_o \left(\frac{\omega}{c} r \right) + E_4 \, Y_o \left(\frac{\omega}{c} r \right) \tag{I-12}$$

$$H = i \sqrt{\frac{\epsilon_o}{\mu_o}} \left[E_3 \, J_1 \left(\frac{\omega}{c} r \right) + E_4 \, J_1 \left(\frac{\omega}{c} r \right) \right] \tag{I-13}$$

where E_3, E_4 are two additional arbitrary constants.

At r = 0, the function E must be finite; consequently:

$$E_2 = 0 \tag{I-14}$$

If the wall of the cavity is assumed to be a perfect electric conductor, E must vanish at $r = r_2$. Thus from (I-12), we have:

$$E_4 = - E_3 \frac{J_o \left(\frac{\omega}{c} r_2 \right)}{Y_o \left(\frac{\omega}{c} r_2 \right)} \tag{I-15}$$

and in the region (I-11), the electromagnetic field is given by:

$$E = E_3 \left[J_o \left(\frac{\omega}{c} r \right) - \frac{J_o \left(\frac{\omega}{c} r_2 \right)}{Y_o \left(\frac{\omega}{c} r_2 \right)} Y_o \left(\frac{\omega}{c} r \right) \right] \qquad \text{(I-16)}$$

$$H = i E_3 \sqrt{\frac{\epsilon_o}{\mu_o}} \left[J_1 \left(\frac{\omega}{c} r \right) - \frac{J_o \left(\frac{\omega}{c} r_2 \right)}{Y_o \left(\frac{\omega}{c} r_2 \right)} Y_1 \left(\frac{\omega}{c} r \right) \right] \qquad \text{(I-17)}$$

At the surface $r = r_1$, both E and H must be continuous. Thus, taking into account the condition (I-14), we obtain the system of equations:

$$J_o \left(\frac{\omega}{c} \varkappa r_1 \right) E_1 - \left[J_o \left(\frac{\omega}{c} r_1 \right) - \frac{J_o \left(\frac{\omega}{c} r_2 \right)}{Y_o \left(\frac{\omega}{c} r_2 \right)} Y_o \left(\frac{\omega}{c} r_1 \right) \right] E_3 = 0$$

$$\varkappa J_1 \left(\frac{\omega}{c} \varkappa r_1 \right) E_1 - \left[J_1 \left(\frac{\omega}{c} r_1 \right) - \frac{J_o \left(\frac{\omega}{c} r_2 \right)}{Y_o \left(\frac{\omega}{c} r_2 \right)} Y_1 \left(\frac{\omega}{c} r_1 \right) \right] E_3 = 0$$

(I-18)

By virtue of (I-18), ω must satisfy the equation:

$$\varkappa \frac{J_1 \left(\frac{\omega}{c} \varkappa r_1 \right)}{J_o \left(\frac{\omega}{c} \varkappa r_1 \right)} = \frac{J_1 \left(\frac{\omega}{c} r_1 \right) Y_o \left(\frac{\omega}{c} r_2 \right) - J_o \left(\frac{\omega}{c} r_2 \right) Y_1 \left(\frac{\omega}{c} r_1 \right)}{J_o \left(\frac{\omega}{c} r_1 \right) Y_o \left(\frac{\omega}{c} r_2 \right) - J_o \left(\frac{\omega}{c} r_2 \right) Y_o \left(\frac{\omega}{c} r_1 \right)}$$

(I-19)

By solving (I-19), we obtain the complex values of ω. The real part of ω gives the resonant frequency of the cavity and the imaginary part gives the damping of the oscillations, due to the energy losses inside the plasma.

B. Resonant Frequency and Damping of the Oscillations

Let us assume first:

$$\varkappa = 1 \tag{I-20}$$

In this particular case, Eq. (I-19) reduces to:

$$J_o\left(\frac{\omega}{c} r_2\right)\left[J_o\left(\frac{\omega}{c} r_1\right) Y_1\left(\frac{\omega}{c} r_1\right) - J_1\left(\frac{\omega}{c} r_1\right) Y_o\left(\frac{\omega}{c} r_1\right)\right] = 0 \tag{I-21}$$

$$\frac{2\,c}{\pi\,\omega\,r_1} J_o\left(\frac{\omega}{c} r_2\right) = 0 \tag{I-22}$$

Thus the resonant frequencies of the cavity without the plasma in the region $0 < r < r_1$ are given by the roots of the Bessel function J_o. In particular the fundamental resonant frequency is given by:

$$\frac{\omega}{c} r_2 \sim 2.40 \tag{I-23}$$

Let us suppose now that the refractive index of the plasma is:

$$\varkappa = 1 - \delta \tag{I-24}$$

where δ is a complex quantity, such that:

$$|\delta| << 1 \tag{I-25}$$

The new resonant frequency of the cavity will be

$$\omega = \omega_o + \Delta\omega \tag{I-26}$$

where ω_o is the frequency corresponding to $\varkappa = 1$. In a general case $\Delta\omega$ is a complex quantity and we assume:

$$|\Delta\omega| << \omega_o \tag{I-27}$$

By virtue of (I-25) and (I-27), in a first-order approximation, Eq. (I-19) becomes:

$$\frac{2c}{\pi\omega r_1} J_o\left(\frac{\omega}{c} r_2\right) + Y_o\left(\frac{\omega}{c} r_2\right)\left[J_o\left(\frac{\omega}{c}\varkappa r_1\right) J_1\left(\frac{\omega}{c} r_1\right) - \varkappa J_1\left(\frac{\omega}{c}\varkappa r_1\right) J_o\left(\frac{\omega}{c} r_1\right)\right] \sim 0 \tag{I-28}$$

Let us call:

$$\frac{\omega_o}{c} r_1 = x_o \qquad \text{(I-29)}$$

we have

$$\frac{\omega}{c} \varkappa r_1 = \frac{r_1}{c} (\omega_o + \Delta \omega) (1-\delta) \sim x_o (1+\alpha) \qquad \text{(I-30)}$$

where

$$\alpha = \frac{\Delta \omega}{\omega_o} - \delta \qquad \text{(I-31)}$$

In Eq. (28) we have:

$$J_o\left(\frac{\omega}{c} \varkappa r_1\right) J_1\left(\frac{\omega}{c} r_1\right) - \varkappa J_1\left(\frac{\omega}{c} \varkappa r_1\right) J_o\left(\frac{\omega}{c} r_1\right)$$

$$\sim \left[J_o(x_o) + J_o'(x_o)\, x_o\, \alpha\right] \left[J_1(x_o) + J_1'(x_o)\, x_o \frac{\Delta \omega}{\omega_o}\right]$$

$$- (1-\delta) \left[J_1(x_o) + J_1'(x_o) x_o \alpha\right] \left[J_o(x_o) + J_o'(x_o) x_o \frac{\Delta \omega}{\omega_o}\right]$$

where J' are the derivatives of the Bessel functions:

$$J'(x_o) = \left(\frac{d\, J(x)}{dx}\right)_{x=x_o} \qquad \text{(I-33)}$$

If (I-31) is taken into account, (I-32) reduces to:

$$\delta \left\{J_o(x_o)\, J_1(x_o) - x_o \left[J_o'(x_o)\, J_1(x_o) - J_o(x_o)\, J_1'(x_o)\right]\right\} \qquad \text{(I-34)}$$

On the other hand:

$$J_o'(x_o) = -J_1(x_o); \quad J_1'(x_o) = J_o(x_o) - \frac{1}{x_o} J_1(x_o) \tag{I-35}$$

Thus:

$$J_o'(x_o)\, J_1(x_o) - J_o(x_o)\, J_1'(x_o) = -J_o^2(x_o) - J_1^2(x_o) + \frac{1}{x_o} J_o(x_o)\, J_1(x_o) \tag{I-36}$$

and (I-34) becomes:

$$\left[J_o^2(x_o) + J_1^2(x_o)\right] x_o\, \delta \tag{I-37}$$

Hence, Eq. (28) reduces to:

$$\frac{2c}{\pi \omega_o r_1} J_o\left(\frac{\omega}{c} r_2\right) + Y_o\left(\frac{\omega}{c} r_2\right) \left[J_o^2\left(\frac{\omega_o}{c} r_1\right) + J_1^2\left(\frac{\omega_o}{c} r_1\right)\right] \frac{\omega_o}{c} r_1\, \delta \sim 0 \tag{I-38}$$

The first term in (I-38) transforms to:

$$\frac{2c}{\pi \omega_o r_1} J_o\left(\frac{\omega}{c} r_2\right) \sim -\frac{2 r_2\, \epsilon}{\pi \omega_o r_1} J_1\left(\frac{\omega_o}{c} r_2\right) \tag{I-39}$$

and Eq. (38) becomes:

$$\frac{\Delta\omega}{\omega} \sim \frac{\pi}{2}\left(\frac{r_1}{r_2}\right)^2 \frac{\omega_o r_2}{c} \frac{Y_o\left(\frac{\omega_o}{c} r_2\right)}{J_1\left(\frac{\omega_o}{c} r_2\right)}\left[J_o^2\left(\frac{\omega_o}{c} r_1\right) + J_1^2\left(\frac{\omega_o}{c} r_1\right)\right] \delta \tag{I-40}$$

which gives the change of the resonant frequency and the damping of the oscillations, due to the plasma, assuming that the plasma represents a small perturbation of the empty cylindrical cavity.

In order to satisfy the condition (I-25), we assume in Eq. (I-8):

$$\omega_p \ll \omega \tag{I-41}$$

Thus for $\omega = \omega_o$, the refractive index becomes:

$$\varkappa \sim 1 - \frac{1}{2}\frac{\omega_p^2}{\omega_o^2}\frac{1 + i\frac{\nu}{\omega_o}}{1 + \frac{\nu^2}{\omega_o^2}} \tag{I-42}$$

i.e.,

$$\mathrm{Re}\ (\delta) \sim \frac{1}{2}\frac{\omega_p^2}{\omega_o^2}\frac{1}{1 + \frac{\nu^2}{\omega_o^2}} \tag{I-43}$$

and

$$Im(\delta) \sim \frac{1}{2} \frac{\omega_p^2}{\omega_o^2} \frac{1}{1 + \frac{\nu^2}{\omega_o^2}} \frac{\nu}{\omega_o} \qquad \text{(I-44)}$$

By means of (I-43) and (I-44), we may evaluate from Eq. (40) both the real and the imaginary parts of $\Delta \omega$.

It is necessary to emphasize that in order to detect a change of the resonant frequency of the cavity, the order of magnitude of the imaginary part of $\Delta \omega$ must be smaller than the order of magnitude of the real part of $\Delta \omega$. Otherwise the effect of the plasma would be primarily a broadening of the resonance curve of the cavity. This condition is satisfied if:

$$\nu \ll \omega_o \qquad \text{(I-45)}$$

Consequently, the resonant frequency of the empty cavity gives the maximum value of the collision frequency which allows the possibility of measuring the change of the resonant frequency due to the plasma. For instance, for a 3 cm wavelength cavity, the maximum value of ν would be:

$$\nu_{max} \sim 10^{10} \qquad \text{(I-46)}$$

If ω_o corresponds to the fundamental resonant frequency of the cavity, given by (I-23), Eq. (I-40) becomes:

$$\frac{\Delta \omega}{\omega_o} \sim 3.71 \left(\frac{r_1}{r_2}\right)^2 \left[J_o^2 \left(2.4 \frac{r_1}{r_2}\right) + J_1^2 \left(2.4 \frac{r_1}{r_2}\right)\right] \delta \qquad \text{(I-47)}$$

We observe that the real part of $\Delta \omega$ is a positive quantity, which means that the resonant frequency of the cavity increases with the injection of the plasma in the central region $0 < r < r_1$. Furthermore, the resonant frequency increases rapidly with the dimension r_1.

The plasma frequency ω_p is related to the electron density n_e by the equation:

$$\omega_p = \left(\frac{n_e q_o^2}{\epsilon_o m_e}\right)^{\frac{1}{2}} \qquad \text{(I-48)}$$

where q_o, m_e are the electric charge and the mass of an electron. The numerical value of $\omega_p/2\pi$ is:

$$\frac{\omega_p}{2\pi} \sim 8.97 \, n_e^{\frac{1}{2}} \qquad \text{(I-49)}$$

where n_e is the number of electrons per cubic meter. Thus assuming always a 3 cm wavelength cavity, the useful range

of the order of magnitude of n_e which may be measured with this technique is:

$$O(n_e) \leq 10^{18} \text{ el/m}^3 \qquad \text{(I-50)}$$

APPENDIX II

PRINCIPLE OF OPERATION OF THE EXTERNAL CAVITY PROBE

The reflection properties of an electromagnetic wave of angular frequency ω_o at the interface of an overdense collisionless plasma ($\omega_p > \omega_o$, $\nu = 0$) can be used as the principle of operation of a probe intended to measure electron densities.

The basic idea is to have a partially open resonant cavity. When this device is immersed in an overdense plasma it becomes a closed structure with the resonant frequency a function of the penetration of the electromagnetic field inside the plasma. This penetration is a function of the electron density, consequently a correlation between resonant frequency and electron density can be established.

The propagation constant inside the plasma is imaginary and equal to

$$k_2 = i \frac{\omega_o}{c} \sqrt{\frac{\omega_p^2}{\omega_o^2} - 1} \qquad \text{(II-1)}$$

where $i = \sqrt{-1}$

c = speed of light in a vacuum.

For $\omega_p >> \omega_o$

$$\left| k_a \right| \sim \frac{\omega_p}{c} \qquad \text{(II-2)}$$

Thus the penetration depth of the electromagnetic wave inside the plasma is given by

$$\left| \frac{1}{k_a} \right| \sim \frac{c}{\omega_p} \qquad \text{(II-3)}$$

The results are essentially the same if either a plane or a cylindrical geometry is considered.

An analysis of the electromagnetic performance (resonant frequency versus electron density) of a probe using this principle of operation can be made using the model shown in Fig. 40.

A cylindrical cavity formed by two perfectly conducting parallel planes and a cylindrical electromagnetically transparent sheet of internal radius r_o, which separates the internal region of the cavity from the plasma region, are assumed. The thickness of the cylindrical wall is assumed negligible. The plasma located outside of the cylinder is uniform and the metallic planes are assumed infinite in extent.

For $\omega_p < \omega_o$ the electromagnetic field is radiated in the radial direction between the metallic planes, and a well defined resonance condition is not found. Only an overdense plasma $\omega_p > \omega_o$ will lead to a total reflection of the electromagnetic wave. A change in ω_p means a change in penetration depth and consequently of the resonant frequency.

The TE_{011} mode seems to be a suitable one because it has no currents between the plasma and the walls of the cavity.

The dispersion equation is

$$\frac{1}{x}\frac{J_1(x)}{J_0(x)} = -\frac{1}{y}\frac{K_1(y)}{K_0(y)} \qquad \text{(II-4)}$$

where J_0 and J_1 are the Bessel functions of the first kind of order $_0$ and $_1$ respectively, x and y are given by

$$x = r_o\sqrt{\frac{\omega^2}{c^2} - \frac{\pi^2}{Z^2}} \qquad \text{(II-5)}$$

$$y = r_o\sqrt{\frac{\omega^2}{c^2}\left[\left(\frac{\omega_p}{\omega}\right)^2 - 1\right] + \frac{\pi^2}{Z^2}} \qquad \text{(II-6)}$$

where c is the velocity of light in vacuum. The solution

can be obtained graphically but the analysis of the asymptotic behavior can be performed very easily. Assume $\omega_p >> \omega$. In Eq. (II-4) one has

$$\lim_{\frac{\omega_p}{\omega} \to \infty} x = x_o = 3.832$$

where x_o is the first root of $J_1(x) = 0$ and

$$\lim_{\frac{\omega_p}{\omega} \to \infty} \frac{K_1(y)}{K_o(y)} = 1$$

Thus Eq. (II-4) yields

$$\frac{1}{x} \frac{J_1(x)}{J_o(x)} \sim \frac{1}{y} \qquad \text{(II-7)}$$

By substituting in Eq. (II-7)

$$x = x_o + \delta_x \text{ with the condition } \left|\delta_x\right| << x_o$$

one has

$$J_1(x) \sim J_o(x_o)\delta_x$$

and the equation simplifies to

$$\frac{\delta_x}{x_o} \sim -\frac{1}{y_o} = -\frac{c}{r_o \omega_p}$$

The resonant frequency of the cavity is $\omega = \omega_o + \delta_\omega$ where ω_o is the resonant frequency when $\omega_p \to \infty$. ω_o is given by

$$\omega_o = c\sqrt{\frac{\pi^2}{z_o^2} + \frac{x_o^2}{r_o^2}}$$

In Eq. (II-8) one has

$$x = r_o\sqrt{\frac{\omega_o^2}{c^2} - \frac{\pi^2}{x^2} + \frac{2\omega_o}{c^2}\frac{\delta_\omega}{\omega_o}} = x_o\left[1 + \frac{\omega_o r_o}{c^2}\frac{1}{x_o^2}\frac{\delta_\omega}{\omega_o}\right]$$

Thus

$$\frac{\delta_x}{x_o} = \frac{\omega_o^2 r_o^2}{c^2}\frac{1}{x^2}\frac{\delta_\omega}{\omega_o}$$

and Eq. (II-7) yields:

$$\frac{\delta_\omega}{\omega_o} = -\frac{\omega_o}{\omega_p}\frac{x_o^2}{\left(\frac{\omega_o r_o}{c}\right)^3} = -\frac{k}{\sqrt{n_e}} \qquad \text{(II-8)}$$

where

$$k = \frac{\omega_o x_o^2}{\left(\frac{\omega_o r_o}{c}\right)^3 \frac{e}{(m\epsilon_o)^{\frac{1}{2}}}},$$

n_e is the electron density; ϵ_o the permittivity of a vacuum; e and m are the electron charge and mass, respectively. One can conclude that the relative change of

resonant frequency of the cavity is inversely proportional to the square root of the electron density.

To estimate the range of application of this probe $\frac{\delta\omega}{\omega_o} = Q^{-1}$ may be assumed to give the minimum detectable frequency shift, i.e., the resolution of the instrument.

$$\left(\frac{\delta\omega}{\omega_o}\right)_{min} = \frac{1}{Q} = \frac{\omega_o}{\omega_p} \frac{x_o^2}{\left(\frac{\omega_o r_o}{c}\right)^3}$$

For $\omega = 2\pi \times 3$ KM$_c$, $r_o = 8$ cm, $x_o = 3.83$ we can expect a Q of 10^3 as a maximum value. One gets $\omega_p = 1.8 \times 10^{12}$ rad/sec corresponding to $n_e = 10^{15}$ e/cm^3, giving margin for additional reduction of the sensitivity.

On the other hand the condition $\omega_o \leq \omega_p$ must be satisfied. Consequently the minimum electron density is 10^{11} e/cc for the operating frequency of 3 KM$_c$/sec.

It is worthwhile pointing out that the minimum operating frequency is related to a maximum acceptable size for the cavity. The flow field boundary layer and the plasma transport processes may change the electron density close to the wall. The thickness of this region of nonuniform plasma distribution must be smaller than the penetration

depth of the electromagnetic wave in the plasma. Preliminary calculations indicate that this condition can be satisfied up to a range of electron densities of the order of 10^{14} e/cc, where the penetration depth of the electromagnetic field is estimated to be of the order of 1 mm.

Additional limitations are encountered when one considers the effects of collision frequency. When $\nu \neq 0$ the equation for the frequency shift with $\frac{\omega_o}{\omega_p} << 1$ is:

$$\frac{\delta\omega}{\omega_o} \sim \frac{x_o^2}{\left(\frac{\omega_o r_o}{c}\right)^3} \frac{\omega_o}{\omega_p} \sqrt{1 - i\frac{\nu}{\omega_o}}$$

Thus in order to obtain a simple correlation between the actual frequency shift $R_e\left(\frac{\delta\omega}{\omega_o}\right)$ and the electron density, one must have $\frac{\nu}{\omega_o} < 1$. For this condition the relation given in Eq. (II-8) can be used. The plasma generated during the reentry is estimated to satisfy this condition as well as the plasmas obtained in the shock tubes used to check the probe.

A possible configuration of a probe to measure electron density in a supersonic flow according to this principle is shown in Fig. 41.

The final dimensions of the probe will change linearly with the microwave wavelength being used, with the square root of the relative dielectric constant of the material filling the cavity and with the use of more sophisticated resonant structures. The maximum diameter of the probe shown in Fig. 33, (10 cm wavelength, $\epsilon_r = 4$) is estimated to be approximately 3 inches. Smaller sizes can be obtained by reducing the wavelength; however, this will raise the minimum measurable electron density, consequently the range of operation will be narrowed because the upper limit, 10^{14} e/cm^3, is fixed essentially by boundary effects.

APPENDIX III

LOW PHASE VELOCITY STRUCTURE PROBE

A probe can be developed with the basic idea of measuring the propagation properties of a dielectric waveguide located in the ionized flow field. In order to describe the principles of operations of such a probe assume a dielectric rod of circular cross section of radius r_o, located in a plasma. A detailed study of the propagation properties of a dielectric rod can be found in Ref. 9.

Let $\varkappa_1$ be the index of refraction of the dielectric rod. If the medium surrounding the rod is a uniform lossless plasma its index of refraction is given by

$$\varkappa_2 = \sqrt{1 - \left(\frac{\omega_p}{\omega}\right)^2} \qquad \text{(III-1)}$$

where ω_p is the plasma frequency and ω is the angular frequency of the electromagnetic field. Furthermore, assume a fundamental TM mode of operation of the dielectric waveguide. The dispersion equation is:

$$\frac{\varkappa_1^2}{x}\frac{J_1(x)}{J_0(x)} = -\frac{\varkappa_2^2}{y}\frac{K_1(y)}{K_0(y)} \qquad \text{(III-2)}$$

where J_0 and J_1 are the Bessel function of the first kind of order 0 and 1 respectively. K_0 and K_1 are the modified Hankel functions of order 0 and 1 respectively. x, y are given by

$$\left.\begin{aligned} x^2 &= k_0^2 \varkappa_1^2 r_0^2 - k_z^2 r_0^2 \\ y^2 &= - k_0^2 \varkappa_2^2 r_0^2 + k_z^2 r_0^2 \end{aligned}\right\} \qquad \text{(III-3)}$$

k_0 is the propagation constant in a vacuum and k_z is the axial propagation constant in the dielectric waveguide.

Assume for instance that the frequency of the electromagnetic wave is given. Thus k_0 is known and the solution of the system of Eqs. (III-2) and (III-3) determines a value of k_z as a function of the index of refraction $\varkappa_2$ of the plasma. Therefore a measurement of k_z (i.e., the axial wavelength of the electromagnetic field) can be correlated to the electron density of the plasma surrounding the rod.

Assume first that the rod is surrounded by a very weak plasma, (i.e. $\omega_p << \omega$) and let x_0, y_0 be a pair of values for x and y which satisfy Eq. (III-2) in the limiting case $\varkappa_2 = 1$; $(\omega_p = 0)$.

If k_{zo} is the axial propagation constant in the limiting case of zero electron density, the solution of

Eqs. (III-2) and (III-3) for a small value of $\left(\frac{\omega_p}{\omega}\right)^2$ leads to a value $k_{zo} + \delta k_z$ where

$$\delta k_z = \frac{k_o^2 G'(y_o) - \frac{2y_o}{r_o} G(y_o)}{2k_{zo}\left[x_1^2 F'(x_o)\frac{y_o}{x_o} - G'(y_o)\right]} \cdot \left(\frac{\omega_p}{\omega}\right)^2 \qquad \text{(III-4)}$$

In this equation $G(y_o)$ is the value of

$$G(y) = \frac{1}{y}\frac{K_1(y)}{K_0(y)} \qquad \text{(III-5)}$$

at $y = y_o$ and $G'(y_o)$ is the derivative of $G(y)$ with respect to y at $y = y_o$.

$F'(x_o)$ is the derivative of

$$F(x) = \frac{1}{x}\frac{J_1(x)}{J_0(x)} \qquad \text{(III-6)}$$

at $x = x_o$.

It is of interest to observe that the shift in the propagation constant k_z is proportional to the electron density.

Equation (III-4) assumes that no propagation of the electromagnetic field occurs in the radial direction.

APPENDIX IV

INTERNAL CAVITY PROBE OPERATING MANUAL

The suggested equipment consists of a cw microwave generator with a power output on the order of 20 mw and a frequency range as wide as that specified for the particular probe being used (2 to 2.3 KM_c for the 10 cm wavelength probe and 8.6 to 10.8 KM_c for the 3 cm wavelength probe) a wavemeter for the same frequency range, an oscilloscope with a sensitivity up to 1 mv/cm, a recording camera, a directional coupler, a crystal detector with output indicator, an isolator and the components required to interconnect the above-mentioned elements.

A schematic of the set-up is shown in Fig. 44. The microwave power generator is a klystron with its corresponding power supply; the output is fed through an isolator and a directional coupler which delivers a sampling signal to the frequency measuring system composed of a wavemeter, crystal detector and an indicator (a milliammeter or an oscilloscope).

From the directional coupler the signal is delivered to the probe.

Both the 10 and the 3 cm wavelength probe operates as a transmission cavity; the holders contain the crystal detectors and the coaxial cables carrying the microwave signal from the input to the cavity where the coupling is performed with a loop; a second loop picks up the transmitted signal and delivers it to the crystal detector. Both input and output of the probes are BNC connectors, the one mounted ahead is the input for the 3 cm wavelength probe and the output for the 10 cm and vice versa. This is shown in Fig. 44.

The output from the probe is connected to the oscilloscope and recording system. It is convenient to connect a resistance at the output of the crystal to compensate for the capacities and improving the time resolution of the recorded measurement. A value of a few thousand ohms is adequate to obtain resolution of the order of microseconds.

An appropriate foregoing system should be used to command the oscilloscope. For the calibration of the probes use has been made of heat transfer gauges acting as triggers. The probe in use should be mounted exposed to the plasma flow; it can be held in place by using the two threaded holes located in the back of the holder. Sufficient room should be allowed for the ionized gas to flow around the

probe without shocking. The teflon windows covering the cavity gap have been designed to withstand the sudden pressure jump that occurs at the end of the test up to about 30 psi.

The following steps indicate a systematic approach to perform the measurement of electron densities.

1. Determine the resonant frequency of the cavity without plasma. The frequency of the microwave generator is changed until an output from the probe is found. By using the wavemeter this resonance frequency (f_o) is measured.

2. The maximum expected electron density is estimated and the corresponding frequency shift (Δf) can be found in Fig. 37. The microwave generator is set at a frequency $f_o + \Delta f$.

The sensitivity of the oscilloscope can be selected considering that the output of the probe goes down with respect to the value obtained when determining f_o at a rate of one order of magnitude for each order of magnitude in electron density. Those values change over wide limits and the more convenient value can be found only by performing the measurement.

The sweep velocity of the oscilloscope is selected according to the expected direction of the plasma flow and the delay introduced in the trigger because of its location relative to the probe.

3. Firing of the shock tube and interpretation of the photographic traces.

The main point is to determine whether the maximum electron density of the plasma flowing inside the probe is above or below the expected one, corresponding to the preset value of Δf. If a double peak appears in the recording of the oscilloscope trace it indicates that the value of Δf was too low or that the peak electron density has been underestimated; a single peak indicates that both estimated and real electron densities are close and no peak shows an overestimation of the electron density. It is convenient to start the determination with a double peak trace and perform several runs increasing the Δf until a single peak appears and then decays. The inspection of the traces give the value Δf_c corresponding to the peak electron density.

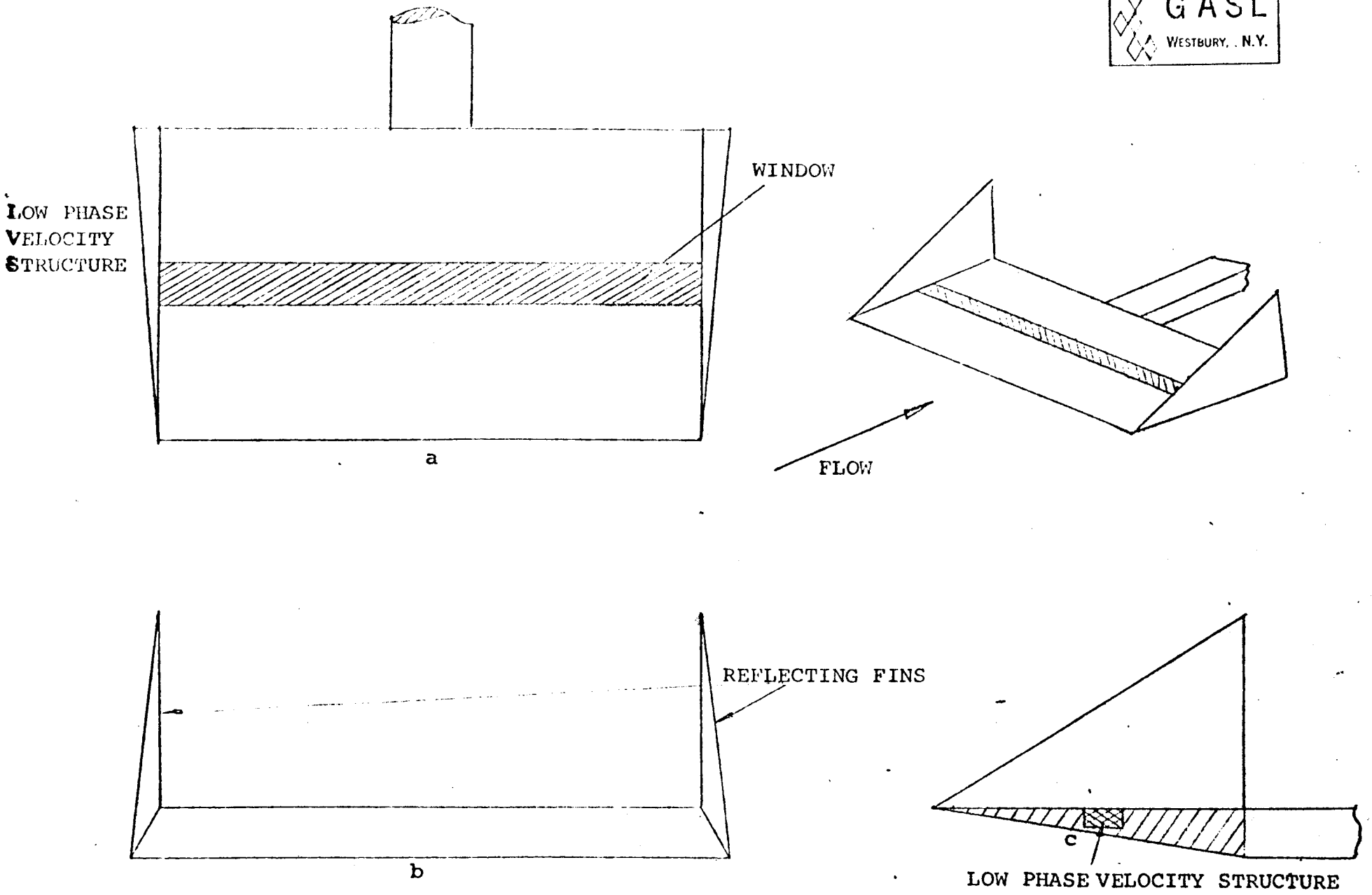

FIGURE 43. POSSIBLE CONFIGURATION OF THE LOW PHASE VELOCITY PROBE FOR A SUPERSONIC FLOW FIELD

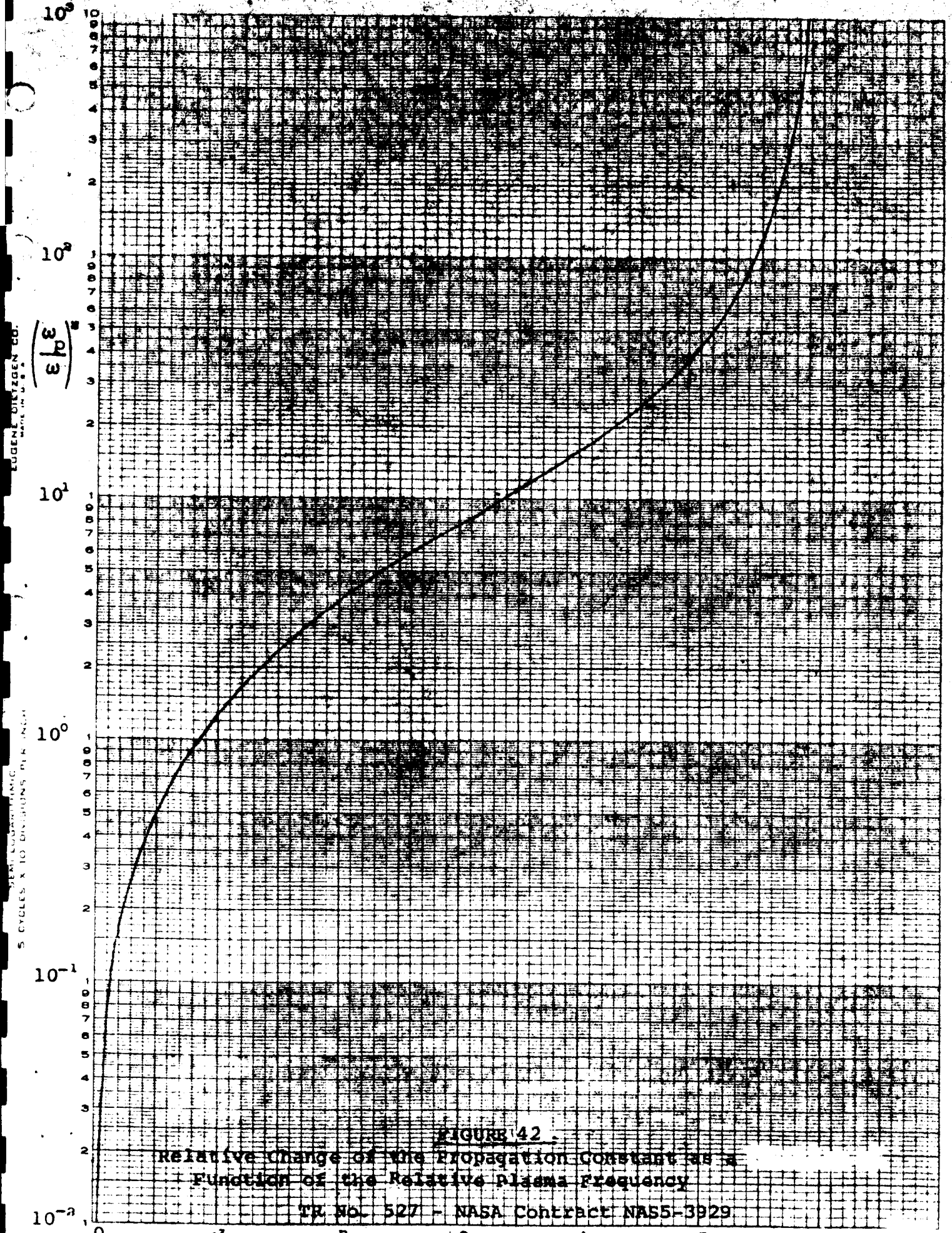

FIGURE 42.
Relative Change of the Propagation Constant as a Function of the Relative Plasma Frequency

TR NO. 527 - NASA Contract NAS5-3929

Project 8017 **DISTRIBUTION LIST**

FINAL REPORT - NASA Contract NAS5-3929

	No. of Copies
Office of the Director National Aeronautics & Space Administration Goddard Space Flight Center Glenn Dale Road Greenbelt, Maryland 20771	1
Office of the Assistant Director, SS&SA National Aeronautics & Space Administration Goddard Space Flight Center Glenn Dale Road Greenbelt, Maryland 20771	3
Office of the Assistant Director, T&DS National Aeronautics & Space Administration Goddard Space Flight Center Glenn Dale Road Greenbelt, Maryland 20771	3
Office of Technical Services National Aeronautics & Space Administration Goddard Space Flight Center Glenn Dale Road Greenbelt, Maryland 20771	3
Library National Aeronautics & Space Administration Goddard Space Flight Center Glenn Dale Road Greenbelt, Maryland 20771	2
Mr. M. C. Saunders, Code 248 National Aeronautics & Space Administration Goddard Space Flight Center Glenn Dale Road Greenbelt, Maryland 20771	2
Technical Information Division, Code 250 National Aeronautics & Space Administration Goddard Space Flight Center Glenn Dale Road Greenbelt, Maryland 20771	4
Dr. Richard Lehnert, Code 513 National Aeronautics & Space Administration Goddard Space Flight Center Glenn Dale Road Greenbelt, Maryland 20771	1 reproducible and 102